UNIVERSITY OF TECHNOLOGY SYDNEY

Doctorate Thesis

Key Techniques for Traffic Information Acquisition Sensor Networks

Faculty of Engineering and Information Technology

School of Electrical, Mechanical and Mechatronic Systems

Student: Zhiguo Li

Supervisor: Steven Su

August 2019

CERTIFICATE OF ORIGINAL AUTHORSHIP

I, Zhiguo Li, declare that this thesis is submitted in fulfilment of the requirements for the award of Doctor of Philosophy, in the Faculty of Engineering and Information Technology at the University of Technology Sydney.

This thesis is wholly my own work unless otherwise reference or acknowledged. In addition, I certify that all information sources and literature used are indicated in the thesis.

This document has not been submitted for qualifications at any other academic institution.

This research is supported by the Australian Government Research Training Program.

Signature:

Date:

Acknowledgement

First and foremost, I would like to convey my many thanks to the remarkable people who provide support, motivation, knowledge, friendship and love on my journey to pursuit a PH.D.

Special recognition must be given to Dr. Steven Su and Dr. Peiyuan Qin for their expertises, supervision and encouragement throughout the course of this project. I am particularly grateful for his wisdom that has inspired me to be a life-long learner and a passionate seeker of knowledge, and for his always being the first subject to test our new setup instrumentation, even though some of them were quite tough. I thank you with the deepest of respect.

I would like to give special thanks to Professor Jay Guo who spent lots of time to give insights into my thesis. I also express tremendous gratitude towards Professor Honghui Dong in Beijing Jiaotong University and my former colleague Mr. Kun Tang for the great support on experiments, data sharing as well as discussions about the research and help in many cases. I am indebted to all of the volunteer subjects, who have given their precious time to participate in the experiment and helped me to collect the data.

Finally, and most importantly, I would like to thank my family - my wife Xin Liu and my lovely children of Ethan, Joshua, Annabel and Esther, for their love and being backbone during this period of my life. Thanks also go to my parents and all my relatives in China. Without their eternal love and support, I would not be who I am today. I love you and God bless you.

Abstract

Road traffic information acquisition technologies have the capability to provide important information for intelligent transportation systems (ITS) by employing sensor networks, especially for detecting the road network information in dots, sections or large-scale areas. Sensor network plays a vital role in acquiring road traffic information of ITS. By exploiting spatial-temporal models, traffic flow models or correlation models, the traffic information of road sections and networks can be derived from the traffic data of some key points in the road for the temporal and spatial correlation. Furthermore, because of the constraints of space-time correlation, project investment and construction cost, the investigation of traffic information acquisition by employing sensor network technologies has become an important research direction of ITS. As a result, the investigation of the theories, techniques, sensors, and methodologies of traffic information acquisition sensor network (TIASN) has been a significant research topic.

Based on specific requirements on real time, accuracy and completeness for traffic information acquisition, this thesis has focused on the following key challenges: (1) new algorithm to acquire traffic flow based on multi-functional geomagnetic sensor; (2) efficient optimization methods for TIASN; (3) efficient calibration method for Inertial Measurement Unit (IMU); (4) effective testing method for urban rail transit sectional passenger flow.

In this dissertation, motivated by the above challenges, a thorough investigation is presented on a novel multi-parameter sensing method of traffic information by using a multi-function geomagnetic sensor (MFGS). Furthermore, in order to improve the efficiency of IMU based traffic monitoring, the calibration and its associated experimental design schemes are developed for the two-key tri-axial sensors in an IMU, i.e. tri-axial magnetometers and tri-axial accelerometers. At the end , we study the short-term prediction methods of sectional passenger flow and selects Back-Propagation (BP) neural network combined with the characteristics of sectional passenger flow itself.

Contents

List of Abbreviations

ITS	Intelligent transportation system
TIASN	Traffic information acquisition sensor network
MFGS	Multi-function Geomagnetic sensor
IMU	Inertial Measurement Unit
MTFs	Mix Traffic Flows
SN	Sensor Network
GPS	Global positioning system
INS	Inertial Navigation System
MEMS	Micro Electro Mechanical Systems
TAs	Tri-axial Accelerometers
TMs	Tri-axial Magnetometers
TGs	Tri-axial Gyroscopes
WSN	Wireless sensor network
DWVDA	Double window vehicle detection algorithm
GSVDA	Go-stop vehicle detection algorithm
ADWVDA	Adaptive DWVDA
SVDA	Stationary vehicle detection algorithm
IoT	the internet of things
ED	End device
RP	Repeater point
AP	Access point
FP	Fusion point

CP	Centre point
RFID	Radio Frequency IDentification
RIP	Routing Information Protocol
OSPF	Open Shortest Path First
OLSR	Optimized Link State Routing Protocol
AODV	Ad hoc On-Demand Distance Vector Routing
DoE	Design of Experiments
FIM	Fisher Information Matrix
CCD	Central Composite Design
BBD	Box-Behnken Design
MSE	Mean Square Error
OLS	Ordinary Least- Squares
AHRS	Attitude and Heading Reference System
A/D	Analog/Digital
SLP	Sensor location problem
TIC	Traffic information credibility
PoI	Point of Interest
PoS	Point of Sensor
ICF	Information credibility function
RICF	Road information credibility function

List of Publications

[1] Wenlong, Peng, Li Zhiguo, Pang Shaohuang, Jia Limin, Tian Yin, Chen Jianxiao, and Dong Honghui. "Access point research in rail train safety monitoring sensor network." In Digital Manufacturing and Automation (ICDMA), 2012 Third International Conference on, pp. 157-160. IEEE, 2012.

[2] Li, Qian, Yong Qin, Ziyang Wang, Zhongxin Zhao, Minghui Zhan, Yu Liu, and Zhiguo Li. "The research of urban rail transit sectional passenger flow prediction method." Journal of Intelligent Learning Systems and Applications 5, no. 04 (2013): 227.

List of Figures

List of Tables

1. Background

1.1. Introduction

As the recent rapid development of world economy, the amount of motor vehicles and level of mobility on roads has been dramatically increased. The demand of traffic system has significantly raised. The quality of services related to road traffic have been challenged. The road traffic information is complicated and also variable due to the interaction of mix traffic flows (MTFs) which consist of different objects such as motor vehicles, non-motor vehicles and pedestrians, the interaction between MTFs and roadways, the restraint between MTFs and their surrounding environment.

Road traffic information is the basic variable, including multi-traffic parameters such as flow, velocity, occupancy-rate and route time. Road traffic information acquisition includes the successive stages of MTF data's acquisition, generation, communication, storage and further process. The road traffic information acquisition provides the important fundamental data for intelligent transportation systems (ITS), which promotes the effectiveness of traffic control and traffic guidance strategy by the timely, accurate and comprehensive road traffic information.

Nowadays, the traffic congestion has already been a universal problem all over the domestic metropolises. The release of traffic congestion highly depends on the efficient synergism of related service, control and dispatch which strongly requires the comprehensive acquisition and fully utilization of the traffic information. Therefore, in order to essentially enhance the safety level, advance the operation efficiency and promote emerging industry, the related technologies for traffic information acquisition sensing network (SN) is imperative for ITS.

The physical basis of traffic state information acquisition is composed of physical sensors and their complete sets of systems. At present, there are many types of sensors used in the road traffic system, such as ring coils, radar guns, infrared tachymeters, ultrasonic tachometers and so on, which are used for road traffic flow and velocity statistics. The sensors of the related application system include infrared tachometer, stress and strain gage, ultrasonic gage and gas alcohol detector. The sensors used for road infrastructure monitoring include temperature, stress and strain gage, fibre grating, etc. The existing traffic sensor features single, multi-use of wired communication, installation is not convenient enough, these factors lead to the realization of large-scale, network deployment. With the application of ITS in urban road management, it has put forward new requirements for the low cost, multi-function, easy installation, easy maintenance and large-scale deployment of traffic sensors.

Single sensor detection performance, multi-sensor networking, and large-scale deployment optimization are critical for accurate access to road and even road traffic status information. Accurate access to traffic state information requires multiple sensors in the network space-time collaboration. Therefore, how to configure the sensors reasonably and how to construct the traffic information acquisition sensor network (TIASN) becomes the key technology for the accurate, comprehensive and efficient access to the road traffic state information. The existing situation is usually a variety of sensors to achieve an application service, ITS further development requires the sensor to form a variety of applications to meet the demand for large-scale deployment, detection of a variety of traffic environment sensor network. Therefore, the problem of single sensor traffic information multi-parameter sensing, regional sensor network optimization and construction, the sensor network layout optimization under large-scale deployment has become an important topic in academia, and industry.

Nowadays, there is an urgent need for large-scale traffic information acquisition in urban roads, expressways, and even national and county roads. The number of traffic sensors and related networks and system deployments has exploded. With the development of microelectronics technology, wireless communication technology and computer technology, the cheap, reliable traffic related products and systems have been becoming more and more available, and the cost of transportation sensor-related products and systems is decreasing rapidly. In addition, the types of traffic application systems needed by ITS in urban traffic management are increasing, which are mostly based on accurate and comprehensive traffic information acquisition. This research provides an application basis for the study of the multi-parameter traffic information sensing, sensor network topology optimization, sensor placement optimization and so on. Therefore, the research in this direction has important theoretical and practical significance.

On the other hand, GPS (Global positioning system) devices in the motor vehicles become more and more important when vehicles are on the road and make the traffic flow. For strap-down Inertial Navigation System (INS), an inertial measurement unit (IMU) is directly installed in the vehicle. Thus, the navigation precision of INS depends on the measuring accuracy of IMU. An inertial measurement unit (IMU) is an electronic device that measures and reports a body's specific force, angular rate, and sometimes the orientation of the body, using a combination of accelerometers, gyroscopes, and sometimes magnetometers. Since the INS updates the data rapidly and possesses the advantages of high short-term accuracy and stability, it can provide comprehensive navigation data, such as the location, speed, or the attitude of the carrier. Therefore INS plays a very important role in civilian navigation.

With the rapid development of Micro Electro Mechanical Systems (MEMS) technology it allow the size reduction of the chip-based inertial sensors in IMU (e.g. Tri-axial Accelerometers (TAs), Tri-axial Magnetometers (TMs), Tri-axial Gyroscopes (TGs) and also for the production of IMU-enabled GPS devices. An IMU enables a GPS receiver to work when GPS signals are unavailable, such as in tunnels, inside buildings, or when electronic interference is around. Therefore, Calibration of TAS and TMs becomes crucial.

Due the quickly expended size of population and city size, the development of road construction is far behind of the development of urbanization especially in the tier-one cities in China, such as Beijing Shanghai and Guangzhou. The demand of building urban rail transit is raised to relief the traffic pressure on road. And the high peak period of urban rail is key part to test and challenge the capacity of the rail network and also provide very important information to future expansion of rail network planning and design. Therefore the close control and forecast of the passenger flow is essential. And sectional passenger flow prediction especially in the important stations are one of most important elements.

1.2. Research Topics

Urban traffic problem (such as congestion, pollution, accidents, etc.) has been a serious problem facing in many large cities all around the world. Currently, ITS is one of the primary methods in the urban road network, which can improve the testability, observability and controllability of the traffic system. This is done by placing a certain number of traffic sensors to obtain real-time traffic information.

It is an important support for ITS in large-scale road traffic information acquisition. It is a key technology to realize the single-point, cross-section and regional traffic flow information acquisition in the network by sensor network technology. The real-time, accuracy and comprehensiveness of the traffic information of single-point and section are related to the real-time, accuracy and comprehensiveness. Due to the temporal and spatial correlation of traffic information, road sections and road network traffic information are often based on the traffic information of key points on the road, which is derived from the spatio-temporal model, traffic flow model and relational model. In addition, due to the spatial and temporal correlation of traffic information and engineering capital, construction costs and other constraints, research for single node, cross-section, sensor node traffic information multi-parameter sensing, sensor network topology optimization and network construction, large-scale deployment of sensor networks Layout optimization technology has become the focus of urban traffic research direction, the direction of the relevant theory, technology and methods of research has important theoretical and practical significance.

In some complex traffic environment such as inside a tunnel or somewhere when even GPS may be inaccessible, an Inertial Measurement Unit in the vehicle can still predict the pitch and roll information by integrating the measurements of TAs and TGs, without error accumulated with time. However, when only accelerometers and gyroscopes are used, the heading of vehicle is hard to estimate. That brings Tri-axial Magnetometers (TMs) to IMU and combined TMs with IMU to provide more accurate navigation information in terms of attitude and heading. Given the down sized IMU and every sensor embedded, the mobile navigation used in traffic control and monitoring becomes more and more popular. And how to calibrate TAs and TMs in the IMU is most important part of setting work and Auto-Calibration is one of the main research topics in this area.

With highly maintained traffic issues on the road, the urban rail train network expansion become the main way to reduce public transportation problems. Given the urban rail train is convenient, one time, not impacted by weather and cost economic, most of public choose to urban rail train to go to work or schools. And continuous population growth of some tier-one cites make the existing rail network under challenge. To avoid over passenger flow in some key sections and intersections, the passenger control and prediction is crucial. The research regarding how to best predict the passenger flow and give the support information of traffic control is very important.

1.3. Research Status and Analysis

The related technologies and methods of sensor network applied to traffic information acquisition have attracted the attention of scholars and engineers all of the world, and formed more and more related theories, methods and systems.

1.3.1. Wireless Sensor Network

Sensor Network has three main function which are acquisition of data, processing and transfer. Sensor network together with communication and computer technology constitutes main three pillars of information technology.

Wireless Sensor Network (WSN) [1-8] is a set of lots of static or dynamic senor combined together in the form of a self-configured mode in which the information is gathered from monitored field through wireless links. The data is forwarded through multiple nodes, and with a gateway, the data is connected to other networks like wireless Ethernet.

In WSN, there are many types of sensors to gather all different parameters in many scenarios such as earthquake, temperature, humidity, vibration, noise, pressure, intensity, electromagnetism, speed, direction and size of moving subject etc. It applies in all sort of industries including military, aviation, medical, environment, healthcare, modern living, anti-explosion, ocean analysis and many other

sectors. Data retrieved from sensors is passed through the network to a main location to be observed and analyzed.

1.3.2. WSN Network Topologies

The typical structure [9-15] of a WSN are various topologies as shown below.

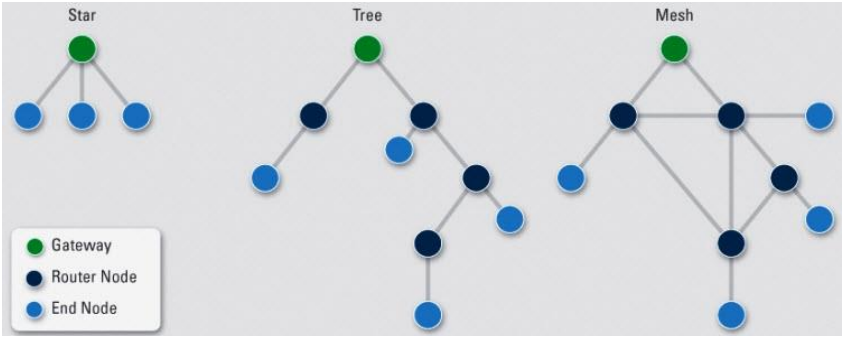

Fig.1-1 Wireless Sensor Network Topologies

Star Topology

Star topology is a topology of communication, in which each node connects directly to a gateway. One gateway can send or receive a message to several remote nodes. The nodes can't talk to each other.

Because each single node is independent, the gateway has to manage the node within the distance or range which data is transmissible between the end node and gateway. But there is also an advantage in this star topology. It is easy to manage the far end node in a low cost and minimum power consumption mode. The sizes of this topology vary from the amount of connections to the interchange.

Tree Topology

Tree Topology is like a combination of star topology, in which each node first connects to a node higher in the tree, and then to the gateway. Tree topology makes network expansion easier and also make error detection becomes convenient. But this network relies on the bus cable a lot. All the network will become failure if the cable breaks.

Mesh Topologies

Mesh topology is more complex topology in which data transmission from one node to another becomes even easier as long as within its radio transmission range. Data need to be forwarded by an intermediate node if one node is out of radio communication range. The advantage of mesh

topology is easy isolation and failure detection. And the disadvantage is the network is sometimes huge and requires lots investment and maintenance.

1.3.3. Key factors of Wireless sensor network

Large Scale

To acquire the accurate information, the number of sensors which are deployed in the system could be over thousands or even more. There are two presentations of large scale.[16-17] One is in a large geographical area, there are many sensors for instance in the scenario of bush fire monitoring network. Many sensors need to be deployed in all different locations in a massive area. The other is lots of sensors are deployed very intensively in a relatively small space.

Large scale sensor network has following advantages: the information received from different spacial views are more economic; the accuracy rate of information has been increased through distributed processing method; the requirement of accuracy level of single node has been softened; the existing redundant nodes make the system more fault-tolerant; the large number of sensors can also cover more monitoring area and reduce the blind monitoring area.

Self-configure

During the application of sensor networks, some sensors have to be placed in the rural area or the places without infrastructure [18-21]. The distance between the sensors is not pre-defined, the relationship before the neighbor sensors has not been set up. It makes the node in the network has self-configure ability which allows network to work properly and the data captured by the sensor can still be transmitted in the network through the topology and network protocols. In some cases, part of sensors may lose their function by dead battery or other environmental impacts. The number of sensors will decrease. In some cases, to achieve better monitor result or accuracy, the backup sensors will be added to network and make the number of sensors increase. That will make the network topology will change accordingly. Self-configure function is required to set up to adapt these situations dynamically.

Reliability

WSN is occasionally set up in very tough nature environment. In some cases, the place is hard to reach by human beings. The sensor and devices are exploded outdoor suffering strong sun light, rain, wind and sometimes destroyed by nature animals or other people [22-25]. This requires the sensor need to be tough and resistant.

Because the restriction of working environment and the large amount of sensors, it is very hard to maintain a high-level care on each of devices. It makes the network security become one of the most important issues. And fault tolerant is also a big impact to the reliability.

Data as the center

The development of internet is to start with PC as terminal and then connect the terminals into the network. The terminal also can exist as an isolated device out of network. In internet IP address is the single tag for each of computer and device. Resource allocation and information transfer rely on the IP address of the terminals, routers and servers [26-30]. To visit a device on internet, the first thing needs to know is the IP address.

WSN is a type of task-oriented network. Without the network, the isolated single sensor couldn't do any task. The node and device in WSN also have a tag, and they talk to each other through network communication protocol. In most of cases the sensors are randomly deployed and relationship between the nodes and their tags are dynamic. It means the tag and location of the node or device are not bound together. The user of WSN send request to the network not to any particular device and the network get the information to pass it to the user. This kind of command is more related to the tradition of human's nature language communication. So WSN is a network with data as the center.

Cooperative on tasks

Cooperative on tasks includes date acquisition, processing, saving and transmission. Through the cooperation, the sensors can work together to get more accurate information about the monitoring subjects. It also reduces the disadvantage of lack of the storage or processing capability of single unit. The units cooperatively work together to accomplish the complicated tasks.

1.3.4. Related Application of WSN

WSN is to acquire the real information in the physical world. The information is diversified and in many different kinds of format. Different WSN is designed to work with different physical parameters in different industries. So, the demand of WSN is totally different case by cases, not only in hardware platform and software system, but also in network protocols. So unlike internet with unified communication protocol platform, each WSN was designed to have its own ones. Even some of WSN has similarity, the majority of WSN care more about the differences which means the applicable to project the system was designed, the better result will be achieved by WSN. Customized design of each WSN based on the project requirement is main character of WSN compared to the traditional network designs.

WSN is designed and deployed in many industries [31-39]. Most of cases it was designed to monitor data, especially in the rural area where wired network is nearly impossible to establish or cost a fortune to set up. Wireless devices can be left in the rural for long time and only be called back or replaced when there is faulty or dead battery. The typical WSN applies in video surveillance, transportation monitoring, aviation controls, robotics, motor vehicles, healthcare sector and automation.

In recent years, the rapid development of sensor networks, especially wireless sensor networks (WSNs), has provided technical support for the real-time, networked and large-scale acquisition of various types of information in the transportation field [40]. The idea of wireless sensor networks was originally proposed by the US military [41]. As early as 1978, the US Department of Defence Advanced Research Institute Program began to fund Carnegie-Mellon University for distributed sensor network research, which is seen as the embryonic form of wireless sensor networks. The concept of Internet of Things (IoT) has been proposed by academia and industry [42-44], and the data perceived by the sensor network as one of the important sources of mass information of the Internet of Things has greatly expanded the application of sensor networks range, showing that the technology is in more rich application prospects.

The development of sensor networks has greatly facilitated the acquisition of environmental awareness and information [45-48]. At present, the most research achievements of sensor networks in the world are from the United States, Canada, Britain, Germany and Japan. Sensor network research started in the 1980s, in recent years, with the rapid development of microelectronics technology, computing technology, nanotechnology and wireless communications technology, it becomes possible to create cheap, micro, low power, multi-function sensor nodes.

In the area of sensor network application research, Nanyang R & D University of Singapore developed a large-scale real-time weather monitoring system based on wireless sensor networks in 2007 [49], which aims to enhance the environment protection awareness by automatically detect regional weather changes and predict climate change, global warming and other environmental issues. In this project, hundreds of mini weather stations are deployed in more than 100 universities or high schools in Singapore, each weather station contains several detection nodes that can measure weather parameters such as temperature, rainfall, humidity, wind speed and wind direction. The information with 5-15min sampling cycle was transferred to the data centre. In 2008, Harvard University and BBN deployed a large-scale wireless sensor network system in Cambridge, Massachusetts based on the City Sense project [50], mainly for monitoring a wide range of weather and air pollution. City Sense system consisting of more than 100 sensor nodes can monitor the air temperature, atmospheric pressure, relative humidity, wind direction, wind speed, rainfall, CO2 concentration, sound level and other environmental information, one data sample per hour. The data

was sent to the base station by multi-hop routing technology. In the same year, the University of Virginia completed a wireless sensor network project called MetroNet [51], which developed a pedestrian monitoring system to make use of pedestrian data collected in various stores across the city to make certain predictions. The system will deploy sensors in the store's doors and windows, counting the number of pedestrians in a period of time, in order to get the information of the store's advertising effect, the weather conditions, the most visited store and so on. In the field of intelligent transportation, as early as 1995, the US Department of Transportation proposed the National Intelligent Transportation System Project Planning which will be fully in operational by 2025. The program seeks to integrate advanced information technology, communication technology, sensor technology, control technology and computer technology into the integrated terrestrial traffic management, and establish a real-time, accurate and efficient of the integrated transport management system. The system uses large-scale wireless sensor network and GPS positioning system and other resources, not only maintaining all vehicles in the efficient, low-power state, automatically keeping distance, but also recommending the best driving route, and warning the potential faults [52].

In China, the research of sensor network system started late, but the related technology, standards, application developed rapidly [53-60]. Many universities and research institutions, such as Tsinghua University, Southeast University, Harbin Institute of Technology, Wuhan University, Zhejiang University, Chang'an University, and the Chinese Academy of Sciences have carried out the sensor network research, and more and more institutions and research institutions are joining to this field of research. In the field of intelligent transportation, Shenyang Institute of Automation of Chinese Academy of Sciences proposed an expressway traffic monitoring system based on wireless sensor network. This system adopted image sensor, which can effectively monitor high-speed road sections under low visibility and ice. Liu Xinxin of Wuhan University proposed a traffic light control system based on wireless sensor network, the sensor nodes on the road surface carrying the ultrasonic transceiver module which were used to detect the traffic flow in each direction lane. Based on the technical advantages of wireless sensor network, this thesis studies the method of automatic detection of highway traffic accident using wireless sensor network technology, aiming at the physical characteristics of traffic events which are common in highway traffic. Jia Tong from Southeast University proposed a wireless sensor network-based real-time monitoring system for roadside slope, the wireless sensor network using GPRS to achieve the remote monitoring of highway slopes which has obvious advantages of real-time, intelligence and low cost, can widely been applied to real-time monitoring of dam and reservoir facilities. Hui Meng, et al used the wireless sensor network and amorphous localization algorithm, combined with a wireless camera and related mobile platform to monitoring and positioning the fire of subway station or tunnel, which has great significance for the timely detection of subway fire and timely rescue.

1.4. Contributions and Organization of the Thesis

1.4.1. Contributions

A) High-accuracy traffic information multi-parameter sensing based on single geomagnetic sensor. In order to fast and accurately acquire traffic information, a novel multi-parameter sensing method of traffic information is proposed by using a multi-function geomagnetic sensor (MFGS), which is shown in Chapter 3. Compared with manual investigation, floating car technology, and several isolated traffic information acquisition methods, the developed multi-parameter sensing method based on MFGS is able to acquire information without any limitation by time. Furthermore, it has advantages of low cost, transmitting information wirelessly and ease of implementation. These enable the developed MFGS to be deployed in large-scale, which meet the needs of the road network in full-time and space and large-scale traffic information acquisition.

B) Various vehicle detection algorithms such as double window vehicle detection algorithm (DWVDA), Go-stop vehicle detection algorithm (GSVDA) and ADWVDA (Adaptive DWVDA) are compared for the first time for different application needs, which is shown in Chapter 3. By comparing these algorithms, the most appropriate algorithm for single-point vehicle speed acquisition method based on single-module and dual-module MFGS can be found. The various algorithms and methods compared in this chapter have been verified in actual road scenarios, which proves the practicability and effectiveness of each algorithm and method.

C) A new type of TIASN network and its optimization method is presented in the thesis. The architecture and function of TIASN are analyzed in terms of information standardization and subnet topology optimization of TIASN, which is given in Chapter 4

D) In order to improve the efficiency of Inertial Measurement Unit (IMU) based traffic monitoring, the calibration and its associated experimental design schemes were investigated for the two-key tri-axial sensors in an Inertial Measurement Unit (IMU), tri-axial magnetometers and tri-axial accelerometers. Furthermore, we introduce new methods to assess the quality of each individual experiment in terms of desired experimental characteristics, such as orthogonality, D-optimality, and G-optimality.

E) We also proposed a new method to simultaneously identify both the TA and TM 9-parameter models with certain optimality in Chapter 6. The effectiveness of the proposed experimental schemes have been demonstrated for the auto calibration of a recently developed μ-IMU which includes a 9-axis motion tracking chips.

F) Lastly we studied the short-term prediction methods of sectional passenger flow and selects BP neural network combined with the characteristics of sectional passenger flow itself. With a case study, we designed three different schemes. We used MATLAB to realize the prediction of the sectional passenger flow of the Beijing subway Line 2 and made comparative analysis. The empirical research shows that combining data characteristics of sectional passenger flow with the BP neural network have good prediction accuracy.

1.4.2. Organization of Thesis

The organizational structure of this thesis is as follows:

The first chapter is the introduction, showing the research background and significance of the main work.

The second chapter describes the background information about traffic information acquisition sensor network and geomagnetic sensor. More particularly, it studies the multi-parameter comprehensive acquisition of the traffic information based on single geomagnetic sensor, focusing on the accurate and real-time acquisition of traffic flow and vehicle speed based on the single-geomagnetic sensor.

In chapter three, a vehicle classification method based on single geomagnetic sensor is studied, and the time-frequency characteristics and multiple algorithms analyzed.

The fourth chapter is the mesoscopic research, involving the sensor network of traffic information acquisition. The methods of network node semantic coding, physical topology optimization and communication topology are researched, and the methods are validated by scenario and data examples.

In the fifth chapter, we investigates the calibration and its associated experimental design schemes for the two-key tri-axial sensors TAs and TMs in an IMU. For the commonly used 9-parameter models, we adopted a 12-observation rotatable G-optimal experimental scheme. Based on our previously proposed linearization approach, we linearized both the 9-parameter tri-axial accelerometers and magnetometers and the parameters of both two sensors can be simultaneously identified with acceptable accuracy. We also proposed two other experimental schemes and investigated their efficiency based on the analysis of their information matrices.

In the sixth chapter, the calibration and its associated experimental design scheme for the tri-axial magnetometers were discussed. The Icosahedron scheme is proved to be rotatable. And for this 12-observation experiment scheme, a simple linearization approach is applied for the parameter estimation. This algorithm can be easily implemented in a micro-controller with low computational

capacity. We also proposed online recursive least square algorithms for both 6-parameter and 9-parameter models when fast calibration is need. Experimental results showed the effectiveness of these calibration approached. It should be noted that the precision turntable is not required to ensure the desired calibration accuracy although these calibration methods utilize the projection of the local earth's magnetic field as a calibration input.

In the seventh chapter, short term sectional passenger flow forecasting is studied based on the historical data of Beijing Subway Line 2. BP neural network is used to predict sectional passenger flow. Three schemes are found feasible when the features of sectional passenger flow are combined to predict. Moving over more advanced video surveillance and face recognition system will be used together to verify the result of prediction and make the forecasting model more practical and accurate.

In the last chapter, the main conclusions of this thesis are analysed and summarized. Based on the experience of the research, the next research plan is given.

2. Traffic Information Acquisition Sensor Network and Geomagnetic Sensor

2.1. Traffic Information Acquisition Sensor Node

"Traffic information" has a rich connotation and extension. Traffic information includes traffic facilities information, traffic flow information, parking lot information, traffic incident information, traffic environment information, and sometimes even traffic road network information (such as road grades, fees, interchange connections, traffic management information, etc.) and so on. The traffic information in this thesis mainly refers to dynamic traffic information, which is narrow and basic traffic information, that is, traffic flow parameter information (such as flow, speed, occupancy, headway, vehicle stop) and traffic flow Models, etc..

Access to traffic information is now largely dependent on various types of traffic sensors. Traffic sensors are the "sensory organs" of traffic information, which are mainly fixed traffic detection technology [61-68] and floating vehicle technology [69-76]. Floating vehicle method is currently the most common travel time acquisition technology. Investigators drive a specific vehicle (such as a taxi with GPS positioning) on a pre-selected route, measuring the time taken and the distance travelled. In order to save manpower and improve the efficiency of data processing, floating car investigators can be through special instruments and equipment, such as EDMI or GPS receiver to assist in the recording, processing data [77-78]. The cost of this method is high, and it is not convenient for large-scale, network and long-time observation. This thesis focuses on fixed traffic detection technology.

With the continuous development of microelectronic technology, sensing technology, computer technology, communication technology and advanced manufacturing technology, as well as the continuous innovation of ITS technology, the market opportunity and the increasing demand of application, promote the industry and academia to develop new Detection technology [79-82], so more and more types of traffic sensors used in traffic information acquisition. Existing traffic sensor technology is divided into three categories: intrusion detection technology, non-invasive detection technology, road detection technology [83-84]. Intrusive detectors are installed beneath pavements of roads or bridges, by drilling (for example, some magnetic detectors) on a road surface (e.g. induction coil detectors) or by excavating pipes under the road surface (e.g. some models Magnetic detector, road tube detector, piezoelectric detector and weighing detector, etc.), or on the road directly fixed (such as the road tube detector) and other ways to install. Non-intrusive detectors do not need to be placed directly above the road surface or buried below the road surface, this detector is usually installed in the driveway or lane next to the main passive infrared detector, active infrared detector, microwave Radar detectors, ultrasonic detectors, acoustic detectors and video detectors,

etc. [77]. Off-road detection technology is mainly a non-fixed detection method, such as floating car technology, cellular communications, and remote sensing images.

For the fixed traffic detection technology, performed the performance evaluation for different types of traffic sensors, such as data type, detection accuracy, installation and maintenance cost. Table 2-1 shows the performance of different traffic sensors. Type of traffic flow parameters.

For large scale deployment of applications, the sensor cost and installation costs are still high. Many scholars are committed to define the characteristics of different sensors [85-86] in order to select the appropriate cheap traffic sensors to reduce ITS costs; other sensors to detect various types of traffic information. The researchers have developed the corresponding vehicle detection algorithm to reduce the complexity of the algorithm to improve the speed of operation [87-90]. The different types of traffic sensors have different application costs and detection errors. Table 2-1and Table 2-2 give the life cycle cost estimates for different types of traffic sensors when they are applied to two-way six-lane freeway traffic flow information detection. The test error rate of different traffic sensors is for different traffic flow parameters [83-84].

Table 2-1 and Table 2-2 to be continued in following pages.

Note: √, can provide the data type; ×, cannot provide the data type.

Table 2-1 Data types of detector devices

Sensor type	Device name	Traffic flow	Traffic velocity	Vehicle Length	Occupancy	Existence
Induction coil	Inductive loop	√	√	√	√	√
Geomagnetic sensor	3M micro loop	√	√	√	√	√
	SPVD	√	√	×	×	√
Pneumatic road tube detector	Pneumatic Road Tube	×	×	×	×	×
Passive infrared sensor	ASIM IR 224	√	√	√	×	√
	ASIM IR 254	√	×	×	√	√
	Eltec model 842	√	√	√	×	√
	Siemens PIR-1	√	×	×	√	√
Positive infrared sensor	Autosense II	√	×	×	×	×
Doppler radar sensor	TC 26-B	√	√	√	×	×
	TDN-30	√	√	×	×	×
	Loren	√	√	×	√	√
Microwave radar sensor	Accuwave 150LX	√	√	√	×	√
	RTMS	√	×	×	√	√
Ultrasonic sensor	TC-30	√	√	√	×	√
	Lane King	√	×	×	×	√
Passive acoustic sensor	SmarTek SAS-I	√	×	×	√	√
	SmartSonic TSS-I	√	√	√	×	×
Video sensor	Autoscope	√	√	√	√	√
	Video Trak	√	√	√	√	√
	Traficon	√	√	√	√	√
	Vantage	√	√	√	√	√
	Traffic Vision	√	√	√	√	√

Table 2-2 Estimated life-cycle costs for a typical freeway application (for 6 lanes)

Device name	Unit		Installation		Maintenance cost/a	Lifecycle (Year)
	Number	Cost	Mounting	Cost		
Inductive loop	12	$9,000	Inbuilt	Included	$700	5/15
3M Microloop	6	$13,125	Inbuilt	Included	$200	15
Autosense II	6	$36,000	O	$3,200	$600	7
ASIM IR 254	6	$4,200	O/S	$3,200/$1,200	$600	7
Seimens PIR-1	6	$6,600	O	$3,200	$600	7
RTMS	1	$6,600	O/S	$2,400/$400	$200	7
TC 26B	1	$1,470	O/S	$2.400/$400	$200	7
SmarTek SAS-1	1	$7,000	S	$800	$400	7
Autoscope solo	1	$9,800	O/S	$3,000/$1,000	$400	10
VideoTrak 900	1	$17,400	O/S	$3,000/$1,000	$400	10
Traficon	1	$8,000	O/S	$3,000/$1,000	$400	10

Compared with various traffic sensors, the geomagnetic sensor has its unique advantages, such as climate adaptability, low cost, convenience process, small size, fast installation and wireless transmission [83-84] [91-92]. In addition, there are many traffic information fusion algorithms based

on geomagnetic sensors, which can synthesize many important parameters of traffic information, such as speed, flow, time occupancy, stop discrimination, vehicle classification, etc. Because of these advantages, the geomagnetic sensor is easy to compose a cheap sensor network which can provide a possibility for large-scale deployment in the entire city adapting to the demand of full-time, network and large-scale traffic information acquisition.

In terms of traffic velocity acquisition, many scholars have studied the speed acquisition methods based on geomagnetic sensors [93-95]. These methods often require multiple sensors (two or more) to be used in conjunction with two adjacent sensors at a certain interval d , the detection system writes down the time difference t of the vehicle through the two sensors, and computes the vehicle speed by $v = d / t$. In some special sections, such as bridges, tunnels, curve sections, ramp entrances, etc., there is no suitable places for a number of sensors spaced at intervals, resulting in reduced applicability of this method. In addition, as for the single-lane flow detection, one sensor is enough, this method in the detection of traffic flow speed will increase the system construction costs.

Traffic information is becoming more and more important for ITS [96-97]. Along with the continuous popularization of ITS technology, the information such as the proportion and distribution of vehicles on the road is important for traffic planning, management and toll. Also, vehicles at a variety of regional road need to be real-time classified, such as the intersections with speed and load restrictions, highway toll stations, large parking lot. In addition, the traffic information provides the basic data and reference [91-92] for the application of the traffic flow forecast, the traffic regulation efficiency evaluation, the toll collection system, the vehicle weight limitation, the environmental impact assessment, the vehicle priority control, the roadbed life estimation and the road section overhaul. In recent years, many scholars have tried vehicle detection, classification algorithms by means of video [98-99], audio [100-104], coil [103-104] and geomagnetism [91-94] [105-106]. Yang Zhaosheng developed an offline classification system using the length, axle number, axle weight and other parameters as an input to solve the automatic classification problem in highway toll system [82]. Chen Qiang made traffic classification according to the two types of vehicle samples using the sound sensor to collect noise signals outside the vehicle [102]. Jeng studied the vehicle classification by the data fusion of the vehicle output of the coil, the number of axles, the KNN algorithm. Coifman and Kimb studied the car-length-based vehicle classification method using a single coil detector [77-78]. In recent years, the research of vehicle classification based on geomagnetism sensor has aroused the attention of scholars. Cheung and Varaiya used the actual data collected by the geomagnetic sensors to make classification according to the 13 classes of vehicles proposed by FHWA [91-92]. They used KNN, SVM and other classifiers to study the vehicle classification method for different data sets. Due to data acquisition constraints, the main study focused on 6 types of vehicles (1 type of car and 5 types of trucks) classification with the average accuracy rate around

80%. Kaewkamnerd, established a vehicle classification system based on the characteristics of vehicle induction length, average energy and peak number, and classified the vehicle into four categories: motorcycles, cars, pickups and vans [93-94].The system automatically performs vehicle detection, feature extraction and vehicle classification with the average accuracy rate of 79.66%. Vehicle classification based on sensors such as geomagnetism or coils [91-94] [82] usually rely on the length of the vehicle by two or more sensors obtaining the vehicle speed and deducing the length of the vehicle, which will increase the single-point vehicle classification cost. In addition, there is rarely research on the sample robustness of the model and the efficiency of algorithm implementation.

2.2. Multi-Functional Geomagnetic Sensors

The traffic sensor used in this thesis is a multi-functional geomagnetic sensor (hereinafter referred to as "sensor" or "MFGS"), which is shown in Figure. 2-1.

Fig. 2-1 MFGS product

The typical MFGS is 100mm in diameter and 64mm in height. The MFGS can real-time detect the magnetic field around the sensor, using magneto-resistive effect to turn the magnetic field signal into mV-level voltage signal, then amplified into a V-class voltage by the amplifier. The voltage is processed by the filter to eliminate interference and converted to digital signal through the A/D converter. The size of digital signal is corresponding to the magnetic field changes by vehicle disturbance.

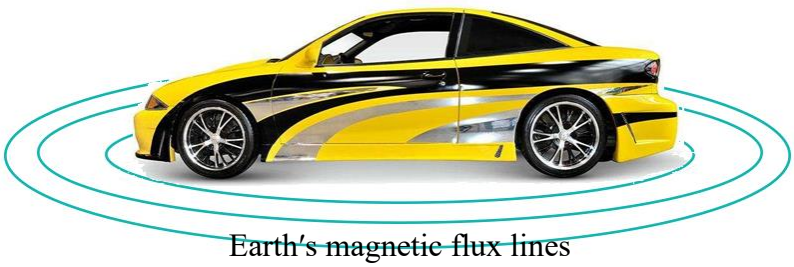

Fig. 2-2 The disturbance of Earth's magnetic flux lines by a vehicle

Figure 2-2 shows the magnetic field disturbance diagram by vehicle. When there is no vehicle in the sensor's surrounding environment, the output is a specific digital quantity (excluding the random noise) which is defined as the sensor reference value y_b. When the vehicle is passing through the sensor, the output is superimposed due to the influence of the ferromagnetic material on the magnetic field, the output is the waveform accumulated by the vehicle disturbance variation and the reference value y_b, defined as the original vehicle waveform. An MFGS detects traffic flow information in a single lane and can comprehensively detect a variety of parameters such as vehicle presence, vehicle stop, vehicle flow, vehicle speed, headway, time occupancy, and even vehicle types. In this thesis, single-module and dual-module geomagnetism sensors are chosen for vehicle detection in different application scenarios, and then study the traffic flow, vehicle speed, vehicle parking or presence, headway and vehicle traffic information such as comprehensive access methods.

Single module sensor can sense three sensitive axes (magnetic field direction), respectively, X, Y, Z axis in three directions, and output the corresponding digital value; dual-module sensor can sense four sensitive axes X, Y, Z1, Z2, respectively. It can output the corresponding digital values and the other module designed to receive only the Z-axis direction of the output. The X axis points to the reverse direction of the vehicle direction and collects the direction information of the vehicle direction. The Y axis is perpendicular to the direction of the vehicle direction and the interference information of the bypass path is collected. The Z axis points to the reverse direction of the gravity direction and collects the vehicle information, finally records the waveform of the vehicle (magnetic disturbance profile). MFGS can set the sensitivity of the axis strength to adapt to different applications when the effective detection range differs.

Multi-functional geomagnetic sensors can be used by wired or wireless communication (depending on different model) according to different application requirements. Wired communication is mainly used to acquire original sensing waveforms for product experiment and parameter calibration. Wireless communication is mainly for traffic flow information acquisition, based on different communication protocols (SimpliciTI, Zigbee, etc.) to form a wireless sensor network.

Another feature of this sensor is the environment self-learning mechanism. When the sensor works, it will measure and record the road environment's inherent magnetic field. During the vehicle detection, the sensor removes the environment inherent magnetic field from the output, so the vehicle waveform data will not be affected by the road environment. For the output may be negative at this time, which is not easy to deal with, the sensor sets the initial reference value for each sensitive

axis output, that is, the aforementioned y_b. Traditional geomagnetism sensor is influenced by the latitude and longitude of the installation location and the ambient temperature. After introducing the environment self-learning mechanism, it can reduce or even eliminate the influence of the two factors on the vehicle waveform output.

2.3. Traffic Information Acquisition Sensor Network

The road traffic information acquisition sensor network has not established a series of technologies and standards, which need more research of standardization. Compared with the traditional sensor network, the road traffic information acquisition sensor network is particularity in the aspects of network node distribution, network node semantics, network node information and communication links, it needs to study the topology optimization method of sensor network based on these characteristics, and then construct a low cost and low power consumption sensor network.

In this thesis, the definition of TIASN is given as follows. The set of sensors, repeaters, access nodes, gateways, servers, other nodes equipment and software system are arranged in the traffic network and traffic management department, connected by wireless or wired communication, in order to obtain the traffic system status. In the entire TIASN network, network devices are distributed at different levels. These devices carry different spatial granularities, time granularities and traffic information types.

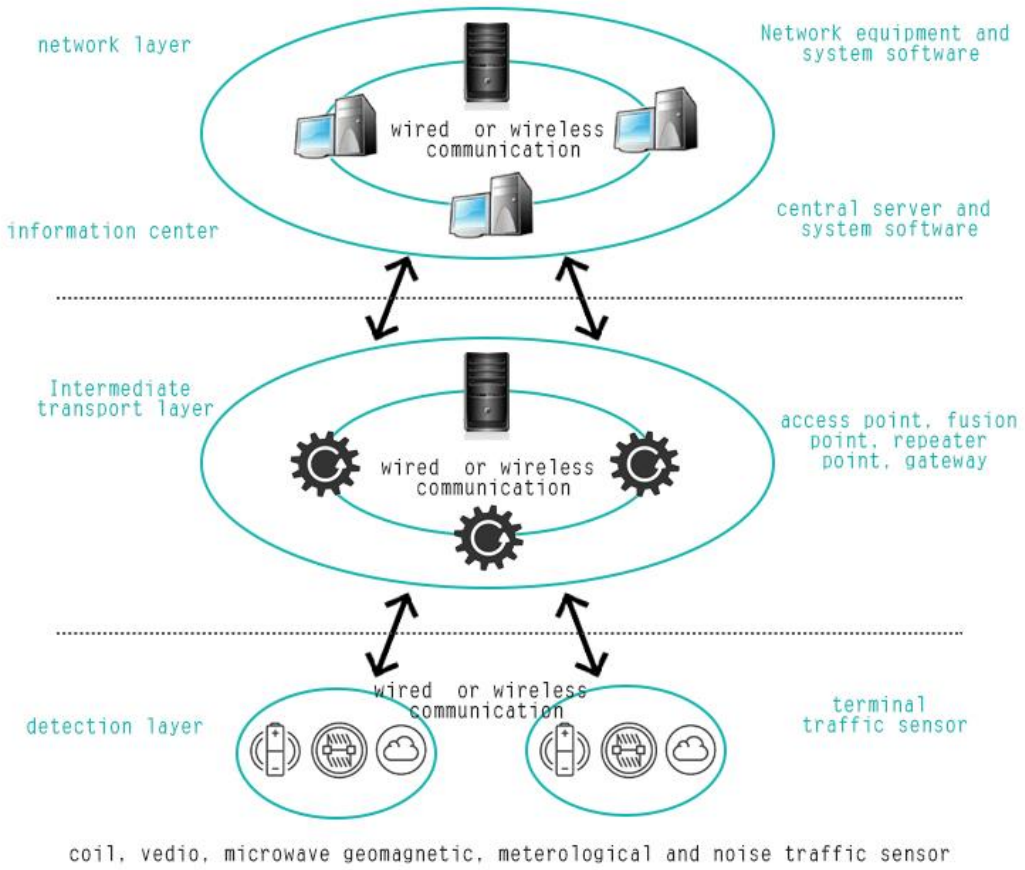

Fig. 2-3 Structure of TIASN and its devices

It can be seen that, in addition to the underlying detection nodes, TIASN also needs various network nodes with different functions to ensure that the traffic information acquired by the underlying detection nodes can be timely and accurately transmitted to local or remote storage and processing devices, supporting the upper application system. Although these network devices are not the focus of this work, they are an indispensable part of the sensor network.

(1) End Device (ED)

TIASN's low-level detection nodes, such as MFGS, other types of traffic flow sensors, road infrastructure sensors, meteorological sensors, etc., for the detection of ITS applications in various types of static and dynamic traffic information, which constitute the entire network traffic information data source, the ED of the test data to the network access node.

(2) Repeater Point (RP)

In the process of wireless communication, in order to effectively extend the transmission distance from ED to AP, RP nodes need to be relayed to transmit the ED information to its destination access node through multi-hop.

(3) Access Point (AP)

The access node is a gateway of the TIASN network. It collects the information of each ED node to which it belongs. It can receive information directly from the ED node or receive information from the RP node. Usually an AP and a number of RP, ED constitute a small TIASN subnet, for the collection and processing of specific areas of traffic information, to complete the regional application system functions.

(4) Fusion Point (FP)

This is used to realize the aggregation and processing of a plurality of TIASN sub-network information, and directly receives information from each AP node. The features include several local information processing functions, and can realize the fusion of a plurality of TIASN sub-network coverage area information and complete several coverage area applications system functions.

(5) Centre Point (CP)

The central node, or the traffic information data centre, connects multiple FPs to realize the collection, processing distribution of traffic information in a large area. It is the traffic information data centre of several regions or the whole city.

According to the size of the research area, there are two types of nodes in a TIASN subnet: ① EDs and an AP, ② EDs, RPs and an AP. FPs and CPs are involved only when multiple TIASN subnets are required and detection information is passed to the data centre. One of the APs and several MFGSs form a small TIASN subnet and transmit the test data to the CP through the FP. In different scenarios, the TIASN network configuration is different, depending on the distance to choose whether the RP is needed.

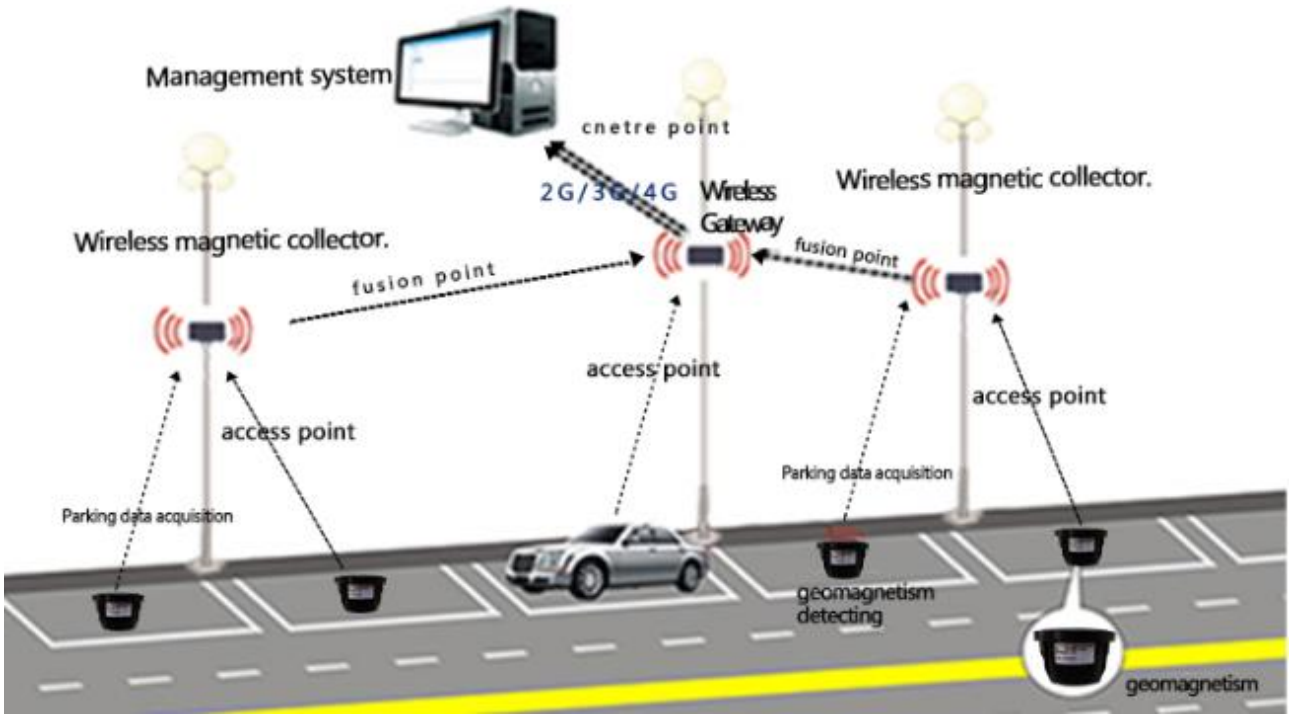

Fig. 2-4 A typical subnet of TIASN and its application scenario for road traffic flow information acquisition.

3. Synthetic Acquisition of Traffic Flow based on Multi-Functional Geomagnetic Sensor

3.1. Traffic Flow Acquisition based on Multi-Functional Geomagnetic Sensor

3.1.1. Vehicle detection Algorithm and Application

Vehicle detection is the first step of MFGS to obtain traffic flow. A good vehicle detection algorithm can improve the accuracy of flow counting, reduce the computational complexity and prolong the service life of the sensor. An adaptive threshold vehicle detection algorithm based on geomagnetism sensor is proposed in the reference document [5], which mainly solves the output drift problem caused by temperature or other environmental factors of the geomagnetism sensor, that is, the reference value of the sensor's sensitive axis output needs to be adjusted to accommodate this slow fluctuation. The algorithm determines whether to update the reference value by discriminating d_X and d_Z, which are the difference between the current output and the historical output value of the X-axis and Z-axis. The forgetting factor α is introduced to determine the weight between the new output value of a sensitive axis and the original reference value when updating the reference value. In addition to the other model parameters that should be determined in the algorithm, three parameters, d_X, d_Z and α, need to be determined from the field data, which increases the uncertainty of calculation and results. Because MFGS has environment self-learning mechanism, which eliminates the influence of temperature, latitude and longitude on the output reference value, this thesis presents a simpler double window vehicle detection algorithm (DWVDA). Because Z-axis can reflect the close and leave information, in order to further reduce the computational complexity of MFGS, only the two windows of Z-axis is initialized to reduce the difficulty of parameter calibration and prolong the service life of nodes.

The DWVDA algorithm is described as follows:

(1) The initial of reference value y_b and two window sizes, including the vehicle proximity determination window w_1 and the vehicle departure determination window w_2;

(2) Starting the vehicle proximity judgment window w_1;

(3) Input the waveform data of each sampling point sequentially, if the sampling data is beyond w_1, turn to (4), record the vehicle adjacent point as p_1, otherwise turn to (2);

(4) Starting the vehicle to leave the discrimination window w_2;

(5) Input the waveform data of each sampling point sequentially. If the sampling data is within w_2, record the vehicle departure point as p_2 and the traffic volume plus 1, and record the waveform between the sampling points p_1 and p_2 as the vehicle waveform, and then turn to (2) continue to detect the next car, otherwise turn to (4).

DWVDA algorithm can get a complete single vehicle waveform and write down the vehicle adjacent to the vehicle and leave the sampling points for the calculation of traffic flow, speed, length, headway, vehicle types and other traffic flow information to provide basic vehicle waveform data, in the following chapters, the research of traffic information acquisition is based on the algorithm.

This algorithm can also detect the situation of vehicle stop movement, that is, the vehicle stops near the MFGS for a period of time to leave. In the algorithm DWVDA, the introduction of variable window w_3, you can get the time to stop the vehicle s_1 and end s_2. In this thesis, the Go-Stop Vehicle Detection Algorithm (GSVDA) is given as follows:

(1) Set the initial width and height of window w_3 to $StopWinWidth$ and $StopWinHeigh$ respectively;

(2) Obtaining p_1 and p_2 using the DWVDA algorithm, then input the waveform between p_1 and p_2 into window w_3;

(3) If there exists continuous waveform points in w_3, note the beginning of w_3 for s_1, enter (4), otherwise enter (6);

(4) Increases $StopWinWidth$;

(5) If several consecutive points are not in w_3, note the end point of w_3 for s_2, enter (6), otherwise enter (4);

(6) End.

Using GSVDA algorithm, not only can determine the vehicle stop time, you can also modify the vehicle waveform. For example, in the geomagnetic sensor-based vehicle classification, vehicle parking situation recognition rate by using the traditional method is low or even cannot identify. Because the input parameters of the vehicle classification algorithm are mainly for the characteristics of normal vehicle waveform extraction, the vehicle stop waveform not only changes the time-domain

characteristics of the vehicle waveform, but also the uncertainty of the time factor. GSVDA algorithm can cut off the waveform data between s_1 and s_2 re-splicing new vehicle waveforms between p_1 and p_2 which can effectively improve vehicle classification accuracy.

In addition, when the vehicle stops at the top of the MFGS, the sensitive axis output is a constant value which is far different from the reference value y_b , then by modifying the DWVDA algorithm, a simpler Stationary Vehicle Detection Algorithm (SVDA) can be obtained.

The SVDA algorithm for real-time vehicle discrimination is described as follows:

(1) Initialize reference value y_b , stop reference value difference d_y and suspension determination window w_4 ;

(2) Input the waveform data of each sampling point in turn;

(3) If the distance between sampling point data in the width of w_4 and d_y is greater than y_b , turn to (4), otherwise turn to (6);

(4) If the sampling point data in (3) are all within w_4 , turn to (5);

(5) The output detection state is "Vehicle Exists", turn to (2);

(6) The output detection status is "No Vehicle", turn to (2).

Using the SVDA algorithm, a single function parking sensor can be developed for vehicle detection and management in car park. As a result of single function, simple algorithm, and the non-directional laying, these parking geomagnetic sensors with low cost, longer life, easy to lay features are convenient for all types of large underground park, street parking spaces, large-scale parking spaces, improving the intelligent management level of car park.

The intelligent parking management and guidance system can be realized by using the SVDA algorithm and the sensor network node described in section 3.1. The system can acquire the parking status and the time point when the vehicle enters and leaves the parking space by installing the parking sensor and real-time analysis. At the macroscopic level, real-time parking status is the dynamic attracting points of traffic flow, which explains the source of traffic flow and the end of traffic flow in order to carry out targeted police deployment for the effective induction and management. On the microscopic level, real-time parking status information shows the real-time usage of each parking space, which is convenient for real-time statistics of the utilization ratio of large-scale parking lots

and on-street parking spaces for convenient parking management, planning and billing. It can provide data support for parking monitoring, parking information release, urban parking guidance and off-site parking forensics applications. According to the collected parking space usages and traffic flow information, an accurate parking guidance function can be realized by means of guidance screen, broadcasting, network, mobile equipment, etc., which can reduce manpower cost, searching time and pollution, and provide decision-making basis for city planning and road planning.

The specific functions of intelligent parking management and guidance system are as follows:

(1) Parking status real-time detection

A parking sensor is located in the centre of each parking lot for real-time detection of parking occupancy. When the parking space geomagnetism sensor detects that some street parking space j is occupied by the vehicle i, the parking status is set to "Occupied" and triggers the parking sensor timer to obtain the time $t_{i,in}$ which the vehicle i starts to park at the parking space; When leaving, the parking status is set to "Vacant" and the time $t_{i,out}$.

In this way, the TIASN composed of parking sensor, RP, AP and so on, can transfer the real time occupancy and vacant time of the parking spaces to the MFA or the detachment centre to realize real-time detection of the whole network or regional parking resources.

(2) The space-time statistics of the parking status

By analysing the occupied and vacant time series $T_j = \left\{ t_{1,in}, t_{1,out}, \mathrm{L}\ , t_{i,in}, t_{i,out}, \mathrm{L}\ , t_{n,in}, t_{n,out} \right\}$, the spatial and temporal distribution status $T_{j,occupied}$ of parking space j is obtained. $T_{j,occupied} = t_{i,out} - t_{i,in}$, $T_{j,vacant} = t_{i+1,in} - t_{i,out}$. If 1 stand for the parking space is occupied, 0 stand for the parking space is vacant, the spatial and temporal distribution status of the parking space can be described by 0-1 sequence, $S_t = \left\{ s_{1,}(t), s_2(t), \mathrm{L}\ , s_j(t), \mathrm{L}\ , s_m(t) \right\}$, where $s_j(t) = 0\ or\ 1$. If the time discretization is performed, the space-time distribution of the parking spaces can be represented by the two-dimensional 01 matrix ST, $ST = \left[s_1(t_i), s_2(t_i), \mathrm{L}\ , s_j(t_i), \mathrm{L}\ , s_m(t_i) \right]$.

(3) Statistical analysis of bureau level and detachment level of parking spaces

According to the real-time parking spaces information obtained by the intelligent parking management and guidance system, the bureau/detachment level server, the different sizes of regional parking space information is prepared to analyse the spatial and temporal distribution of

parking spaces in time and space, and statistically analyse parking space related data of different spatial granularity. Bureau level is mainly about the status of parking spaces, such as the proportion of time, space balance and other information, providing reference for the new parking plan, different regions of the different regions of the development of charges, car OD estimation, etc. Detachment level is mainly about the specific situation of the parking space distribution in the jurisdiction, including the demand for sub-area parking space, the status of the real-time parking status and the parking status information such as parking spaces for the management of parking, traffic control and other traffic management.

(4) Parking supervision, publish, planning and parking guidance

Using the system, according to the parking status information, the traffic control station can judge whether the parking spaces are occupied reasonably and then supervise the parking spaces. The parking spaces can be distributed in real time according to the status of the parking spaces and the status data. According to the status of the sub-regional parking spaces and the proportion of the relevant sections of the traffic flow characteristics, rational plan the parking spaces (especially on-street parking spaces), location and quantity. At important junctions, parking status, number of occupants and location of the parking spaces are displayed on the display screen, and parking guidance is provided for the traveller to reduce the waiting time searching for parking space and reduce the interference of the parking vehicles to the traffic flow of the adjacent road sections.

3.1.2. Secondary Environment Adaptive Vehicle Detection Algorithm

In high congestion scenarios, such as traffic jams, ramp, highway toll stations, and congestion-prone sections, these vehicles travel slowly, with a small front-to-rear distance, even below 100 cm, resulting in low MFGS vehicle detection rate. In project applications, it is already a common problem that almost all unidirectional interactive traffic sensors (different from the detection method using on-board RFID) exist for the high accuracy vehicle detection in the high congestion level. The reference [43] studied the factors of traffic sensors detection performance such as environment and traffic condition, combined with his research results and my study.

Although MFGS has environment self-learning mechanism, in the case of high congestion, the reference value y_b of DWVDA algorithm cannot return to the original level in time due to the distance between the front and rear vehicles too close to the neighbouring vehicles, leading to the failure when the geomagnetic environment return to baseline level without vehicle impact. On this basis, this thesis designs adaptive detection algorithm (ADWVDA), similar to the adaptive threshold vehicle detection algorithm of reference [5] , ADWVDA algorithm based on DWVDA adding update mechanism of reference value y_b (The first time for the MFGS itself to achieve the geographical

environment adaptive, the second time for the traffic flow environment adaptive). Field tests show that the algorithm can achieve high vehicle detection accuracy in high congestion scenarios.

ADWVDA algorithm update mechanism is as follows:

$$newy_b = (1-\alpha)oldy_b + \alpha \times buffery_b(w_5) \tag{3.1}$$

$newy_b$ is the new reference value, $oldy_b$ is the newly used reference value, w_5 is the second adaptive window; $buffery_b$ is the mathematical expectation when the sampling points of the neighbouring vehicles are in the window w_5, otherwise the $buffery_b$ value is null; α is forgetting factor.

ADWVDA update conditions:

$$|buffery_b - oldy_b| < dr_1 \ and \ |buffery_b - y_b| < dr_2 \ and \ buffery_b \neq null \tag{3.2}$$

In the formula, dr_1 and dr_2 are the short-term drift and long-term drift of the traffic flow. ADWVDA algorithm needs to calibrate dr_1, dr_2, α, w_5 and other parameters.

3.1.3. Experiments and Analysis

In this thesis, the parameters of each vehicle detection algorithm proposed are calibrated by using MFGS to collect urban road traffic data and video.

(1) The experimental scenario Ⅰ

The experiment is based on the MFGS at the traffic lights of the Beijing Jiaotong University, which is used to verify the algorithm of DWVDA and realize the general road traffic information detection.

MFGS was used to collect the data of the traffic data at different time points in the experiment scene, and the continuous geomagnetic waveform data set with different traffic flow was obtained. The data sets were named after the MFGS time (year, month, day and hour).

The DWVDA algorithm achieves a high accuracy rate of more than 99% in the test scenario-traffic volume detection, and the overall statistical error is lower, only 0.25%. The sample set of this experiment contains many factors such as different climate and temperature difference (summer and winter), peak-peak traffic flow (midday peak and late peak), signal change (traffic flow in green light and car-following in red light). The test results do not reflect the differences under these factors,

indicating that the MFGS and DWVDA algorithms used in this thesis have good robustness to these factors in traffic information acquisition.

(2) The experimental scenario II

This experiment is used to verify the detection results of ADWVDA algorithm in the high congestion scenario. The experimental scene in Xi'an, a main road layout MFGS.

In the second experiment, MFGS collects the 24-hour vehicle waveform data from 24:00 on November 24th, 2016 and uses the ADWVDA algorithm proposed in this thesis to validate the method. the 24th and 25th at a number of time points of the traffic flow state, we can see that from 8:00 on the 24th, the traffic flow began to increase, then the traffic congestion degree increases, the phenomenon of vehicle stop-and-go gets serious, and the vehicle is closely followed, in this case DWVDA algorithm's detection error increased.

Because of the large amount of data, this thesis uses hourly traffic volume as the unit of statistics, using uninterrupted video data (18: 00-19: 00 and 02: 00-03: 00 hours is incomplete, not statistics) to calculate the hourly traffic of the lane. In order to compare the applicability of different algorithms, this thesis uses the collected 24-hour continuous waveform data for scene reproduction, respectively, using DWVDA and ADWVDA algorithm for vehicle detection. Under the high congestion scenario, the DWAVA algorithm has an average absolute error of 7.07% in 24 hours. After introducing the secondary environment adaptive mechanism, the ADWVDA algorithm reduces the error to 2.54%, and the traffic flow detection at all times the accuracy rate is greater than 90%. Figure 3-1 and Figure 3-2 show the hourly traffic statistics and statistical error distribution for DWVDA and ADWVDA, respectively. As can be seen from Figure 3-2, the detection error of ADWVDA algorithm is smaller, especially in the high congestion period. It can effectively reduce the vehicle detection error. However, there are still some errors in some periods, such as 6: 00-8: 00 and 22: 00-00: 00 in the non-high congestion periods. By analysing the video data and waveform data, there are some reasons: ① long-time manually statistics error; ② video acquisition equipment replacement corresponds to a slight error; ③ the probability of vehicle lane change makes the man-made statistics ambiguous. The above reasons are mostly due to the following statistical errors. In this study, only the single-lane statistics are used, in practice, the traffic flow is mostly cross-section. If the lanes are parallel to the MFGS, the traffic flow statistics of the cross-section will be negligible.

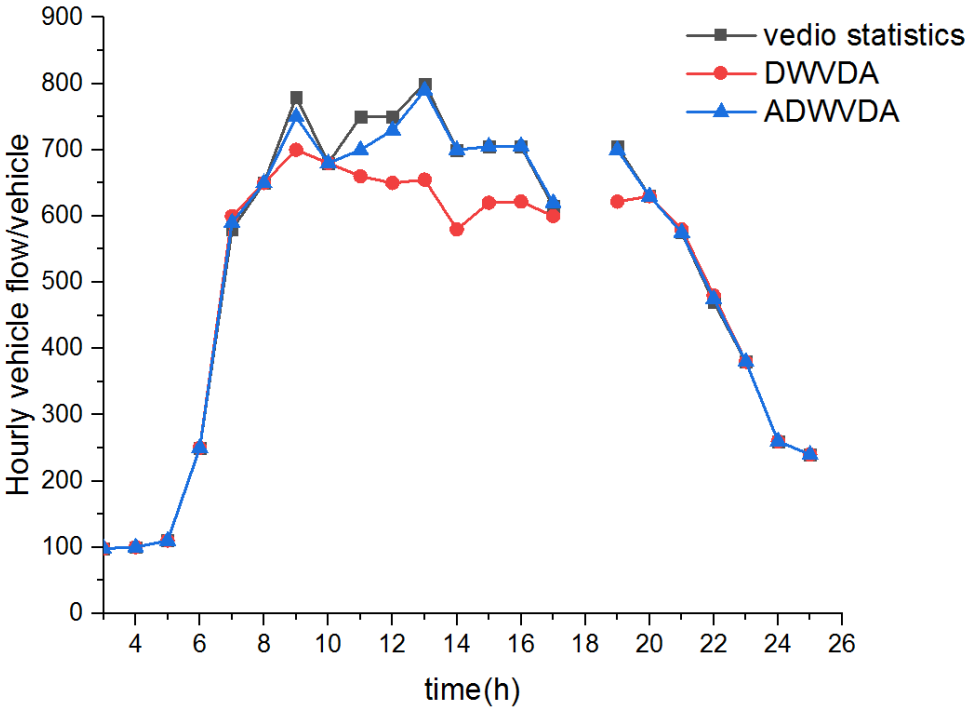

Fig. 3-1 DWVDA and ADWVDA based hour traffic counting of experiment scenario 2

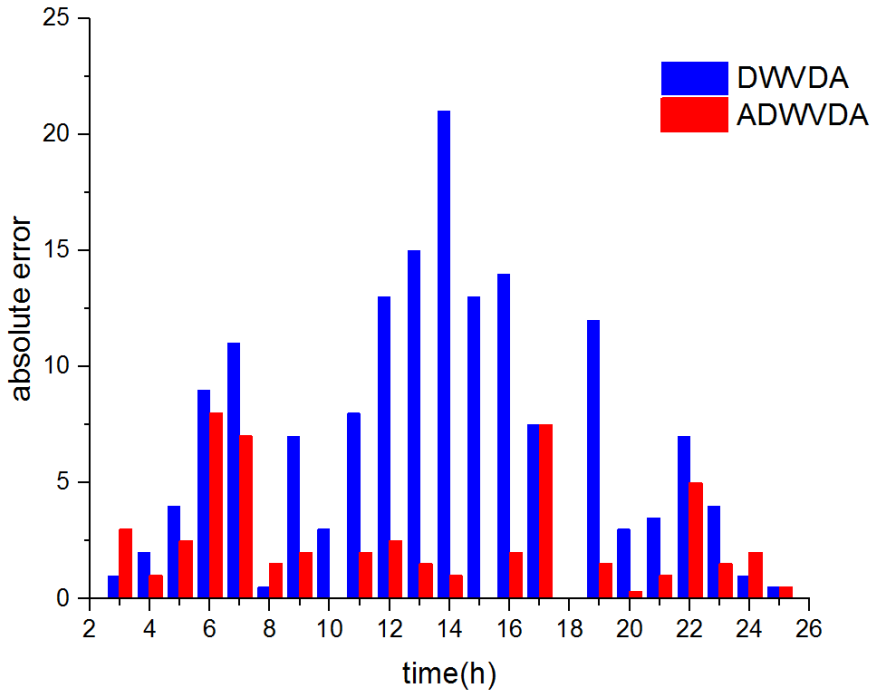

Fig. 3-2 DWVDA and ADWVDA based percentage error of experiment scenario 2

Using the vehicle detection algorithm in this thesis, the MFGS not only gives the number of traffic flow in a given time period, but also gives the time point when the vehicle arrives and departs from the MFGS, which makes it possible to estimate the traffic flow.

3.2. Vehicle Speed Acquisition Method based on Multi-Functional Geomagnetic Sensor

It is very important to obtain the speed of each vehicle for estimating the traffic flow velocity of all-time network. Floating vehicle technology estimates the average travel speed of the road section of the average speed from single vehicle, using the vehicle camera identification system which is similar to the road traffic flow sampling, to estimate the average speed of the corresponding sections. These techniques provide a reference to the overall situation estimation of the traffic flow, but the method cannot pay attention to the details of the vehicle operation because of the lag of the traffic flow state estimation and the untypical sampling value. MFGS is able to reflect the detailed characteristics of traffic flow at the same time, such as headway, vehicle time slot and vehicle speed as described above. In reference [5], a statistical method for estimating the velocity of a traffic flow using a single geomagnetic sensor is presented. In this section, a vehicle speed estimation method based on one single module and a dual module MFGS is studied [107]. This method not only obtains the average speed, median speed, but also can obtain the time and space distribution of the vehicle speed of the road network and provide more detailed basic data for real-time traffic guidance, traffic signal control, traffic accident and congestion detection and other applications.

3.2.1. Vehicle Speed Dual-Module Sensor Acquisition Method

The distance between the two modules L_c leads to two waveforms offset, which just depends on the speed of vehicles at this time. Assuming that d_s is the offset of the Z1 axis and Z2 axis waveform, the vehicle speed v_{double} based on the two-module MFGS is estimated as follows:

$$v_{double} = \frac{L_c \times 3.6 \times f_s}{d_s} \left(\mathrm{km/h}\right) \tag{3.3}$$

Compared with the traditional method of estimating the vehicle speed with two detectors at a certain distance, the cost of the method is reduced by 50%, and the influence of the two detectors on the estimation result is also eliminated. However, the distance L_c is smaller (the limitation on the individual sensor volume in engineering), so d_s is smaller. In the case where f_s is constant, from function (3.3), the time vehicle passing through the distance L_c is d_s / f_s . It can be seen that the smaller the d_s , the greater the error of the velocity estimation. In order to reduce the error caused by

the small d_s , this thesis introduces interpolation method to improve the speed estimation accuracy. Let k_{interp} be the interpolation multiple, then the vehicle's estimated time resolution is increased from $1/f_s$ to $1/\left(f_s \times k_{interp}\right)$ which can improve the vehicle speed estimation accuracy. At this time, the vehicle speed v_{double} is:

$$v_{double} = \frac{L_c \times 3.6 \times f_s \times k_{interp}}{d_s\left(k_{interp}\right)}\left(\mathrm{km/h}\right) \tag{3.4}$$

Where $d_s\left(k_{interp}\right)$ is the offset of Z1-axis and Z2-axis after k_{interp} multiples?

3.2.2. Experiments and Analysis

The experimental scenario I (the sensor in this scenario is a dual-module MFGS and the single-module MFGS vehicle estimation method using only the Z1-axis output data). The vehicle speed estimation method proposed in this thesis is validated by the data set 201605211118. Using live video and the data set, the traffic flow status at 11:00 AM on May 21, 2016 was reproduced. There were 45 vehicles, which were stopped 3 times due to pedestrian traffic lights.

Table 3-1 gives the vehicle speed estimation results and errors for each method. The average absolute error of v_{single} and v_{double} are 4.12 $\mathrm{km/s}$ and5.90 $\mathrm{km/s}$ respectively, and the average absolute error is 0.33 $\mathrm{km/s}$ (1.54%) and 0.91 $\mathrm{km/s}$ (4.32%) respectively. In addition, combined with SVDA algorithm, 3 cases pedestrian traffic lights were all well detected, respectively, the 4,15 and 29 vehicles.

Table 3-1 Results and errors of vehicle speed estimation based on single chip and double chips MFGS

Number	$v_{average}$	v_{single}	v_{double}	v_{single}-MAE	v_{double}-MAE
1	33	31	20	1.6	12.6
2	47	34	33	12.9	13.6
3	19	13	22	6.2	3.0
4	0	0	0	0.0	0.0
5	8	8	11	0.1	3.2
6	13	30	29	16.8	15.4
7	14	12	14	1.9	0.4
8	34	33	25	1.1	9.1
9	31	29	22	2.2	9.1
10	25	30	18	5.0	6.8
11	30	44	40	14.0	9.9
12	27	37	17	10.2	10.1
13	11	10	18	0.3	7.3
14	29	21	25	7.8	3.9
15	0	0	0	0.0	0.0
16	12	14	8	2.3	4.0
17	19	17	22	1.7	3.4
18	17	13	18	3.7	1.5
19	27	40	22	13.2	4.6
20	30	25	22	5.0	7.8
21	34	27	25	7.1	9.1
22	19	16	20	2.7	1.2
23	26	26	29	0.1	2.7
24	22	16	25	6.1	2.9
25	21	17	20	3.8	0.9
26	31	32	22	0.8	9.1
27	31	33	25	1.8	6.3
28	14	10	22	3.9	8.3
29	0	0	0	0.0	0.0
30	13	19	17	5.6	3.2
31	14	18	15	3.9	1.2
32	16	16	29	0.4	12.9
33	20	15	17	4.7	3.1
34	27	21	25	5.8	1.8
35	24	19	33	4.8	9.1
36	33	28	29	4.6	4.1
37	33	34	25	1.4	7.6
38	23	16	20	6.7	2.8
39	11	10	11	0.9	0.2
40	17	19	22	1.6	4.7
41	23	21	22	1.7	0.5
42	28	27	20	0.8	7.8

43	47	42	29	4.9	18.3
44	19	12	29	3.2	19.7
45	5	3	7	1.5	2.1
average	**21.40**	**21.07**	**20.49**	**4.12**	**5.90**

3.3. Summary

In this chapter, based on the actual engineering and application requirements of ITS, a multi-parameter acquisition method of traffic flow information based on single geomagnetism sensor is studied by using the self-developed MFGS. Compared with manual survey, floating vehicle technology and several isolated points, the single-geomagnetism sensor multi-parameter acquisition method can obtain all-weather information, and it can support wireless communication, easy deployment and low-cost installation, making the MFGS to facilitate large-scale deployment, so as to meet the road network full time and space, large-scale traffic information access needs. This thesis introduces the MFGS and its TIASN, and gives the vehicle detection algorithms such as DWVDA, SVDA and ADWVDA, which are suitable for different application requirements. Using these algorithms, the single vehicle speed acquisition method based on single module and dual module MFGS is studied. The algorithms and methods proposed in this chapter have been validated in practical road scenes, and the practicability and effectiveness of the algorithms and methods are proved.

4. Optimization for TIASN

In Traffic Information Acquisition Sensor Network (TIASN), sensors that are placed strategically to sample the road traffic information. The sensors send out the information sampled to a central data access point. The central data access point aggregates all information retrieved from all sensors and constructs a real-time monitoring of the road traffic by TIASN.

However, typical wireless sensors have very limited transmission range. It is not always possible for the sensors to transmit their sensing information directly (one hop) to central data access points. In latest research of sensor networks, it is common to construct a sensor network where sensors may relay data for other sensors in order for the central data hub to cover a larger area and a larger number of sensors. That is, the sensors in TIASN forms a mesh data network.

Note, to avoid confusion in terminology, we will use data traffic or traffic to denote the information flow transmitted in the TIASN mesh network and use road traffic to denote the traffic of vehicles on the road. We will also use nodes, end devices (EDs), and sensors interchangeably in this chapter.

In addition to the limited wireless transmission range mentioned above, sensors have also scarce resource such as power capacity and computation capability. The forwarding of the data traffic from each sensor to the central data hub should take these limitations into consideration. The classical routing approach, which routes traffic through the smallest hop counts, shortest path routing, does not suit the wireless sensor mesh networks. Ultimately, we need to devise a routing mechanism that routes traffic efficiently within the constraint of transmission bandwidth, power capacity and computation capability. That is, the optimization for TIASN is essentially a traffic routing optimization problem.

In this chapter, we will firstly go through the state of the art in network routing problems; Secondly, we will give a formal definition for the optimal routing problems; Finally, we apply an interior point Newton’s method, which has a second-order convergence on convex optimization problems, to the traffic routing in TIASN network.

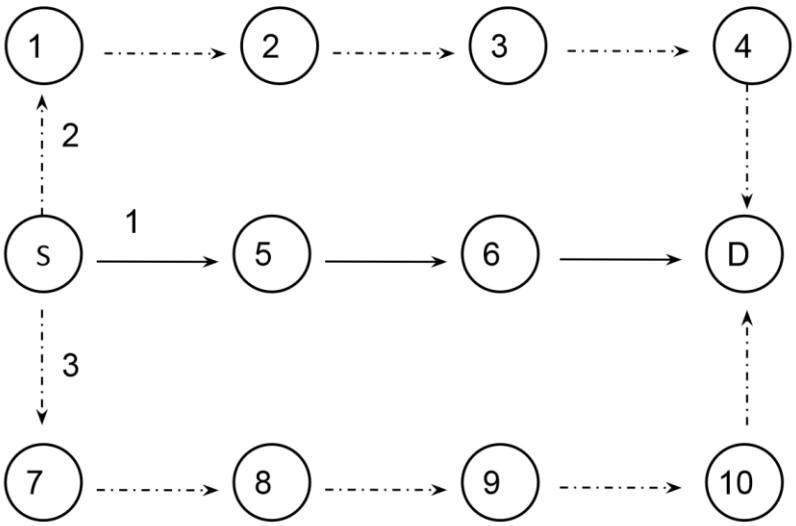

Fig. 4-1: The mesh view of the data traffic routing in TIASN

4.1. State of the Art

Traffic routing is the process of deciding the path of a data packet from source node to destination node among one or multiple potential paths. The goal of the routing task in TIASN is for the nodes to forward their data traffic from the source sensors where the sensing data is sampled to the central data hub where the sensing data is consumed. As in the example shown in figure 1, node S denotes the source sensor and node D denotes the central data hub or the destination node.

In classical shortest path routing, the traffic are routed through the path with the least hop counts between node S and node D, that is, path 1 in the figure. Existing shortest path routing protocols include RIP and OSPF for wired communications, and OLSR and AODV for wireless communications. These protocols are generally based on Dijkstra's algorithm or Bellman-Ford algorithm. They are dynamic and find the shortest available paths for any given communication pair.

However, it is possible that intermediate nodes in path 1 may have a heavy traffic, high interference or low in available bandwidth. Traffic may be routed through path 2 or 3 and is much more efficiently due to lighter traffic conditions despite their longer distance in hop counts. This is very much like going through motor way may reach the destination faster despite traveling a longer distance in vehicular traffic.

Of course, in reality, there might be much more potential paths between node S and node D. And the traffic on each node in a path may be dynamically changing. Therefore, the actual

optimal routing path should be determined in real time based on the traffic and the constraints of each node in the mesh network.

It is possible to formulate the routing problem as an optimization problem and applies a variation of gradient descent algorithm to solve the problem. The issue of doing so is the gradient descent algorithm is typically first order and converges to an optimal solution in a linear or sub-linear speed. In reality, it may take an extremely long time for such an optimization algorithm to reach to an acceptable solution that it is practically suboptimal.

4.2. Problem Formulation

In this section, we give a formal definition of the optimal routing problem in TIASN.

Firstly, we provide mathematical representation of the mesh network and the traffic in the network. A wireless mesh network *G={V,L}* is defined as a set of nodes (or sensors) V and a set of wireless links L. A communication pair w={s,d} consists of a source node where the road traffic information is sensed, and destination node d where the road traffic information is consumed. A path p⊂L is a set of connected links. Let P denote all potential paths in the network between any communication pair. Let Pw denote all paths between a communication pair w. That is Pw is a subset of P.

We denote the traffic demand for communication w as Tw. A data flow fp denotes the data payload that are transmitted over a path $p \in P_w$. The universe of fp,

$F = \{f_p | p \in P\}$, represents all traffic flows of a network. We call F a feasible solution to a routing task if for any w, $T_w = \sum_{p \in P_w} f_p$.

The data load $\bar{f_a}$ of node a, is the summation of all flows that run through it:

$$\bar{f_a} = \sum_{p \in P_w} \delta_{ap} f_p \quad (1)$$

Where

$$\delta_{ap} = \begin{cases} 0 & if\ a\ not\ \in p \\ 1 & if\ a \in p \end{cases}$$

We define N_a as the set of neighbours of node a, and accordingly define N_a as the neighbouring traffic of node a:

$$N_a = \sum_{x \in N_a} \bar{f_x}$$

Next, given a mesh network defined above, we need to define the optimality of the routing problem. There can be two ways of defining an optimality: cost minimization and utility maximization:

4.2.1. Optimality: Cost Minimization

Communication delay is a strong indicator of underlying transmission ability, interference and workload over a medium. Communication delay is a direct result of the transmission capacity of a node. When a node is under heavy usage, it incurs a high delay to the traffic that runs through it. In addition, in TIASN, the road traffic information needs to be communicated in a real-time fashion. Therefore, it is natural to use the delay of the network as the cost function that the optimal routing algorithm tries to minimize.

We define a latency function $l(\cdot)$ over one hop. It takes the data load of the medium as input. We assume the latency function to be convex increasing. We define the cost function over one node, Ca, as the latency experienced by all communications that run through the node.

$$C_a = l(\bar{f_a} + N_a)\bar{f_a}$$

The cost of a network is given accordingly.

$$C(F) = \sum_{a \in V} C_a$$

Given a network and the traffic demand, the objective of our solution, namely the network optimum, is to find a feasible F that minimizes the network cost.

$$\underset{F}{minimize}\ C(F) \tag{2a}$$

$$\text{s.t.} \sum_{p \in P_w} f_p = T_w \tag{2b}$$

$$F \geq 0 \tag{2c}$$

$$g(F)<C \tag{2d}$$

The equality constraint (2b) means that the traffic distributed along all possible routes sums to the traffic originated from the source, that is, to guarantee the feasibility of the solution. The inequality constraint (2d) is trivial in that there can be no negative traffic. The inequality constraint (2d) is called the capacity constraint. It is a set of constraints that are imposed by the network and device conditions.

The basic form of the capacity constraint can be given as:

$$RT \leq C_{NETWORK} \tag{3}$$

where R is the linear matrix that describes the connectivity among sensors, an example of this connectivity matrix is shown in Figure 4-2.

$C_{NETWORK}$ is the vector that represents the link capacity in communication bandwidth. It is also possible to add further inequality constraints to the capacity constraints, such the minimum battery life before a node can take any relays for other nodes. We use the general form (2d) to denote all potential inequality constraints relating to capacity.

$$\begin{cases} G_{1,1}x_1 + G_{1,2}x_2 + G_{1,3}x_3 + G_{1,4}x_4 = b_1 \\ G_{2,1}x_1 + G_{2,2}x_2 + G_{2,3}x_3 + G_{2,4}x_4 = b_2 \\ G_{3,1}x_1 + G_{3,2}x_2 + G_{3,3}x_3 + G_{3,4}x_4 = b_3 \\ G_{4,1}x_1 + G_{4,2}x_2 + G_{4,3}x_3 + G_{4,4}x_4 = b_4 \end{cases}$$

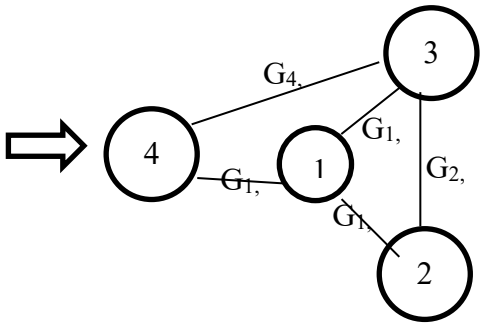

Fig. 4-2 Connectivity matrix

4.2.2. Optimality: Utility Maximization

In the previous section, we have chosen the communication delay as the objective function that the optimal routing algorithm to minimize. It is easily shown that using a cost as the objective function to minimize is mathematically equivalent to using a utility function as the objective function to maximize. The most trivial way of transforming a cost minimizing problem to a utility maximizing problem is to add a negative sign to the cost function and to maximize the negative of the cost function.

Since the maximizing and minimizing problems are equivalent, it can be beneficial to discuss a proper utility maximization that may be used in real world situation. For example, it is common to use traffic throughput of a mesh network as the utility function. The optimal solution to such a utility function is an optimal routing that achieves the most data throughput over a network. Another possible utility function that is suitable for mesh sensor networks is the battery life. The optimal solution to such a utility function is an optimal routing that achieves the long lifetime of a battery-powered mesh sensor network.

$$maximize \ \sum_{i=1}^{i=S} U_i(T_i) \tag{4}$$

T>0

g(F)<C

Here U is the utility function of each sensor. To represent a throughput maximization problem, U could be given as log (T); to represent battery life maximization problem, U could be given as log (P) where P is the set of the battery life of all sensors.

Note we apply logarithm function to the throughput or the battery life as the objective function. The motivation for this transformation is to make the optimization problem convex, which can be solved efficiently. It can be demonstrated that the application of the logarithm function does not impact the optimal solutions.

It has been demonstrated in previous work that the delay minimization problem (2) and (4) are both convex.

4.3. Interior Point Newton's Method

We can formulate the sensor network communication as follows:

$$maximize \ \sum_{i=1}^{i=S} U_i(T_i) \tag{5}$$

$$subject\ to\ RT \leq C$$

T>0

Here U is the utility function of each sensor and T is the traffic/request throughput across the sensor network. R is the linear matrix that describes the connectivity among sensors. With the help of auxiliary variables E such that RT +ε = C, the problem can be transformed into non-negative constraints and equality constraints. Applying the interior-point method, the problem becomes:

$$minimize\ y(x) = -\sum_{i=1}^{S} U_i(x_i) - \mu \sum_{i=1}^{S+L} \log\,(x_i) \tag{6}$$

Subject to Ax=C

where x={T,ε}, A={R,I}. This equality constrained problem can be addressed by iterative steps:

$$\begin{cases} \Delta x^{(t)} = -\nabla^2 y\left(x^{(t)}\right)^{-1}\left(\nabla y\left(x^{(t)}\right) + A^T v^{(t)}\right) & (7) \\ \left(A\nabla^2 y\left(x^{(t)}\right)^{-1} A^T\right) v^{(t)} = -A\nabla^2 y\left(x^{(t)}\right)^{-1} \nabla y\left(x^{(t)}\right) & (8) \end{cases}$$

Since the utility function $U_i(T_i)$; i = 1:::S is defined on each single-path communication, y(x) is separable with respect to each xi; i = 1:::S + L. Both$\nabla^2 y(x)$ and$\nabla^2 y(x)^{-1}$ are diagonal. The primal step (7) is separable therefore can be solved locally at each source node and each link, given the value of the dual variable $v^{(t)}$. However, the dual step (8) is not separable and cannot be directly addressed in a distributed manner. The major contribution of Wei's distributed Newton method is to apply a matrix splitting technique to solve the dual step distributivity. For the purpose of convenience, denote $G = A\nabla^2 y\left(x^{(t)}\right)^{-1} A^T$ and $b = -A\nabla^2 y\left(x^{(t)}\right)^{-1} \nabla y\left(x^{(t)}\right)$. The dual step (8) is written as

$$Gv^t = b$$

where G is a L × L matrix, $v^{(t)}$and b are both L ×1 vector.

Matrix splitting is a type of iterative method to solve the above equation system. It splits G = M + N and solves

$$M\tilde{v}^{(k+1)} = b - N\tilde{v}^{(k)} \tag{9}$$

If a matrix splitting approach converges, as $k \to \infty$, the value of $\tilde{v}^k$ approaches $\tilde{v}^{(k)}$, which is the solution of equation (8). In fact, the Jacobi method and the Gauss-Seidel method can be classified as matrix splitting approaches.

We propose to split G into three parts: 1) a diagonal matrix D with diagonal element $(D)_{i,i} = (G)_{i,i}$; 2) a residual matrix B = G - D; 3) a diagonal matrix $\bar{B}$ with diagonal element $\bar{B}_{i,i} = \sum_{j=1}^{L} (B)_{i,j}$ Therefore, we have

$$G = \underbrace{(D + \bar{B})}_{M} + \underbrace{(B - \bar{B})}_{N}$$

where $D + \bar{B}$ is diagonal.

It has been proved that as long as the matrix splitting approach converges to a certain neighbourhood of the solution to dual step, i.e. $v^{(t)} \pm \varepsilon$ for some small error ε, then the interior-point Newton's method converges quadratically to a neighbourhood of the network optimum.

The iterative algorithm that update the solution set can be given as follows:

Algorithm 1 Algorithm of the sensor utility maximization algorithm

Starting with an initial value $x^{(0)}$, $\mu = \mu^{(0)} > 0$, $0 < \gamma < 1$ and $\varepsilon > 0$ repeat:

1. Find the solution $\tilde{T}^*$ to the equality constrained problem (6) using Newton's method

2. Update the solution: T =$\tilde{T}^*$

3. Update the control scalar: $\mu = \gamma\mu$ until the stopping criterion is satisfied: mμ < ε

At the beginning, each sensor starts to transmit their sensing data through a predefined set of paths. As traffic are sent to the central data hub, feedback is sent back to the source nodes piggybacking the response messages. All nodes along the paths adjust their routing decisions based on the update mechanism given above for the second round of data transmission. This completes one iteration of the data transmission. It can be argued with a random starting point, this algorithm converges quadratically, that is, second order, towards an optimal routing solution.

4.4. Summary

In this chapter, we have formulated the optimal routing problem for communications in TIASN. We have demonstrated it is possible to structure the problem as an optimization problem with convexity property. We can use either communication delay or traffic throughput as the objective function to optimize. The constraints in wireless mesh network, such as the network capacity or battery life limitations, can all be worked into the equality and inequality constraints of the optimization problems. Finally, we have applied the latest research in convex optimization theory, that is, the interior point Newton's method to convex optimization problem. Such an optimization algorithm will converge to an optimal routing solution quadratically, which is superior than the common well-known gradient descent algorithms suite.

5. Auto-Calibration of Tri-axial Accelerometers within an IMU

5.1. Calibration of TAs

In order to improve the efficiency of IMU based traffic monitoring, this thesis investigates the calibration and its associated experimental design schemes for the two-key tri-axial sensors in an Inertial Measurement Unit (IMU), tri-axial magnetometers and tri-axial accelerometers. For the commonly used 9-parameter models, we adopted a 12-observation rotatable G-optimal experimental scheme. Based on our previously proposed linearization approach, we linearized both the 9-parameter tri-axial accelerometers and magnetometers and the parameters of both two sensors can be simultaneously identified with acceptable accuracy. We also proposed two other experimental schemes and investigated their efficiency based on the analysis of their information matrices.

The rapid development of Micro Electro Mechanical Systems (MEMS) technology enables the size reduction of the chip-based inertial sensors (e.g. Tri-axial Accelerometers (TAs), Tri-axial Magnetometers (TMs), tri-axial gyroscopes, and inertial measurement units (IMUs)). Furthermore, the recently manufactured MEMS sensors and devices are often inexpensive, lightweight, and low power consumption, which motivated their applications in traffic monitoring [108-109]. However, due to the mechanics of their fabrication MEMS internal sensors often have relatively large bias instability and high noise levels; regular calibrations are necessary to ensure the accuracy of their measurement. Unfortunately, for the users of traffic monitoring, the available calibration equipment is often hard to achieve comparable accuracy of sensor calibration performed in a laboratory environment.

Auto-calibration method [110-112] is recently developed to calibrate the MEMS TAs. Although the auto-calibration method is especially suitable for in-field calibration, the quality of the calibration has not received the attention they deserve. In this thesis, the classical Experimental design (DoE) theory [113-115] will be applied to generate experiment schemes for the auto calibration of TAs in order to improve the quality of auto-calibration method.

DoE theory investigates the optimal selection or design of an appropriate input signal to stimulate the system significantly in order to extract the maximum system information under limited number of experiments with physical even constraints. The DoE of traditional accelerometer calibration problem can be addressed by using the well-established DoE theory [116-123]. The key step in experimental design is the calculation and analysis of the Fisher Information Matrix (FIM), which is related to this classical parameter estimation problem. Later, the optimal experimental design may be achieved by maximizing or minimizing a certain index

of FIM. Such an index is often defined in various ways, which lead to several famous design schemes, e.g., D-optimal, E-optimal, ED-optimal[124-125], G-optimal [122-123], and Ds-optimal [126-127] design. Because D-optimality is independent with parameter transformation[122-123], it is often the first choice. In terms of minimization of variance functions, G-optimality is often the most appropriate selection [128].

In this section, we derived one 14-points experimental plan based on Central Composite design (CCD) and two 12-points design from Box–Behnken design (BBD) and Icosahedron design for the most commonly used 6-parameter and 9-parameter models [129-130]. In this study, we also experimentally investigate these two models in terms of mean square error (MSE) when auto-calibration approach is utilized.

For a classical TA calibration, it requires an ideal orientation of the TA along a predetermined direction. In a non-laboratory environment, it is often difficult to implement the design on-site by users of infield traffic monitoring.

To assess the quality of a specific experiment ξ, in our previous studies [133], we provide the following index D-efficiency to evaluate the quality of a particular experiment [134-135]:

$$D_{eff} = \Phi(M(\xi)) / \Phi(M(\xi^*)) \tag{1}$$

where ξ^* and ξ stand for the designed optimal experiment (e.g. BBD/CCD) and a specific experiment respectively, $M(\cdot) \in \mathrm{M}$ is the Fisher Information Matrix (FIM) of an experiment which belongs to the compact set M, and $\Phi(\cdot)$ is the index or criterion function which is often a convex real function on M non-increasing. D-optimality is one of the most commonly used criterion [134-135] which maximizes the determinant of the FIM, in particular,

$$\Phi[M(\xi)] = |M|^{-\frac{1}{m}} \tag{2}$$

Another quality of the evaluation experiment is G-optimality, which aims to minimize the maximum value of the prediction variance:

$$v(x) = \min_{\xi}\left[\max_{m \in R}\left\{n_y x^{(m)T} \Phi\left[M(\xi)\right] x^{(m)}\right\}\right] \tag{3}$$

where $x^{(m)}$ represents model matrix, and n_y is the number of parameters to be identified.

The organization of this study is as follows. The next section will introduce the proposed three experimental plans. In Section 3, we will introduce the experimental results. Section 4 provides conclusions.

5.2. The proposed experimental plans

Classically, accelerometer calibration has been performed in a laboratory environment. In such an environment, the axes can be precisely oriented, so each axis can be individually calibrated [136].

Generally, it can be assumed the model of an accelerometer (or a magnetometer) can be written as a standard second-degree model as follows:

$$y = \beta_0 + \sum_{i=1}^{k} \beta_i x_i + \sum\sum_{i<j} \beta_{ij} x_i x_j + \sum_{i=1}^{k} \beta_{ii} x_i^2 + \varepsilon \tag{4}$$

where $x_1, x_2, \Lambda\ x_k$ are a number of associated control or input variable (the input accelerations in each axis), β_i (β_{ij}) are the unknown coefficients, called as parameters here, and ε is a random experimental error.

Assume a set of n experiment points have been executed. Then, the matrix form of the experiment can be expressed as follows:

$$Y = X\mathrm{B} + \bar{\varepsilon} \tag{5}$$

where $\mathrm{B} \in R^{p\times 1}$ is the vector of the unknown parameters, $Y \in R^{n\times 1}$ is the vector of measurements, the matrix $X \in R^{n\times p}$ is generated by the input signals, and $\bar{\varepsilon} \in R^{n\times 1}$ is the vector of random experiment error.

If we assume that the vector $\bar{\varepsilon} \in R^{n\times 1}$ has a zero mean and a variance-covariance matrix $\sigma^2 I$, the ordinary least-squares (OLS) estimation of $\mathrm{B} \in R^{p\times 1}$ is:

$$\hat{\mathrm{B}} = (X^T X)^{-1} X^T Y \tag{6}$$

The variance matrix of $\hat{\mathrm{B}}$ is then of the form:

$$Var(\hat{\mathrm{B}}) = (X^T X)^{-1} \sigma^2 \tag{7}$$

The variance of $\hat{y}(x)$ is of the form:

$$Var\left(\hat{y}(x)\right) = \sigma^2 x^{(m)T} \left(X^T X\right)^{-1} x^{(m)} \tag{8}$$

The experimental design of classical accelerometer calibration is a linear DoE problem, for which several optimal experimental schemes have been developed [136]. These schemes are designed to enable the FIM matrix, $X^T X$, to fulfil various desired properties such as rotatability, orthogonality, G-optimality and D-optimality.

The auto-calibration is based on the simple fact that the acceleration measured by the 3-axis accelerometer should be equal to the local gravitational acceleration, "1g", under static conditions. The basic rule of automatic calibration is:

$$g = \sqrt{a_x^2 + a_y^2 + a_z^2}$$

A 6-parameters model [129-130] has the following form:

$$\begin{cases} a_x = S_{xx} \cdot (V_x + O_x) \\ a_y = S_{yy} \cdot (V_y + O_y) \\ a_z = S_{zz} \cdot (V_z + O_z) \end{cases} \tag{9}$$

where S_{jj} is sensitivity of each direction, $O_j$is the offset, and V_j is the ADC values that obtained from the μ-IMU. It can be seen that the model (9) cannot be written in the form of equation (4) because it is non-linear for the parameter to be estimated. Thus, classical experimental protocols cannot be directly applied to automatic calibration. However, by using the linearization strategies proposed previously, e.g., [133], the nonlinear model (9) can be locally linearized and transformed in the form of equation (4), and the unknown parameters can estimate recursively. After some modifications of the equation, the experimental design is linear, and linear DoE methods can be applied.

For the auto-calibration model of 6 parameters, we have

$$g^2 = a_x^2 + a_y^2 + a_z^2 + \varepsilon$$

$$= \left[S_{xx} \cdot (V_x + O_x)\right]^2 + \left[S_{yy} \cdot (V_y + O_y)\right]^2 + \left[S_{zz} \cdot (V_z + O_z)\right]^2 + \varepsilon$$

For the equation above, with a pre-calibration for offset, the remaining offset O_x^2, O_y^2 and O_z^2 will be quite small with respect to input signal V_z^2, V_y^2 and V_z^2. In this case, neglecting the items containing O_x^2, O_y^2 and O_z^2, the unknown parameters can be estimated with acceptable accuracy based on the remaining parts of the equation. Finally, we will recursively estimate the neglected items, and show that the estimation will finally converge to the desired values.

We now analyse the equation above after neglecting O_x^2, O_y^2 and O_z^2.

$$g^2 \approx S_{xx}^2 V_x^2 + S_{yy}^2 V_y^2 + S_{zz}^2 V_z^2 + 2S_{xx}^2 V_x O_x + 2S_{yy}^2 V_y O_y + 2S_{zz}^2 V_z O_z + \varepsilon \quad (10)$$

If we let $S_{xx}^2 = \beta_{11}$, $S_{yy}^2 = \beta_{22}$, $S_{zz}^2 = \beta_{33}$, $2S_{xx}^2 O_x = \beta_1$, $2S_{yy}^2 O_y = \beta_2$, $2S_{zz}^2 O_z = \beta_3$, $V_x = V_1$, $V_y = V_2$ and $V_z = V_3$.

Equation (9) can be present as:

$$y = \beta_1 \mathrm{V}_1 + \beta_2 \mathrm{V}_2 + \beta_3 \mathrm{V}_3 + \beta_{11} \mathrm{V}_1^2 + \beta_{22} \mathrm{V}_2^2 + \beta_{33} \mathrm{V}_3^2 + \varepsilon$$

This can be simplified as:

$$y = \sum_{i=1}^{3} \beta_i \mathrm{V}_\mathrm{i} + \sum_{i=1}^{3} \beta_{ii} \mathrm{V}_\mathrm{i}^2 + \varepsilon$$

Since V_i is input signal, the equation is now a linear equation about unknown parameter β_i. Assume, we have N set of experiments. Applying linear least square method for the tri-axial model above

$$\hat{B} = (X^T X)^{-1} X^T Y$$

Where, $X = [\bar{V}_1, \bar{V}_2, \bar{V}_3, \bar{V}_1^2, \bar{V}_2^2, \bar{V}_3^2]$,
$\bar{V}_i = [V_{i1}, V_{i2}, \dots, V_{iN}]^T$,

$$\bar{V}_i^2 = \left[V_{i1}^2, V_{i2}^2, \dots, V_{iN}^2\right]^T,$$

$$(i = 1,2,3),$$

and

$$\hat{B} = \left[\hat{\beta}_1, \hat{\beta}_2, \hat{\beta}_3, \hat{\beta}_{11}, \hat{\beta}_{22}, \hat{\beta}_{33}\right]^T$$

Based on linear least square method, the factor β_i and β_{ii} can be evaluated. With β_i and $S^2 = \beta$ which we defined above, the parameters of sensitive S can be estimated. After that, with β_{ii}, $S_{xx,yy,zz}$ and $2S^2 O = \beta$, the offset O can be obtained. So, the 6 unknown parameters have been solved. It has to be noticed that β_i and β_{ii} are not independent. For example, β_{11} and β_1 include common term $\mathrm{S}_{\mathrm{xx}}^2$ from the definition above. Another important condition here is that a pre-calibration is necessary not only to neglect offset O but also to decide the polarity of S.

For the 9 parameters TAs model, we extend 6-parameters model discussed above to 9-parameters model [129][142-143]. After simplification and comparison, the 9-parameters

model also does not include β_0 term, so the measurements of center point are unnecessary in this experiment plan.

For auto-Calibration model of 9 parameters [129] [142-143]:

$$g^2 = a_x^2 + a_y^2 + a_z^2$$

$$\begin{aligned}
&= \left[S_{xx} \cdot (V_x + O_x) + S_{xy} \cdot (V_y + O_y) + S_{xz} \cdot (V_z + O_z) \right]^2 \\
&+ \left[S_{xy} \cdot (V_x + O_x) + S_{yy} \cdot (V_y + O_y) + S_{yz} \cdot (V_z + O_z) \right]^2 \\
&+ \left[S_{xz} \cdot (V_x + O_x) + S_{yz} \cdot (V_y + O_y) + S_{zz} \cdot (V_z + O_z) \right]^2
\end{aligned}$$

For this 9-parameter model, if we replace x, y, z with 1, 2, 3, this equation can be expanded as:

$$\begin{aligned}
&= \sum_{i=1}^{3} S_{ii}^2 \cdot (V_i + O_i)^2 + 2 \sum_{i=1} \sum_{j \neq i} S_{ij}^2 \cdot (V_j + O_j)^2 \\
&+ 2 \sum_{i=1} \sum_{j \neq i} S_{ij} \cdot S_{jj} \cdot (V_i V_i + V_i O_j + V_j O_i + O_i O_j) \\
&+ 2 \sum_{i=1} \sum_{j \neq i} \sum_{k \neq i, k \neq j} S_{ij} \cdot S_{ik} \cdot (V_j V_k + V_j O_k + V_k O_j + O_j O_k)
\end{aligned}$$

This equation above contains four items. The first item is actually the equation of 6 parameters model. For the second and forth terms, the S_{ij} and S_{ik} represents the un-orthogonal between each axis which is very small compare to S_{ii}. In this case, S_{ij}^2 and $S_{ij} \cdot S_{ik}$ will be extremely small which means the second and forth terms can be also neglect. The neglected items will be estimated and compensated iteratively.

The remaining part of the equation after the simplification can be representing as:

$$\begin{aligned}
g^2 \approx\ & S_{xx}^2 V_x^2 + 2 S_{xx}^2 V_x O_x + S_{yy}^2 V_y^2 + 2 S_{yy}^2 V_y O_y + S_{zz}^2 V_z^2 + 2 S_{zz}^2 V_z O_z \\
& + 2 (S_{xx} + S_{yy}) S_{xy} V_x V_y + 2 (S_{xx} + S_{zz}) S_{xz} V_x V_z + 2 (S_{yy} + S_{zz}) S_{yz} V_y V_z
\end{aligned}$$

Based on 6 parameter model and then define

$$\begin{cases}
2 (S_{xx} + S_{yy}) S_{xy} = \beta_{12} \\
2 (S_{xx} + S_{zz}) S_{xz} = \beta_{13} \\
2 (S_{yy} + S_{zz}) S_{yz} = \beta_{23}
\end{cases}$$

Equation (2) above can be written as:

$$\begin{aligned}
y =\ & \beta_1 V_1 + \beta_2 V_2 + \beta_3 V_3 + \beta_{11} V_1^2 + \beta_{22} V_2^2 + \beta_{33} V_3^2 \\
& + \beta_{12} V_1 V_2 + \beta_{13} V_1 V_3 + \beta_{23} V_2 V_3 + \varepsilon
\end{aligned}$$

The above equation can be simplified as:

$$y = \sum_{i=1}^{3} \beta_i V_i + \sum_{i=1}^{3} \beta_{ii} V_i^2 + \sum_{i<j} \sum \beta_{ij} V_i V_j + \varepsilon$$

Again, the parameters can be estimated based on linear least square method as we discussed for the estimation of 6-parameter model. We will later show that the estimated parameters will approach to real value after regression.

Based on the study of the response surface methodology [131-132], we found well developed two types of optimal experimental method which is suitable for the calibration of Tri-axial Accelerometers model. One is Central Composite Design (CCD); the other is Box-Behnken Design (BBD). Generally speaking, central composite design and Box-Behnken Design are designed to reach the desired orthogonality, rotatability, and D-optimality as discussed in[139]. In this study, beside revised BBD and CCD, we will also discuss an Icosahedron design which is more suitable for this specific model.

A. Central Composite Design (CCD)

Central Composite Design is one of the most popular response surface methodologies when building a second-degree model. It can be used to estimate curvature based on the measurement value from fractional factorial points, axial points and centre points [140].

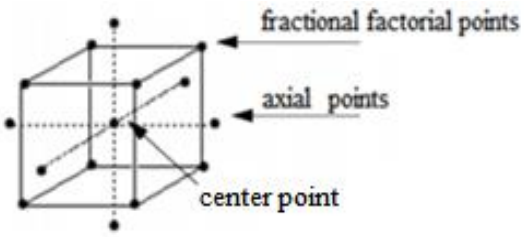

Fig. 5-1 The general structure of three factors CCD

Before applying Central Composite Design, the linearized model of the TAs should be comparing with general three factors quadratic model. The general three factors quadratic model is:

$$\begin{aligned} \mathrm{y} = {} & b_0 + b_1 x_1 + b_2 x_2 + b_3 x_3 + b_{12} x_1 x_2 + b_{13} x_1 x_3 + b_{23} x_2 x_3 \\ & + b_{11} x_1^2 + b_{22} x_2^2 + b_{33} x_3^3 \end{aligned}$$

Normally, Central Composite Design for three factors of second degree system includes 20 runs (or points)[140]. Six runs are for centre points, 8 runs for 8 fractional factorial points, and 6 runs for 6 axial points.

For this experiment design, orthogonal information matrix is expected. But due to the limitation of central composite design and our specific model, the information matrix includes a 3×3 block matrix in the middle for 6 parameters model. For 9-parameters models, the estimation of 6 joint parameters can be independent from each other. The rest 3 joint parameters are dependent as the information matrix is only block diagonal.

As the auto-calibration requires calibrating three axes at the same time, the value of axial points cannot select as $2^{\frac{3}{4}}$. Besides this, the center points cannot be pursued due to the constraint. Compare to classic CCD, center points have to be removed and the value of axial points should be modified to a suitable value. Table 5-1 shows the new proposed CCD design. We replace the 1 in the classic CCD with the actual gravity projected on each axis, and we reuse it for BBD and Icosahedron designs. In this case, three different designs will share the same unit and can be applied to analytical criteria such as D-optimality or G-optimality.

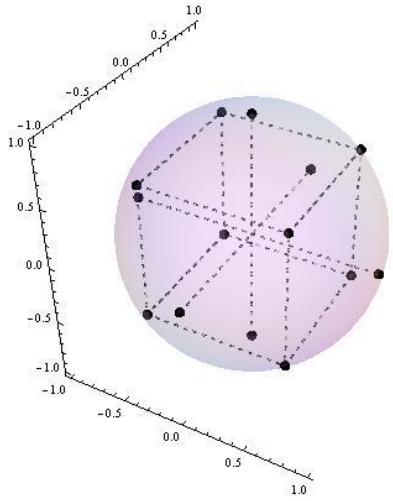

Fig. 5-2 The structure of CCD for TAs models

Table 5-1 Three factors central composite design for Tri-axial accelerometer models

Point	A	B	C
1	$-\sqrt{3}/3$	$-\sqrt{3}/3$	$-\sqrt{3}/3$
2	$\sqrt{3}/3$	$-\sqrt{3}/3$	$-\sqrt{3}/3$

3	$-\sqrt{3}/3$	$\sqrt{3}/3$	$-\sqrt{3}/3$
4	$\sqrt{3}/3$	$\sqrt{3}/3$	$-\sqrt{3}/3$
5	$-\sqrt{3}/3$	$-\sqrt{3}/3$	$\sqrt{3}/3$
6	$\sqrt{3}/3$	$-\sqrt{3}/3$	$\sqrt{3}/3$
7	$-\sqrt{3}/3$	$\sqrt{3}/3$	$\sqrt{3}/3$
8	$\sqrt{3}/3$	$\sqrt{3}/3$	$\sqrt{3}/3$
9	-1	0	0
10	1	0	0
11	0	-1	0
12	0	1	0
13	0	0	-1
14	0	0	1

In this modified CCD, 14 points of experiment requires different arrange of Teas' Points 1 to 8 represent fractional factorial points while points 9 to 14 represent axial points. In order to achieve the requirements of run 1, the gravity should be equally projected along three axes. Consider θ_i ($i \in \{x, y, z\}$) as tilt angle between three axes and gravity. θ_i is equal to $54.74°$ according to geometry (see Figure 2). Based on the same theory, for run 2, the tilt angle θ_x(between x-axis and gravity) is equal 125.26°. Actually, run 3 to 9 are similar to run 1 and run 2 only with different rotation sequence.

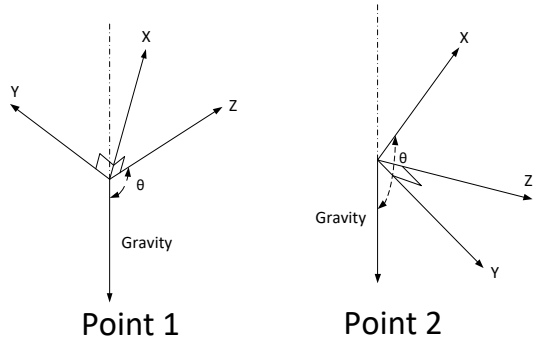

Fig. 5-3 Demonstration of Point 1 and Point 2

For point 9 to point 14, it is designing to measure axial points. In order to achieve it, keep two axes perpendicular to gravity to minimize the influence from gravity while the third axis on the same direction of gravity (or on the opposite direction). Figure 3 below demonstrate the arrangement of points 9, 10, 13 and 14.

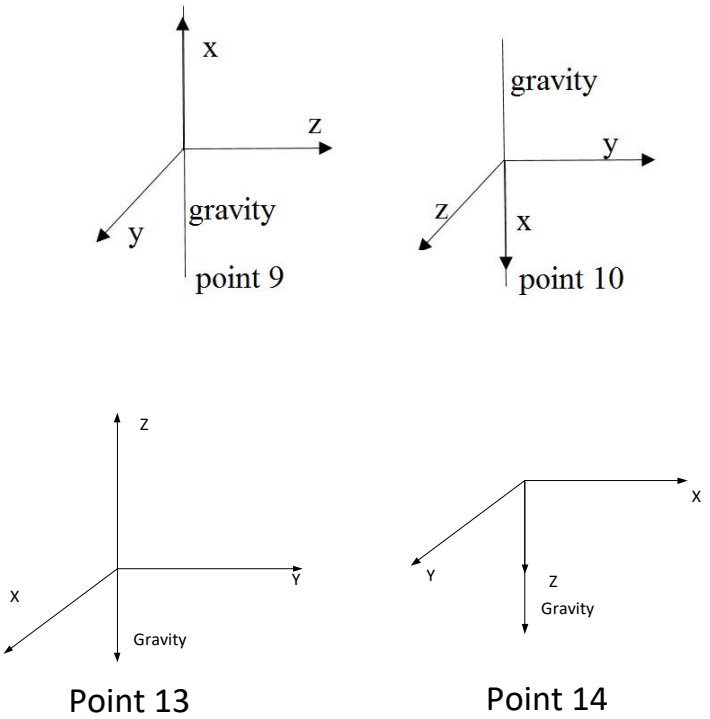

Fig. 5-4 Demonstration of points 9, 10, 13, and 14

Based on the above discussions, three new symbols A, B and C are defined as follows and these definitions are also applied in BBD and Icosahedron Design:

$$\mathrm{A} = \cos\theta_x$$
$$\mathrm{B} = \cos\theta_y$$
$$\mathrm{C} = \cos\theta_z$$

- θ_x: tilt angle between x and gravity
- θ_y: tilt angle between x and gravity
- θ_z: tilt angle between x and gravity

Table 5-2 Tilt angle of teach point to fit in CCD

Point	θ_x	θ_y	θ_z
1	125.26°	125.26°	125.26°

2	54.74°	125.26°	125.26°
3	125.26°	54.74°	125.26°
4	54.74°	54.74°	125.26°
5	125.26°	125.26°	54.74°
6	54.74°	125.26°	54.74°
7	125.26°	54.74°	54.74°
8	54.74°	54.74°	54.74°
9	180°	90°	90°
10	0°	90°	90°
11	90°	180°	90°
12	90°	0°	90°
13	90°	90°	180°
14	90°	90°	0°

B. Box-Behnken Design (BBD)

Box-Behnken Design is another commonly used response surface methodology. It is focused on midpoints of edges of the process space and at the centre [141]. Compare to central composite design, Box-Behnken design are normally less expensive due to the less points required of Box Behnken Design[140].

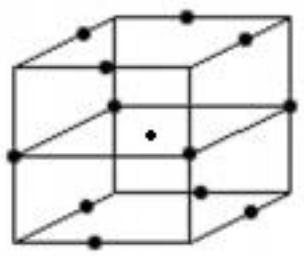

Fig. 5-5 The general structure of 3 factors BBD

Normally, Box-Behnken design requires 15 runs for a three factors second degree system model [140]. 12 runs are for 12 midpoints and 3 runs for centre points. However, due to the limitation of gravity-based calibration and the structure of the TAs model, 3 runs for centre points cannot be pursued. The modified BBD will be reduced to 12 points.

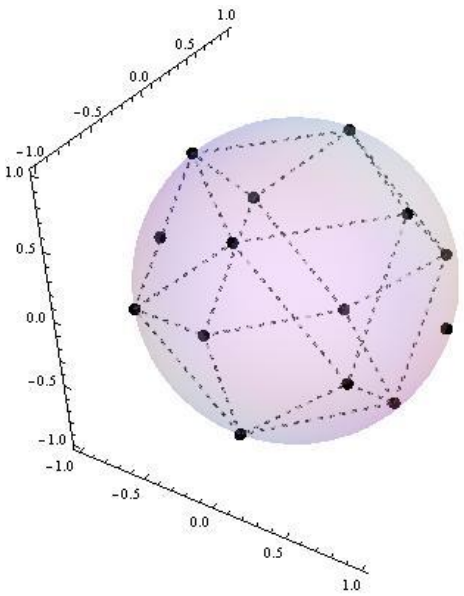

Fig. 5-6 The structure of BBD for TAs models

Table 5-3 Three factors Box-Behnken design for Tri-axial accelerometer model

Point	A	B	C
1	$-\sqrt{2}/2$	$-\sqrt{2}/2$	0
2	$\sqrt{2}/2$	$-\sqrt{2}/2$	0
3	$-\sqrt{2}/2$	$\sqrt{2}/2$	0
4	$\sqrt{2}/2$	$\sqrt{2}/2$	0
5	$-\sqrt{2}/2$	0	$-\sqrt{2}/2$
6	$\sqrt{2}/2$	0	$-\sqrt{2}/2$
7	$-\sqrt{2}/2$	0	$\sqrt{2}/2$
8	$\sqrt{2}/2$	0	$\sqrt{2}/2$
9	0	$-\sqrt{2}/2$	$-\sqrt{2}/2$
10	0	$\sqrt{2}/2$	$-\sqrt{2}/2$
11	0	$-\sqrt{2}/2$	$\sqrt{2}/2$
12	0	$\sqrt{2}/2$	$\sqrt{2}/2$

In Table 5-3, point 1 to point 4 can be arranged as shown in Figure 5-7

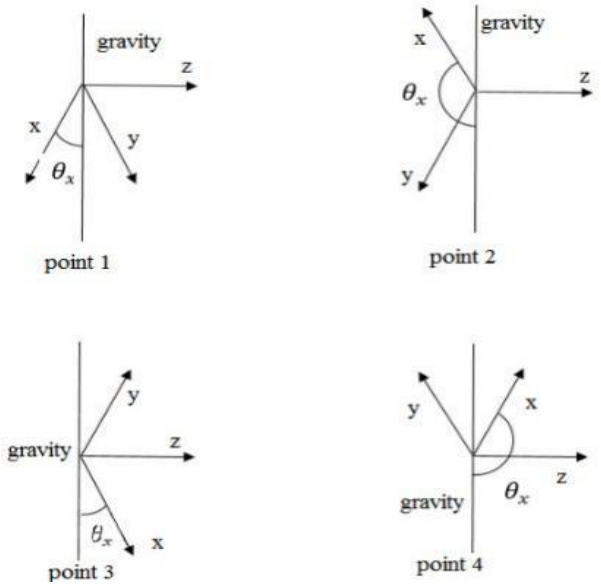

Fig. 5-7. Demonstration of Points 1 to 4

Point 5 to point 12 are similar.

Table 5-4 Tilt angle of each point to fit in BBD

Point	θ_x	θ_y	θ_z
1	45°	45°	90°
2	135°	45°	90°
3	45°	135°	90°
4	135°	135°	90°
5	45°	90°	45°
6	135°	90°	45°
7	45°	90°	90°
8	135°	90°	90°
9	90°	45°	45°
10	90°	135°	45°
11	90°	45°	135°
12	90°	135°	135°

C. Lcosahedron Design

Lcosahedron experiment design is a 12-points space filling design which aiming for the uniformly distribute of experiment points on experimental domains for 6 and 9 parameters TAs models. The idea of Icosahedron design is coming for uniform design.

Due to the constraint of the tri-axial accelerometer model, all the experiment points will be located on the surface of a sphere whose radius equals to the local gravity. Furthermore, these 12 points will construct an Icosahedron whose radius of its circumcircle will be gravity

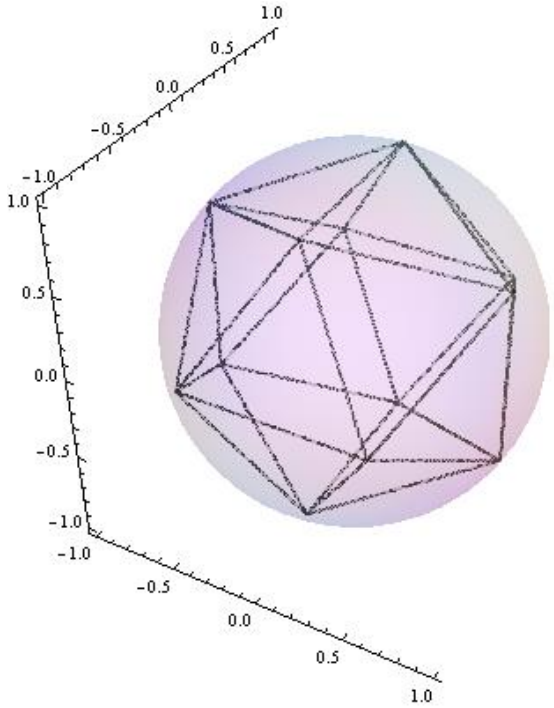

Fig. 5-8 The structure of Icosahedron design for TAs models

For Icosahedron design, if the radius of its circumcircle is 1, the 12 points can be placed as Table 5-5 where assume $a = \sqrt{\frac{2}{5+\sqrt{5}}}$, $= \frac{1+\sqrt{5}}{\sqrt{10+2\sqrt{5}}}$.

Table 5-5 Three factors Icosahedron design for Tri-axial accelerometer model

Point	A	B	C
1	0	$-a$	$-b$
2	0	a	$-b$
3	0	$-a$	b

4	0	a	b
5	$-a$	$-b$	0
6	a	$-b$	0
7	$-a$	b	0
8	a	b	0
9	$-b$	0	$-a$
10	b	0	$-a$
11	-b	0	a
12	b	0	a

The arrangement of Icosahedron design is similar to BBD which will not be presented again. And the definition of A, B and C are the same as CCD and BBD. So, Table 5-6 presents the tilt angle of each point to fit uniform design.

Table 5-6 Tilt angle of each point to fit in Icosahedron Design

Point	θ_x	θ_y	θ_z
1	90°	148.3°	121.7°
2	90°	31.7°	121.7°
3	90°	148.3°	58.3°
4	90°	31.7°	58.3°
5	148.3°	121.7°	90°
6	31.7°	121.7°	90°
7	148.3°	58.3°	90°
8	31.7°	58.3°	90°
9	121.7°	90°	148.3°
10	58.3°	90°	148.3°
11	121.7°	90°	31.7°
12	58.3°	90°	31.7°

Orthogonality:

The information matrixes for all three type of experiment designs in both 6 and 9 parameter model are not fully orthogonal. In fact, they are block orthogonal matrix which shares the same format.

For 6 parameters model:

$$y = \sum_{i=1}^{3} \beta_i \mathrm{V_i} + \sum_{i=1}^{3} \beta_{ii} \mathrm{V_i}^2 + \varepsilon \,,$$

$$Y = XB \,.$$

Where,

$X = [\bar{V}_1, \bar{V}_2, \bar{V}_3, \bar{V}_1{}^2, \bar{V}_2{}^2, \bar{V}_3{}^2]$,

$$\bar{V}_i = [V_{i1}, V_{i2}, \dots, V_{iN}]^T,$$

$$\bar{V}_i{}^2 = \left[V_{i1}^2, V_{i2}^2, \dots, V_{iN}^2\right]^T,$$

$(i = 1,2,3)$,

and

$$B = \left[\beta_1, \quad \beta_2, \quad \beta_3, \quad \beta_{11}, \quad \beta_{22}, \quad \beta_{33}\right]^{\mathrm{T}}.$$

As it is mentioned above, the FIMs share the same format. It is block orthogonal, and the FIM is shown below.

Information matrix for 6 parameter model:

$$\left[\begin{array}{ccc|ccc} X_{11} & & & & & \\ & X_{22} & & & & \\ & & X_{33} & & & \\ \hline & & & X_{44} & X_{45} & X_{46} \\ & & & X_{54} & X_{55} & X_{56} \\ & & & X_{64} & X_{65} & X_{66} \end{array}\right].$$

For 9 parameter model,

$$y = \sum_{i=1}^{3} \beta_i V_i + \sum_{i=1}^{3} \beta_{ii} V_i^2 + \sum_{i<j} \sum \beta_{ij} V_i V_j + \varepsilon \,,$$

$$Y = XB\ ,$$

Where $B = [\beta_1,\ \beta_2,\ \beta_3,\ \beta_{11},\ \beta_{22},\ \beta_{33},\ \beta_{12},\ \beta_{13},\ \beta_{23}]^{\mathrm{T}}$.

$X = [\bar{V}_1, \bar{V}_2, \bar{V}_3, \bar{V}_1{}^{:2}, \bar{V}_2{}^{:2}, \bar{V}_3{}^{:2}, \bar{V}_1.\bar{V}_2, \bar{V}_1.\bar{V}_3, \bar{V}_2.\bar{V}_3]$,

$$\bar{V}_i = [V_{i1}, V_{i2}, \dots, V_{iN}]^T,$$

$$\bar{V}_i{}^{:2} = \left[V_{i1}^2, V_{i2}^2, \dots, V_{iN}^2\right]^T,$$

$(i = 1,2,3)$.

Information matrix for 9 parameter model is as follows:

$$\begin{bmatrix} X_{11} & & & & & & & & \\ & X_{22} & & & & & & & \\ & & X_{33} & & & & & & \\ & & & X_{44} & X_{45} & X_{46} & & & \\ & & & X_{54} & X_{55} & X_{56} & & & \\ & & & X_{64} & X_{65} & X_{66} & & & \\ & & & & & & X_{77} & & \\ & & & & & & & X_{88} & \\ & & & & & & & & X_{99} \end{bmatrix}.$$

It has to be noticed that after the linearization of the non-linear model of tri-axis accelerometer, we use first order variables β to replace second order variables in original model. So even the matrix is block orthogonal, the original unknown parameters are still not independent.

D-optimality:

One target design characteristic of experiment design is D-optimality. The criterion of D-optimality is to maximize the determinant of information matrix (FIM). This aims to the minimization of the size of the confidence ellipsoid for the vector B in equation (4).

According to [139], both original CCD and BBD for 3 factors are not truly D-optimal, but rather D-best. Our modified CCD and BBD do not include the runs for constant terms in full factor second order model. So, the D-optimality will be slighter different from original designs.

Table 5-7 Determinant of fims for three proposed designs

	6 parameter Model	9 Parameter Model
14 Point CCD	1897	1334
12 Point BBD	256	256
12 Point ID	655.38	335.54

Consider two experiments with the same number of points. It is easy to tell that the experiments with larger $\det(X^T X)$ is better. However, this comparison of determinants cannot be applied to experiments with different number of n directly. In order to solve this problem, a matrix called matrix of moments [128] is defined to evaluate the influence of number of runs in experiments when comparing determinant:

Matrix of moments: $M = \left(X^T X\right)/n$.

Now the determinant of matrix of moments will be compared for three designs proposed above.

Table 5-8 Determinant of matrix of moments for three proposed design

	6 parameter Model	9 Parameter Model
14 Point CCD	2.52×10^{-4}	6.45×10^{-8}
12 Point BBD	8.57×10^{-5}	4.96×10^{-8}
12 Point ID	2.19×10^{-4}	6.50×10^{-8}

It is difficult to determine whether the determinant of the information matrix is the largest or not directly. Kiefer developed a continuous counterpart of G optimality criterion and showed that it is equivalent to the continuous D-optimality criterion [144].

Based on the analysis above, we can propose a theorem about the Icosahedron design.

Assumption 1: Assume that:

a. A model represents as equation below:

$$f(x) = \sum_{i=1}^{3} \beta_i x_i + \sum_{i=1}^{3} \beta_{ii} x_i^{\,2} + \sum_{i<j} \sum \beta_{ij} x_i x_j$$

b. $f(\mathrm{x})$ are continuous function in $X, f \in R^m$;

c. $\psi(M)$ is a convex function;

d. $\sum_{i=1}^{3} x_i^2 = 1$.

Theorem 1 [133**]** Under Assumption 1, then the Icosahedron design for $f(\mathrm{x})$ is D-optimal.

Proof:

According to Theorem 2 below, Icosahedron design for $f(\mathrm{x})$ is G-optimal. With the assumptions, the following equation:

$$\max_{\xi} \det\left(X^T X\right)$$

$$\min_{\xi}\left[\max_{m\in R}\left\{n_y x^{(m)T}\left(X^T X\right)^{-1} x^{(m)}\right\}\right]$$

are equivalent [144]. Generally, it means under specific condition, G-optimal is equivalent to D-optimal

In Theorem 2, Icosahedron design will be proved as a G-optimal design for model $f(\mathrm{x})$. Subsequently, Icosahedron design is D-optimal design for model $f(\mathrm{x})$.

Based on this theory, the Icosahedron design proposed above for 9 parameters is D-optimal for our constrained 3 factors 12-run experiment designs. Since the Icosahedron design we proposed is D-optimal for this specific condition, equation (1) and (2) can be applied to evaluate the specific experiment. In this thesis, the modified BBD is also 3 factors 12 run design. It is not D-optimal compare to Icosahedron design. The D-efficiency of BBD is 97.78% for 9 parameter model. This result indicates that BBD is also a very good experiment for 9-parameter model.

G-optimality:

G-optimal design is seeking to minimize the maximum value of the prediction variance in Eq. (3) over the experiment region. G-optimal is an important measurement of performance which indicates good prediction of output throughout the design region. Clearly, one disadvantage of G-optimal is that G-optimal is depending on the location of x instead of a single number.

Now, we introduce Theorem 2 related with G-optimality of the proposed Icosahedron design.

Theorem 2 [133**]** Under Assumption 1, the Icosahedron design is G-optimal for $f(\mathrm{x})$.

Proof:

Recall Eq. (8)

$$Var\left(\hat{y}(x)\right) = \sigma^2 x^{(m)T}\left(X^T X\right)^{-1} x^{(m)}.$$

The scaled prediction variance is defined as:

$$v(x) = \frac{n_y Var\left(\hat{y}(x)\right)}{\sigma^2} = n_y x^{(m)T} \left(X'X\right)^{-1} x^{(m)} \quad (11)$$

Where n_y represents the number of runs and $x^{(m)}$ represents location in the design space.

The G-optimal of above equation is equivalent to

$$\min_{\xi} \left| \max_{m \in R} \left\{ n_y x^{(m)T} \Phi\left[M(\xi)\right] x^{(m)} \right\} \right|$$

According to [131-132]

$$\max_{x \in R} \left\{ v(x) \right\} \geq p \text{ (Number of parameters)}$$

For specific experiment, if

$$\max_{x \in R} \left\{ v(x) \right\} = p$$

Then this experiment design is G-optimal [131-132].

Consider the Icosahedron design proposed above for 9 parameters.

$$X = \left[X_1, \quad X_2, \quad X_3, \; X_1^2, \quad X_2^2, \quad X_3^3, \; X_1X_2, \quad X_1X_3, \quad X_2X_3 \right]^T$$

For these 9 parameters 12-point uniform design, assume $a = \sqrt{\frac{2}{5+\sqrt{5}}}$, $b = \frac{1+\sqrt{5}}{\sqrt{10+2\sqrt{5}}}$

Recall the 12-point Icosahedron design, for this case, we have

$$X = \left[\begin{array}{ccccccccc} x_1 & x_2 & x_3 & x_1^2 & x_2^2 & x_3^2 & x_1x_2 & x_1x_2 & x_2x_3 \\ \hline 0 & -a & -b & 0 & a^2 & b^2 & 0 & 0 & ab \\ 0 & a & -b & 0 & a^2 & b^2 & 0 & 0 & ab \\ 0 & -a & b & 0 & a^2 & b^2 & 0 & 0 & ab \\ 0 & a & b & 0 & a^2 & b^2 & 0 & 0 & ab \\ -a & -b & 0 & a^2 & b^2 & 0 & ab & 0 & 0 \\ a & -b & 0 & a^2 & b^2 & 0 & -ab & 0 & 0 \\ -a & b & 0 & a^2 & b^2 & 0 & -ab & 0 & 0 \\ a & b & 0 & a^2 & b^2 & 0 & ab & 0 & 0 \\ -b & 0 & -a & b^2 & 0 & a^2 & 0 & ab & 0 \\ b & 0 & -a & b^2 & 0 & a^2 & 0 & -ab & 0 \\ -b & 0 & a & b^2 & 0 & a^2 & 0 & -ab & 0 \\ b & 0 & a & b^2 & 0 & a^2 & 0 & ab & 0 \end{array} \right]$$

Follow by X^TX

$$X^TX=\begin{bmatrix} & & & & & & & & \\ 4 & 0 & 0 & 0 & 0 & 0 & 0 & 0 & 0 \\ 0 & 4 & 0 & 0 & 0 & 0 & 0 & 0 & 0 \\ 0 & 0 & 4 & 0 & 0 & 0 & 0 & 0 & 0 \\ 0 & 0 & 0 & 2.4 & 0.8 & 0.8 & 0 & 0 & 0 \\ 0 & 0 & 0 & 0.8 & 2.4 & 0.8 & 0 & 0 & 0 \\ 0 & 0 & 0 & 0.8 & 0.8 & 2.4 & 0 & 0 & 0 \\ 0 & 0 & 0 & 0 & 0 & 0 & 0.8 & 0 & 0 \\ 0 & 0 & 0 & 0 & 0 & 0 & 0 & 0.8 & 0 \\ 0 & 0 & 0 & 0 & 0 & 0 & 0 & 0 & 0.8 \end{bmatrix}$$

Also

$$x^{(m)}=\left[x_1,\ \ x_2,\ \ x_3,\ x_1^2,\ \ x_2^2,\ \ x_3^3,\ x_1x_2,\ \ x_1x_3,\ \ x_2x_3\right]^T$$

$$\begin{aligned} v(x) &= n_y x^{(m)T}\left(X^TX\right)^{-1}x^{(m)} \\ &= 3(V_1^2+V_2^2+V_3^2)+6(V_1^2+V_2^2+V_3^2)^2 \end{aligned}$$

Now consider the region and constrain from assumption e. $V_1^2+V_2^2+V_3^2=1$ so under this constrained:

$$\max_{x\in R}\left\{v(x)\right\}=9$$

According to the definition of G-optimal [131-132], this 12 points Icosahedron design for model $f(\mathrm{x})$ in it is G-optimal.

Based on the same method that we applied to the proof Theorem 2, the value of G-optimality for the rest design is calculated and list in Table 5-9.

Table 5-9 Value of G-Optimality of three types of design

	6 parameter Model	9 Parameter Model
14 Point CCD	8.667	9.2
12 Point BBD	12	12
12 Point ID	9	9

Another important definition here is G-efficiency which is also using to evaluate design when the design is not G-optimal:

$$G_{eff} = \frac{p}{\max\limits_{x \in R}\{v(x)\}}.$$

Rotatability

Rotatability is another criterion that related to prediction variance. Unlike G-optimality, if the prediction variance is constant at all points which are the same distance from the centre of the design. Then this design is rotatable. For this specific experiment for TAs model, if all points locate on a 'sphere' has the same radius, the prediction variance of these points should be the same in order to meet the criterion of rotatability. It is important to notice that the rotatability relate to not only design but also model [140].

Recalling that the equation of prediction variance:

$$Var(\hat{y}(x)) = \sigma^2 x^{(m)\prime}\left(X'X\right)^{-1} x^{(m)},$$

from G-optimality section, it is shown that only 9 parameter 12 points uniform design is rotatable.

For 9 parameter 12 points Icosahedron design:

$$Var(\hat{y}(x)) = 0.75\sigma^2$$

where all the points are located on the sphere andthe radius is 1g from the centre. Based on the same requirement, the rest of the designs proposed above do not match this criterion.

The rotatability is important in this experiment, it represents that the prediction variance of different points is the same.

We define another type of rotatability as space rotatability. In order to explain this space rotatability, we use 12 points Icosahedron design for 9 parameter model as an example.

Recall the 12 points uniform experiment design, assume $a = \sqrt{\frac{2}{5+\sqrt{5}}}$, $b = \frac{1+\sqrt{5}}{\sqrt{10+2\sqrt{5}}}$.

We have D matrix

$$D=\left[\begin{array}{ccc} V_1 & V_2 & V_3 \\ \hline 0 & -a & -b \\ 0 & a & -b \\ 0 & -a & b \\ 0 & a & b \\ -a & -b & 0 \\ a & -b & 0 \\ -a & b & 0 \\ a & b & 0 \\ -b & 0 & -a \\ b & 0 & -a \\ -b & 0 & a \\ b & 0 & a \end{array}\right]$$

Define three rotate matrixes along three axes.

$$Rx=\begin{bmatrix} 1 & 0 & 0 \\ 0 & \cos\theta_x & -\sin\theta_x \\ 0 & \sin\theta_x & \cos\theta_x \end{bmatrix}$$

$$Ry=\begin{bmatrix} \cos\theta_y & 0 & \sin\theta_y \\ 0 & 1 & 0 \\ -\sin\theta_z & 0 & \cos\theta_z \end{bmatrix}$$

$$Rz=\begin{bmatrix} \cos\theta_x & -\sin\theta_x & 0 \\ \sin\theta_x & \cos\theta_x & 0 \\ 0 & 0 & 1_x \end{bmatrix}$$

Now D matrix after rotating D_{new} is defined as:

$$D_{new}=\left(Rx\times Ry\times Rz\times D^T\right)^T=\begin{bmatrix} V_{1new} & V_{2new} & V_{3new} \end{bmatrix}$$

X matrix for 9 parameters model is:

$$X_r=\begin{bmatrix} V_{1r} & V_{2r} & V_{3r} & V_{1r}^2 & V_{r2}^2 & V_3^3 & V_1V_2 & V_1V_3 & V_2V_3 \end{bmatrix}^T$$

It can be proved that the information matrix $(X_r^TX_r)$ is irrelevant with θ_x,θ_y and θ_z which means the information matrix will not change.

Actually, the Information Matrix $(X_r^TX_r)$ is as follows:

$$X_r^T X_r = \begin{bmatrix} 4 & 0 & 0 & 0 & 0 & 0 & 0 & 0 & 0 \\ 0 & 4 & 0 & 0 & 0 & 0 & 0 & 0 & 0 \\ 0 & 0 & 4 & 0 & 0 & 0 & 0 & 0 & 0 \\ 0 & 0 & 0 & 2.4 & 0.8 & 0.8 & 0 & 0 & 0 \\ 0 & 0 & 0 & 0.8 & 2.4 & 0.8 & 0 & 0 & 0 \\ 0 & 0 & 0 & 0.8 & 0.8 & 2.4 & 0 & 0 & 0 \\ 0 & 0 & 0 & 0 & 0 & 0 & 0.8 & 0 & 0 \\ 0 & 0 & 0 & 0 & 0 & 0 & 0 & 0.8 & 0 \\ 0 & 0 & 0 & 0 & 0 & 0 & 0 & 0 & 0.8 \end{bmatrix}$$

Based on the same theory, the above matrix indicates the space rotatability for other designs based on two different model.

Table 5-10 Space Rotatability of experiments

	6 parameter Model	9 Parameter Model
14 Point CCD	NO	NO
12 Point BBD	NO	NO
12 Point ID	NO	YES

This space rotatability is quite helpful during the data acquisition for calibration of Tri-axial sensors, especially, the Tri-axial Magnetometers (TM). It allows initial point to place in any position as long as all the 12 points at the end can construct an Icosahedron where the radius of its circumcircle is gravity or local magnetic field.

When applying this result to the calibration of Tri-axial Accelerometers, it shows that in terms of parameter estimation accuracy, the initial situation of the sensor is not so important as long as the relative position during the calibration can match the proposed design points.

5.3. Experiment Results and Discussion

The equipment we use to pursue these plans is an IMU containing a tri-axial accelerometer. It has 10-bit fix resolution and will increase to 13 bits when g range at $\pm 16g$while maintaining 4mg/LSB scale factor. The key features appeared in the DATA sheet are summarized in Table 5-11.

Table 5-11 Some significant specifications of Tas

Parameter	Min	Typ	Max	Unit
cross-axis		± 1		%
sensitivity (2g range)	230	256	282	LSB/g
0g offset for X, Y	-150	0	150	mg
0g offset for Z	-250	0	250	mg
offset vs. temperature X, Y				mg/°C
offset vs. temperature Z		± 1.2		mg/°C

Based on the described experimental settings in last subsection, we tried to implement the designed CCD, BBD and Icosahedron design experimental plans. It is not supervising that the proposed plans cannot be fully implemented by using the imperfect experimental devices. We assessed the index D-efficiency as proposed in equation (1) in terms of D-optimality. This experiment includes design with different points. Recall Table 5-8, and use 2.52×10^{-4} as D-optimal index for 6 parameter model and 6.5×10^{-8} as D-optimal index for 9 parameter model. Based on this, we compare the D-efficiency of pursued experiments.

Table 5-12 D-efficiency of experiment based on ADXL345

	6 parameter Model	9 Parameter Model
14 Point CCD	93.20%	99.41%
12 Point BBD	92.35%	99.31%
12 Point ID	99.13%	101.78%

In regarding to the comparison between the experiment value and the ideal value, one interesting phenomenon is that the D-efficiency of 9 parameters 12-point Icosahedron design

is larger than 100%. The reason of this phenomenon is that before calibration, the equation below,

$$y = \sqrt{V_1^2 + V_2^2 + V_3^2},$$

is not exactly equals 1g. It is impossible that y is slightly larger or smaller than 1g even this data is collected from perfect points' position. This slight difference will affect the information matrix. Subsequently, for this experiment, we should focus on the difference between D-efficiency and the value of this difference can be positive or negative.

For parameter estimation, we apply the nonlinear least square approach proposed in [129-130], the algorithm in [137-138] for 6-parameters model, and the extended this approach of [137-138] for 9-parameters model. If the experimental data is in required quality, no matter which approaches, in terms of testing Mean Square Error (MSE), both 6-parameters model and 9-parameters model can achieve desired calibration accuracy. The MSE before calibration is 0.0139 and Table 5-13 below indicates the MSE after calibration.

Table 5-13 MSE Of Experiment based on ADXL345

	6 parameter Model	9 Parameter Model
14 Point CCD	0.001310	0.001201
12 Point BBD	0.001128	0.001112
12 Point ID	0.00103	0.001234

5.4. Summary

This Section includes two parts. For the first part, we convert nonlinear TAs models into linear to simplify the equation. This is achieved via simplification and parameter substitution. For a linear model, least square method is applied to solve the unknown parameters. The second part, we investigate the experimental design of a new calibration approach for portable tri-axial accelerometers based on TAs models after linearization. Two experiment plans have been proposed according to Central Composite design and Box–Behnken design. Beside this, we have introduced a new scheme, Icosahedron design. Furthermore, Orthogonality, D-optimality, G-optimality and Rotatability have been compared for three proposed designs. We have proofed that Icosahedron Design is D-optimal, G-optimal and Rotatable for a specific model

that suitable for 9 parameters TAs model. The result shows that with a good design of experiment, MSE of TAs after calibration will decrease significantly which also proofed this linearization method is reliable and efficiency. We hope these proposed experimental plans can be accepted, tested, and improved by the researchers and users of wearable sensors.

6. Auto-Calibration of Tri-axial Magnetometers

In this chapter, we will discuss the calibration and its associated experimental design scheme for the tri-axial magnetometers. For the widely used 6-parameter and 9-parameter models of tri-axial Magnetometers, based on experimental design for Tri-axial accelerometers discussed previously, we selected the 12-observation experiment scheme, i.e., the Icosahedron design, rather than BBD, CCD designs to reduce estimation error. As discussed before, this Icosahedron scheme is proved to be rotatable; before experiment, it is not necessary to estimate the direction of the magnetic field of the Earth, which is quite difficult in infield environment. For this 12-observation experiment scheme, a simple linearization approach is applied for the parameter estimation. This algorithm can be easily implemented in a micro-controller with low computational capacity. We also proposed online recursive least square algorithms for both 6-parameter and 9-parameter models when fast calibration is needed. Experimental results showed the effectiveness of these calibration approach. It should be noted that the precision turntable is not required to ensure the desired calibration accuracy although these calibration methods utilize the projection of the local earth's magnetic field as a calibration input.

6.1. Introduction

For the monitoring of traffic inside a tunnel, even GPS may be inaccessible, an Inertial Measurement Unit can still predict the pitch and roll information by integrating the measurements of TA and Tri-axial Gyroscopes (TG), without error accumulated with time. However, in the absence of a GPS signal, if only inertial sensors (i.e., accelerometers and gyroscopes) are used, it is difficult to estimate the heading (i.e., the yawn angle) within acceptable accuracy.

Magnetometers, commonly used as magnetic compasses, have been widely used to measure heading by sensing the Earth's magnetic field. The measurement error of the magnetometer does not accumulate over time compared to the gyroscope [145]. Therefore, Tri-axial Magnetometers (TMs) are often combined with the IMU to construct an attitude and heading reference system (AHRS).

One of the first magnetic compasses was invented thousands of years ago [129]. With advances in integrated circuit (IC) manufacturing and MEMS sensor technology, TMs have been scaled down and embedded into traffic monitoring systems. Consequently, by integrated with MENS Inertial Measurement Unit (IMU), its use for mobile navigation [146], mobile health/exercise monitoring [131], and especially traffic control/monitoring [147], is popularizing.

Compared to the TA and TG, the TAs have a relatively low accuracy because the magnetometers outputs are polluted by broadband disturbance and noise, stochastic biases due to sensor deficiencies, and unwanted magnetic interference in the vicinity of the sensors [148]. An effective approach to reduce the unwanted magnetic interference (i.e., hard iron and soft iron biases [149]) is infield calibration. Several convenient methods have been offered [129][131][145-149]. However, one of the most popular methods is developed by using Ellipsoid Fitting [145]. In this section, we will apply the linearization approach introduced in the previous sections to develop new calibration algorithms for TM calibration.

Furthermore, to ensure the calibration efficiency, we also discuss the optimal experimental design for TM. As far as we know, the only paper discussing the Experimental Design (DoE) for the auto-calibration of magnetometers is [133], which provided a first investigation of DoE of the auto-calibration for TM.

On the other hand, there are many studies focusing on the experimental design of accelerometers, gyroscopes or IMU calibrations [134][150]. Because of its similarity to the calibration of a three-axis accelerometer, the experimental design of the magnetometer calibration can draw on the idea of a three-axis accelerometer.

We have introduced our previous research results [134][150] for the auto-calibration of tri-axial accelerometers, in which effective linearization methods for both 6-parameter and 9-parameter auto-calibration model were presented. We also showed before, the 12-observation experimental scheme (the Icosahedron scheme) is both G-optimal and rotatable.

Because of the non-orthogonality and misalignment of the triaxial anisotropic magneto resistive sensor, as well as the unwanted magnetic interference, the 6-parameter model may not be sufficient to obtain the desired heading estimate. In this section, we will first examine the effectiveness of the 9-parameter model and its associated 12-observation icosahedral design to evaluate its suitability for calibrating TM through simulation and real time experimentation.

The main reason for testing the suitability of 9-paramter model with 12-observation icosahedral design is the detection of the local magnetic field is much more difficult than that of the local gravity. For in-field calibration of TA, it is nearly impossible to realize the 12-observation Icosahedron design with reference to the local magnetic field. However, the 12-observation scheme is rotatable; we can still simply implement the Icosahedron scheme with reference to local gravity rather than the local magnetic field, and still ensure the G-optimality. This shows that this Icosahedron experimental scheme is especially suitable for the calibration the tri-axial

magnetometers. Even more, due to the rotate-ability, the single experimental scheme can simultaneously implement G-optimal calibrate for both TA and TM in an IMU, and at the same time it can give a relative accurate estimation of the inclination angle of magnetic field.

We also investigated the calibration of TM by using 6-parameter model experimentally. At the same time, to implement fast infield calibration of TM, we also developed a recursive online calibration algorithm for 6-parameter TA model. Its efficiency has been experimentally demonstrated.

This chapter is organized as follows. In section 6.2, the linearized TM model is introduced. In section 6.3, the 12-observation Icosahedron design is re-explored by using numerical analysis. In section 6.4, experimental results are presented. Section 6.5 concludes this chapter.

6.2. TM model and its experimental design

In this section, we introduce the TM model [133] for auto-calibration. Recently, more and more IMUs have been equipped with magnetometers for the AHRS system. For MEMS sensors, accelerometers and magnetometers have similar model structures. The only difference is that local gravity points to the centre of the earth, while the magnetic force of the local geomagnetic field is more horizontal. In this case, the auto-calibration method applied [152] to MEMS TAs should be also efficiency for that of the MEMS TMs. For a TA , define local magnetic field and the measured value as $\mathbf{H}^{\mathbf{r}} \in R^{3\times 1}$ and $\mathbf{H}^{\mathbf{m}} \in R^{3\times 1}$respectively. The typical mathematical model of magnetometer can then be expressed as:

$$\mathbf{H}^{\mathbf{r}} = \mathbf{G}(\mathbf{H}^{\mathbf{m}} + \mathbf{O}) + \mathbf{n}, \tag{1}$$

where $G \in R^{3\times 3}$ is the matrix derived from $\mathbf{G_s} \times \mathbf{G_e}$. $\mathbf{G_s}$ is a diagonal matrix constructed by scale factors, $\mathbf{G_e}$ represents the error from soft iron and/or misalignment? $\mathbf{O} \in R^{3\times 1}$ is the offset and $\mathbf{n}$ is white noise?

The calibration procedure assumes that the amplitude of local magnetic field $\| \mathbf{H}^{\mathbf{r}} \|^2$ remains constants if the model coefficients are well calibrated. That is,

$$\begin{aligned} \| \mathbf{H}^{\mathbf{r}} \|^2 &= [\mathbf{G}(\mathbf{H}^{\mathbf{m}} + \mathbf{O}) + \mathbf{n}]^{\mathbf{T}} [\mathbf{G}(\mathbf{H}^{\mathbf{m}} + \mathbf{O}) + \mathbf{n}] \\ &= (\mathbf{H}^{\mathbf{m}} + \mathbf{O})^{\mathbf{T}} \mathbf{G}^{\mathbf{T}} \mathbf{G}(\mathbf{H}^{\mathbf{m}} + \mathbf{O}) \\ &\quad + 2\mathbf{n}\mathbf{G}(\mathbf{H}^{\mathbf{m}} + \mathbf{O}) + \mathbf{n}^2, \end{aligned} \tag{2}$$

The error distribution of the square norm is a combination of a Gaussian distribution and a chi-square distribution. When the variance of the Gaussian distribution is small compared to

the magnitude of the local magnetic field, the Gaussian distribution error in (2) dominates. In this case, the error of (2) can be considered as an approximate Gaussian distribution. We use ε to denote the error in (2); based on (1) and (2), we have:

$$\| \mathbf{H}^{\mathbf{r}} \|^{\mathbf{2}} = \sum_{i=x,y,z} \left\{ \sum_{i=x,y,z} [G_{ij} \cdot (h_i^m + O_i)]^2 \right\} + \varepsilon \tag{3}$$

where $G_{ij} = G_{ji}$. The model parameters can be identified by minimizing the gap of the following term:

$$\|\mathbf{H}^{\mathbf{r}}\|^2 - h^2 \tag{4}$$

where h is equal to "1"; it is regarded as the magnitude of local magnetic field.

To this end, based on the experimental design theory, for (4), it is necessary for $\| \hat{\mathbf{H}}^{\mathbf{r}} \|^{\mathbf{2}}$ to has minimum variance and the overall variance of $\| \hat{\mathbf{H}}^{\mathbf{r}} \|^{\mathbf{2}}$ is uniform. To directly use classical DoE approach, it is necessary to linearize (3). As discussed for the DoE of TA, the second order polynomial again can be selected for experimental design [136-137]:

$$y = \beta_0 + \sum_{j=1}^{m} \beta_j x_j + \sum_{j=1}^{m-1} \sum_{k=j+1}^{m} \beta_{jk} x_j x_k + \sum_{j=1}^{m} \beta_{jj} x_j^2. \tag{5}$$

To linearize (3) into (5), we have to neglect some trivial terms first. Eq (3) can be expanded as follows:

$$\| \mathbf{H}^{\mathbf{r}} \|^{\mathbf{2}} = \sum_{i=x,y,z} \left\{ \sum_{i=x,y,z} \left[G_{ij}^2 \cdot ((h_i^m)^2 + 2h_i^m O_i + O_i) \right] \right\}, \tag{6}$$

The off-diagonal elements of $\mathbf{G}$ (G_{ij}) for most commercial MEMS magnetometers are around 0 to 5 percent of the diagonal elements of $\mathbf{G}$ (G_{ii}). The offset $\mathbf{O}$ is around 0 to 5 percent of the magnitude of local magnetic field. Based on this fact, we neglect the terms which contain G_{ij}^2 and O_i^2 first. Then, Eq (2) can be simplified as:

$$\| \mathbf{H}^{\mathbf{r}} \|^2 = \sum_{i=x,y,z} G_{ii}^2 (h_i^m)^2 + \sum_{i=x,y,z} 2G_{ii}^2 h_i^m O_i + \sum_{i=x,y,z} \sum_{j \neq i} (G_{ii} + G_{jj}) G_{ij} h_i^m h_j^m + \gamma + \varepsilon, \tag{7}$$

where γ is the neglected terms which will be recursively compensated later, and $G_{ij} = G_{ji}$.

By using substitution technique for (7) and define 9 new parameters as follows:

$$\begin{aligned} G_{xx}^2 &= \beta_{11} & 2G_{xx}^2 O_x &= \beta_1 \\ G_{yy}^2 &= \beta_{22} & 2G_{yy}^2 O_y &= \beta_2 \\ G_{zz}^2 &= \beta_{33} & 2G_{zz}^2 O_z &= \beta_3 \\ 2(G_{xx} + G_{yy}) G_{xy} &= \beta_{12} \\ 2(G_{xx} + G_{zz}) G_{xz} &= \beta_{13} \\ 2(G_{yy} + G_{zz}) G_{yz} &= \beta_{23} \end{aligned} \tag{8}$$

By neglecting γ in (7) first, (2) can then be simplified in the standard polynomial form as:

$$y = \sum_{j=1}^{3} \beta_j x_j + \sum_{j=1}^{2} \sum_{k=j+1}^{3} \beta_{jk} x_j x_k + \sum_{j=1}^{3} \beta_{jj} x_j^2 + \varepsilon, \tag{9}$$

where $h_{x,y,z}^m$ and $\| \mathbf{H}^{\mathbf{r}} \|^2$ are re-writtens as $x_{1,2,3}$ and y respectively. For parameter estimation, the first requirement is to ensure the estimation is unbiased. Although the effect of neglecting γ is minor, it is still required to compensate this effect to achieve unbiased estimation. We introduce the iterative method later.

For the polynomial model in (9), G-optimal experiments can be applied to minimize the maximum variance of $\hat{y}$ [136]. That is the minimum maximum of (4) can be obtained.

The standardized variance of predicted response, for G-optimal experimental design [136], can be reached

$$d(x, \xi_N) = f^T(x) M^{-1}(\xi_N) f(x) = \frac{N \, var(\hat{y}(x))}{\sigma^2}, \tag{10}$$

where $M(\xi_N)$ is the normalized information matrix [138], $f^T(x)$ is the row matrix of all possible values in experiment domain χ from (9), and N is the number of runs. For model 9, $f^T(x)$ is:

$$f^T(x) = [x_1 \quad x_2 \quad x_3 \quad x_1^2 \quad x_2^2 \quad x_3^2 \quad x_1 x_2 \quad x_1 x_3 \quad x_2 x_3] \tag{11}$$

and $M(\xi_N)$ is:

$$M(\xi_N) = \frac{X^T X}{N}, \tag{12}$$

where X is the expected observations. Based on [136], as discussed in the TA section, if the maximum value of $d(x, \xi_N)$ is equal to the number of unknown parameters, then this experimental design can reach G-optimality, i.e.,

$$max\, d(x, \xi_N) = p, \tag{13}$$

p is the number of parameters to be estimated.

As discussed before, this G-optimal experimental design can be achieved by the 12-observations design. Again, defining $a = \sqrt{\frac{2}{5+\sqrt{5}}}$ and $b = \frac{1+\sqrt{5}}{\sqrt{10+2\sqrt{5}}}$, the Icosahedron design is then listed in Table 6-1 (or Table 6-5 three factors Icosahedron design for Tri-axial accelerometer model).

Table 6-1 12 observations Icosahedron experimental design for magnetometer

Observation	x_1	x_2	x_3
1	0	a	b
2	0	-a	b
3	0	a	-b
4	0	-a	-b
5	a	b	0
6	-a	b	0
7	a	-b	0
8	-a	-b	0
9	b	0	-a
10	-b	0	-a
11	b	0	a
12	-b	0	a

The G-optimality for (9) can be easily proved based on (10), (11) and (12), and the standardized variance for (9) based on the design in Table. 1 is:

$$\begin{aligned} d(x,\xi) &= f^T(x)M^{-1}(\xi_N)f(x) \\ &= 3(x_1^2+x_2^2+x_3^2)+6(x_1^2+x_2^2+x_3^2)^2, \end{aligned} \tag{14}$$

where the sum of $(x_1^2+x_2^2+x_3^2)$ is the squared magnitude of local magnetic field. For the Earth's magnetic field, the magnetic force changes from 0.4T to 0.6T. For magnetometers, users typically use them to obtain yaw angles rather than magnetic forces. In this case, we can normalize the magnitude of the local magnetic field to "1h". So we have:

$$\begin{aligned} max\ d(x,\xi) &= 3+6 \\ &= 9, \end{aligned} \tag{15}$$

where the value of $max\ d(x,\xi)$ is the same as the number of the parameters to be identified. As discussed before [151], this Icosahedron experimental design is G-optimal for (9).

Another expected property is rotatability. If an experimental design is rotatable, then variance of predicted response ($\hat{y}$) in experimental domain χ is only related to the distance between center point and observation points [140]. From (14) and (15), the value of $d(x,\xi)$ is only related to $(x_1^2+x_2^2+x_3^2)$, which is the squared distance between center point and experimental points. This clearly shows that the 12-observation design listed in Table6-1 is rotatable.

For this design, it is both G-optimal and rotatable. These two characteristics indicate that the predicted response ($\hat{y}$) has the minimum maximin variance all over the domain χ.

This is not enough for the calibration of the magnetometer. Usually, an accelerometer is needed to determine the horizontal plane [145]. The direction of the magnetic field has an oblique angle to the horizontal plane. For the experiment in question, we have shown that it is spatially rotatable, indicating that only the relative direction/position is important for calibration. Compared to calibration such as [145], there is no need to care about the horizontal plane. To show this spatial rotatability, let's define three rotation matrices. We assume that the tilt angle between the magnetometer and the horizontal plane is θ_x, θ_y and θ_z. Then, the transformation matrices can be expressed as follows:

$$Rx = \begin{bmatrix} 1 & 0 & 0 \\ 0 & \cos\theta_x & -\sin\theta_x \\ 0 & \sin\theta_x & \cos\theta_x \end{bmatrix},$$

$$Ry = \begin{bmatrix} \cos\theta_y & 0 & \sin\theta_y \\ 0 & 1 & 0 \\ -\sin\theta_z & 0 & \cos\theta_z \end{bmatrix},$$

$$Rz = \begin{bmatrix} \cos\theta_x & -\sin\theta_x & 0 \\ \sin\theta_x & \cos\theta_x & 0 \\ 0 & 0 & 1_x \end{bmatrix}.$$

Similar to our proof of TA, in general, for any initial observation, the experimental design can maintain G-optimal as long as all 12 observations can be observed at the "relative" proposed point. Therefore, the misalignment error can be eliminated by the spatial rotatable characteristic.

$$d(x, \xi^{(new)}) = f^T(x)\left(\frac{X^{(new)T} X^{(new)}}{N}\right)^{-1} f(x) = 9 \tag{16}$$

This spatial rotatability provides great convenience for the calibration of the magnetometer. Especially suitable for users who want to calibrate the magnetometer directly without an accelerometer.

6.3. Parameter Estimation and Numerical Analysis

For experimental design, the optimum results can only be obtained in ideal situation. From Table 6-1, the relationship between the expected input and tilt angle of magnetometer is:

In the case of experimental design, the best results can only be obtained under ideal conditions. From Table. 1, the relationship between the expected input of the magnetometer and the tilt angle is as follows:

$$h'_{x,y,z} = \cos\theta_{x,y,z} \tag{17}$$

where $h_{x,y,z}$ is the expected input value in Table 6-1

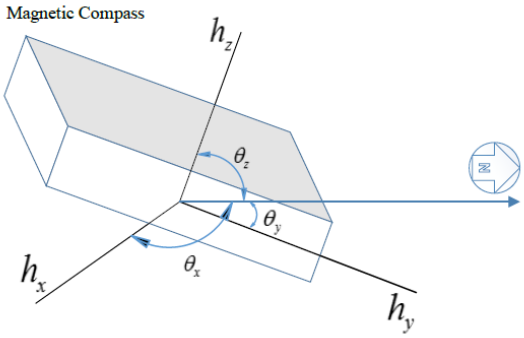

Fig 6-1 The relationship between the expected value in the experimental design and the tilt angle of the magnetometer

In the real world, when auto-calibration methods are used to calibrate unknown parameters, most users of traffic monitoring with an infield environment do not have advanced equipment to obtain precise tilt angles. For this calibration method, calibration can be handled using a simple platform with a suitable tilt angle. Denote the measured value as $\widetilde{X}$. We can estimate the recombined parameters set β by least square estimation:

$$\beta = (\widetilde{X}^T \widetilde{X})^{-1} \widetilde{X}^T Y. \tag{23}$$

With initial $\widetilde{X}^{(0)}$ which is the measured value. According to the procedure, as shown in Figure 6-2, we can use the iterative method to obtain a matrix representing the direction of the experimental scheme without scale factor error and offset.

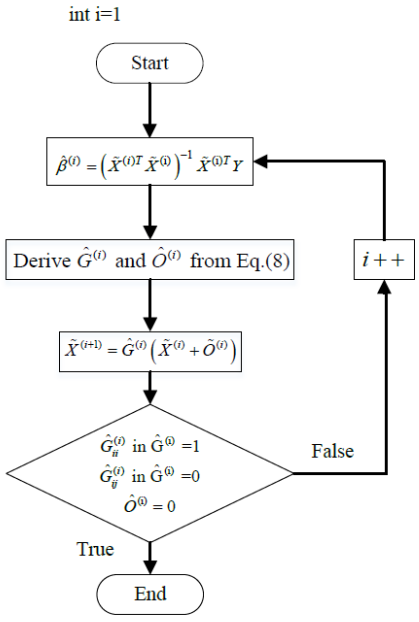

Fig. 6-2 The procedure of the iterative algorithm

Recursively, the estimation of the magnetic field can be calculated as:

$$\hat{\mathbf{H}}^{\mathbf{r(n)}} = \hat{\mathbf{G}}^{(\mathbf{n})}(\Lambda\ \hat{\mathbf{G}}^{(\mathbf{2})}(\hat{\mathbf{G}}^{(\mathbf{1})}(\hat{X}^{(1)} + \hat{\mathbf{O}}^{(\mathbf{1})}) + \hat{\mathbf{O}}^{(\mathbf{2})})\Lambda\ + \hat{\mathbf{O}}^{(\mathbf{n})}). \tag{24}$$

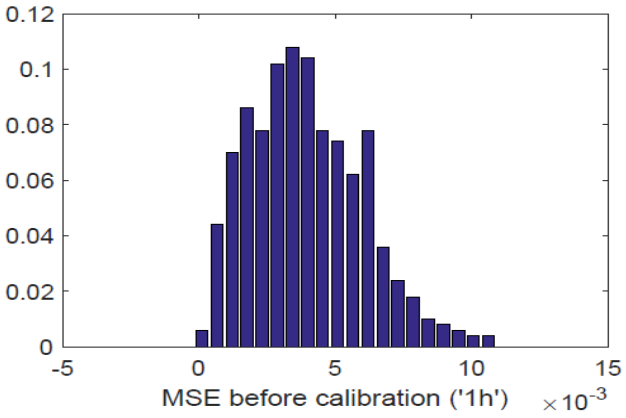

Fig. 6-3 Uncorrected error distribution

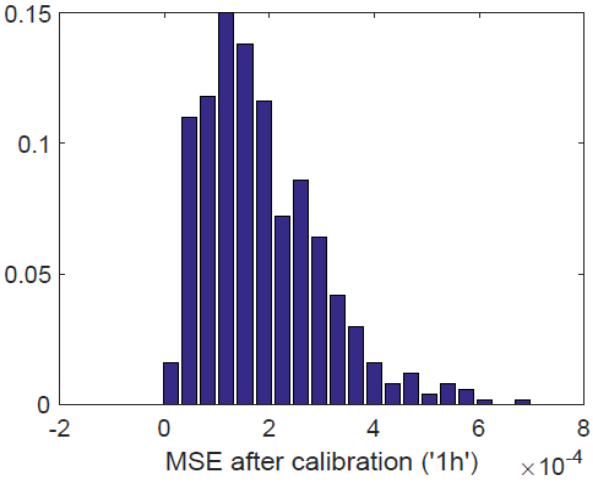

Fig. 6-4 Calibrated error distribution

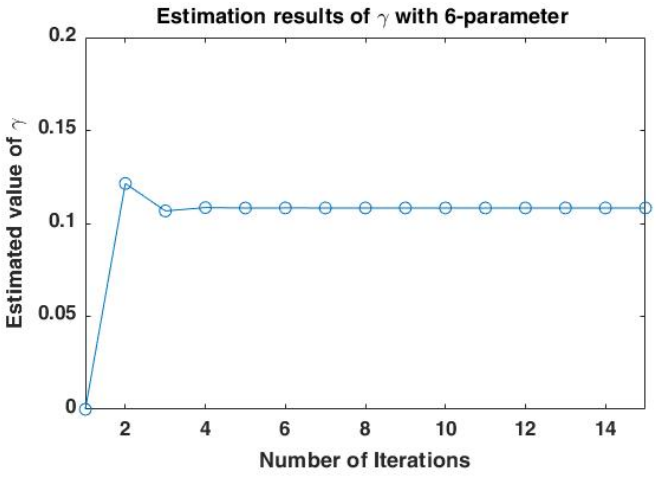

Fig. 6-5 Estimation results of γ with 6-paramter

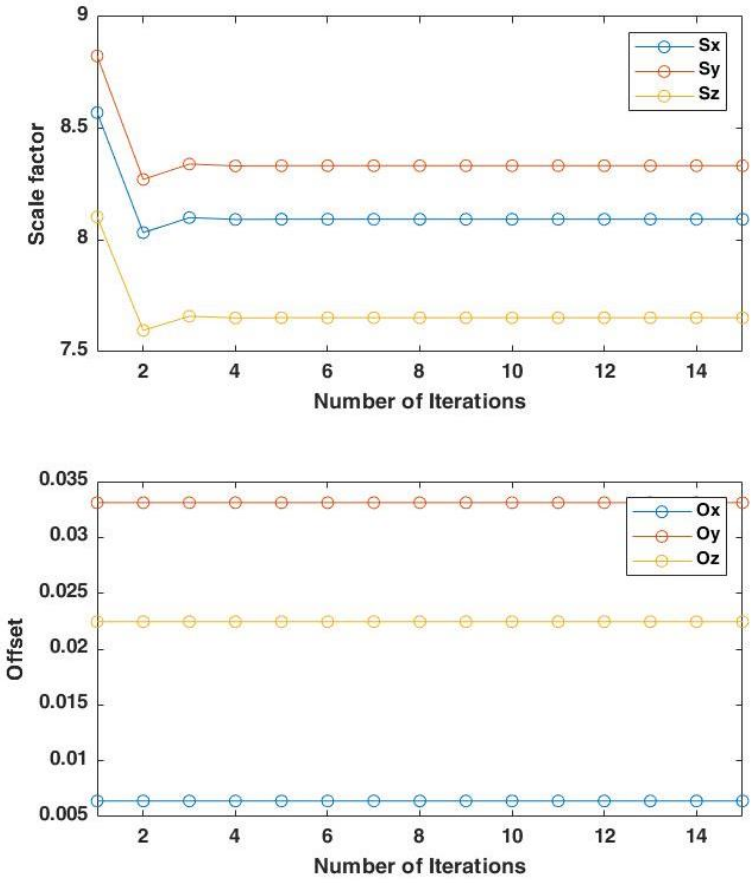

Fig. 6-6 Scale factor and Offset with 6-parameter

From the simulation, it can be seen for most cases, the predicted $\mathbf{H}^{\mathbf{r(n)}}$ will approach real value $\mathbf{H}$ within only 3 iterations. To verify the performance of this method, performed 1000 Monte Carlo simulations.

For TMs, the typical error of scale factor and bias are 5% and 10%. It would cause a substantial variance for angle quantity. To obtain a reliable simulation, the parameters generation in Monte Carlo simulations are assumed as follows. The diagonal element of the scale factor (G_{ii}) follows a uniform distribution $U(-5\%,5\%)$, the off-diagonal element of the scale factor (G_{ij}) follows $U(-1\%,1\%)$ and the offset (O_{ii}) follows $U(-10\%,10\%)$.

For each simulation, parameters will be generated according to the above instructions. In the real world, users who use our methods are less likely to access high-precision devices. As noted above, for this calibration method, a platform with a certain slope is sufficient for this calibration. Using the estimated scale factor and offset, we randomly generate another 100 observations on the sphere. The radius of the sphere is the magnitude of the local magnetic

field (here we use $1h$ for the local magnetic field). In simulation, the noise level is at $U(-0.005,0.005)\ h$. Statistical results for 500 Monte Carlo simulations are provided for the distributed distribution of the magnetometers before and after calibration.

Figures 6-3 and 6-4 show the performance of our calibration method, MSE decreases around 10^{-4} to 10^{-3}.

6.4. Experimental verifications

A recently developed μ-IMU which including a 9-axis motion tracking chips has been applied to verify the proposed calibration approach.

The calibration results of both 6-parameter and 9-parameter models are displayed from Figure 6-5 to Figure 6-10. It can be seen that this method can converge and the estimated results of TM has been greatly improved after calibration from the aspects of magnitude of the magnetic.

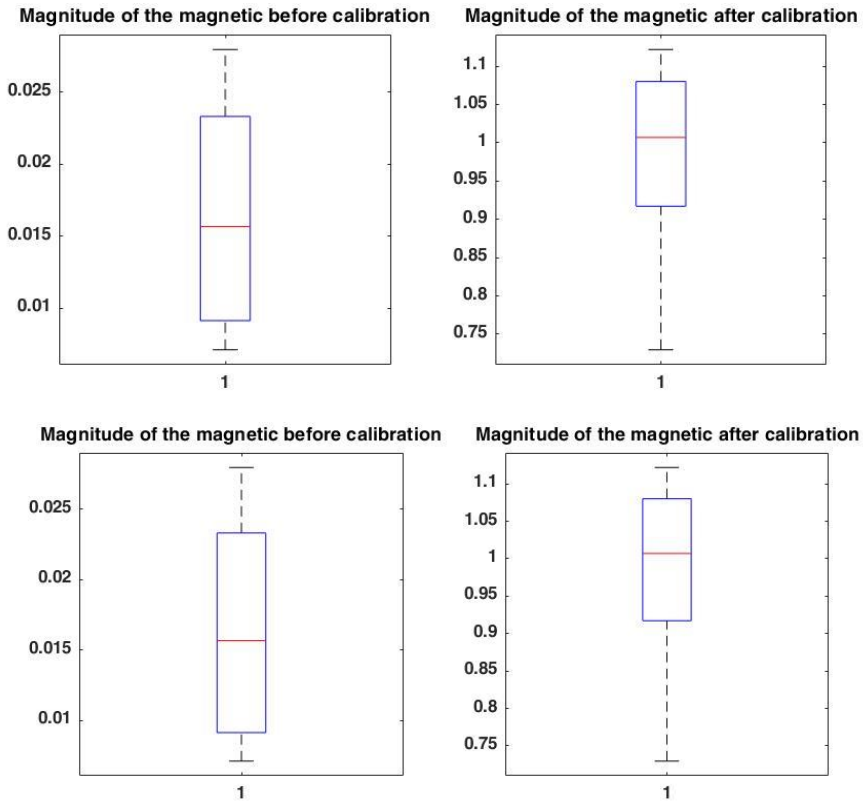

Fig. 6-7 Parameter before and after calibration

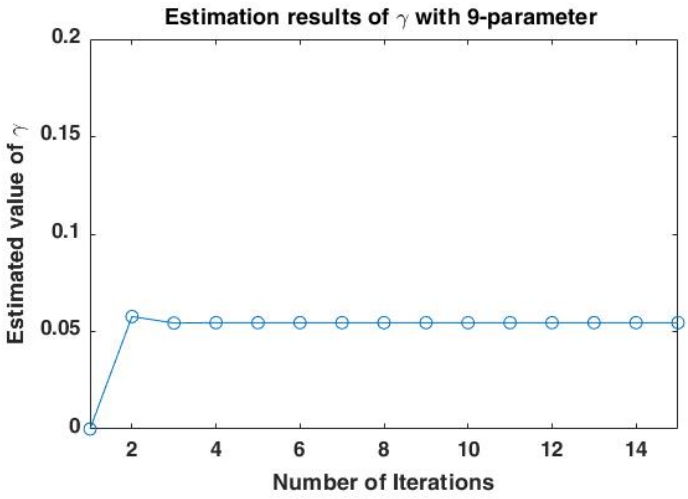

Fig. 6-8 Estimation results of γ with 9-paramter

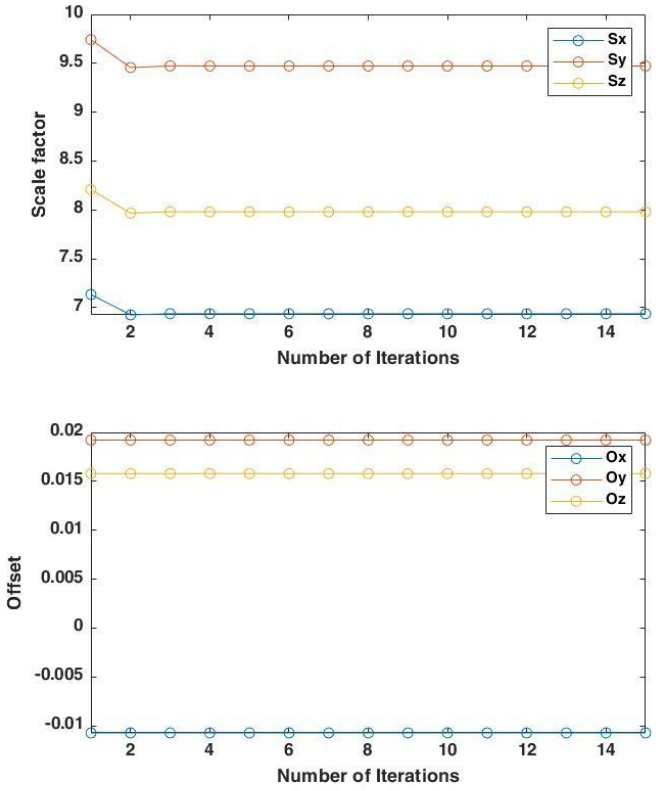

Fig. 6-9 Scale factor and Offset with 9-parameter

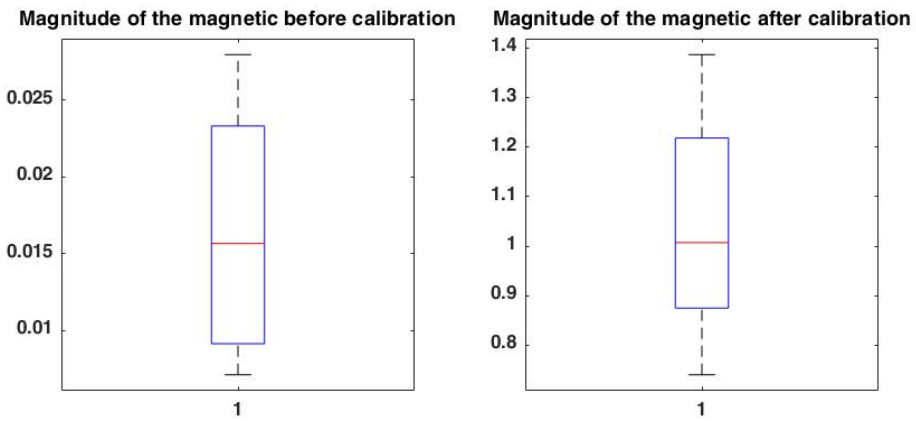

Fig. 6-10 Parameter before and after calibration

Based on the identified TA and TM models, we calculated the angle between the local gravity and local magnetic field, the closest angle of 12 points to the real inclination 64° 18' is 66° 54'. It is indicated that the angle can be estimated with desired accuracy (the mean relative error of 12 points is 0.1162).

6.5. Summary

This chapter investigates an experimental design for the automatic calibration of magnetometers for the 6-parameter and 9-parameter models of MEMS TMs. An iterative algorithm is used to solve unknown parameters during calibration. Based on the results of the 1000 Monte Carlo simulation, the measurement error of the TM after calibration was significantly reduced. The experimental results also show the effectiveness of the proposed approach.

We hope this calibration method and iterative algorithm can provide the user with an easier way to improve the accuracy of the TM and at the same time improve the performance of the AHRS magnetometer.

7. The Research of Urban Rail Transit Sectional Passenger Flow Prediction Method

7.1. Introduction

In recent years, the domestic urban rail transit is under rapidly development, for instance, a complex road network structure, high passenger demand growth and others will come into the future network of urban rail transit in Beijing. Hence whatever in planning, construction or operation stage, the close control and forecast of the passenger flow is inseparable. One of the very important parts for the sectional passenger flow is the short-term forecast which is what traffic sequence is going to happen in short team. On the other way, typical time series with long temporal dependence will be long term forecast. And meanwhile, it is also very necessary for the research of forecasting methods. The study on short-term sectional passenger flow forecasting methods will be shown by this text based on the investigation on the Beijing subway Line 2.

7.2. Overview of Sectional Passenger Flow

The passenger flow volume in a particular place of the subway line at a unit time is referred by the sectional passenger flow. An essential element of forecasting is the prediction on sectional passenger flow. The premise of traffic organization for smoothly working is to grasp the present situation and changes of the passenger flow. It is greatly significant to manage and control, set reasonable operation scheduling plan and track the Quality of Services.

It is indispensable for the analysis of passenger flow in forecasting. It could be seen that bimodal pattern in a day time is belonged to the passenger flow of Beijing subway Line 2 and the weekend passenger flow is greater than usual by combining with the passenger flow features of Beijing subway Line 2. And holidays, weather conditions, season, emergencies and many other factors [153-156] can affect passenger flow as well.

7.3. Research of the Forecasting Methods

7.3.1. Short-Term Passenger Flow Forecasting Methods

In the short-term passenger flow forecasting, methods[157-160] are commonly used for forecasting includes:

- Research on traditional algorithms, such as regression method, time series and so on, concentrates on the law of the passenger flow sequence itself.

- Modern algorithms, such as genetic algorithms, neural networks.

- Combinational algorithms combining traditional methods with modern algorithms.

Among them, the artificial neural network, indexed as neural networks, is on the basis of physiological changes in the brain. It can stimulate the brain's structure and function, so it is a computer-realized information processing system.

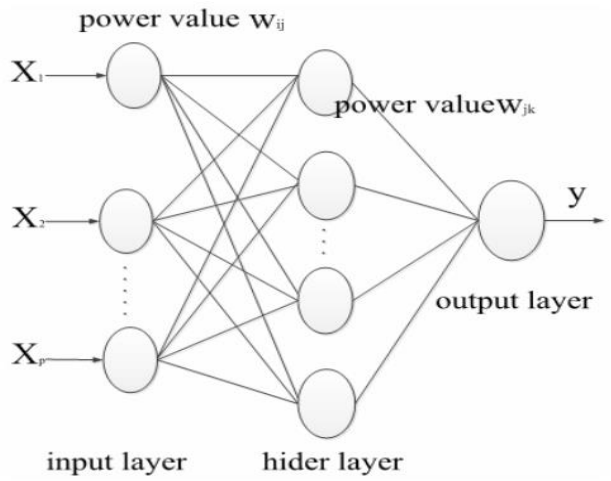

Fig. 7-1 Schematic diagram of BP neural network

7.3.2. Sample Analysis and Data Selection

The collected raw data is from 1 March 2014 to 31 March 2014, of which the daily passenger flow volume is from 6 am to 23 pm every 30 minutes of each section of Beijing subway Line 2. Enough samples, representative and uniform distributions are required by reasonable sample selection, hence the characteristics of sectional passenger flow must be analysed firstly before undergoing passenger flow forecasting.

Because of the prominence of Monday morning rush hour and Friday evening peak compared with other periods, four parts including Monday, Tuesday to Thursday, Friday, weekends, divides one week. Due to the large passenger flow and Fuxingmen being a transfer station, the section of Fuxingmen to Fuchengmen of Beijing Subway Line 2 is selected and studied by this thesis. The use of the data between Tuesday and Thursday morning peak hours (6 am to 10 am, down line) brings some representations on this prediction. The selected data will be normalized before training for ensuring that the sample is reasonable.

7.3.3. BP Neural Network

BP neural network, the full name of which is Back-Propagation neural network, is a learning algorithm developed by McClelland, Rumelhart, in 1986. Currently, vast majority neural network models using BP methods, or its variants are widely taken in practical applications [161][162]. The schematic diagram of BP neural network is presented in Figure 7-1.

This type of network usually includes three parts: input layer, hidden layer and output layer. Different sectional passenger flow is represented by p nodes contained in input layer. Forecast sectional flow is represented by Y in output layer. The actual situation will determine the number of hidden layer nodes.

Accurate forecast is based on suitable network structure. And some conclusions can be made by a large number of experiments: s-shaped tangent function tansig is taken by the transfer function of hidden layer; s-shaped logarithmic function logsig is adopted by output unit, gradient descending, which trains dx when considering BP neural network, is adopted by training function. After largely repeated studies and trainings, the parameters can be adjusted and reasonable mapping relationship between input and output can also be set up.

7.4. The Instance of Predicting Sectional Passenger Flow

Based on the features of sectional passenger flow, its prediction problems of urban rail transit are studied in this chapter by taking advantages of BP neural network model and MATLAB neural network toolbox for the stimulation of schemes.

7.4.1. Solutions Design of Sectional Passenger Flow Forecast

Each section, the passenger flow volume of which is intrinsically linked with the near time of it, is one part of the network; This leads to the essential link between the passenger flow volume of the section and its near section. A large amount of external factors including weekend, holidays, weather, season, can influence sectional passenger flow. Hence the prediction accuracy can be increased by taking these factors into consideration [163-166]. Sectional passenger flow will be predicted by the use of the following three scenarios which is shown in Table 7-1, and BP neural network is applied in these methods.

The previous three periods and the current period can be viewed as input vectors, and the next period of the sectional passenger flow can be forecast based on them.

Table 7-1. Solutions design of sectional passenger flow forecast.

Type of prediction	Solution Description
On the basis of the relevant time	Predict the sectional passenger flow of the T + 1 time period by using passenger flow of researched section of the T time period and previous 30 minutes time period
On the basis of the relevant section	Predict the sectional passenger flow of the T + 1 time period by using passenger flow of researched section, the relevant section of the T time period and previous 30 minutes time period
Consider other factors	Predict the sectional passenger flow of the next day by using the sectional passenger flow of the previous day and influenced factors (holidays, weather, season) of the next day

On this condition, as the structure shown in Figure 7-2, the network is four-dimensional input, one-dimensional output.

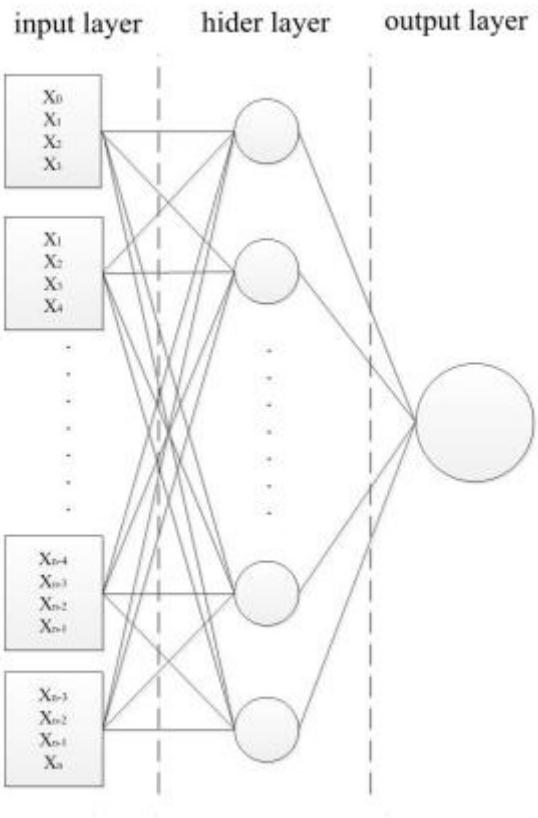

Fig. 7-2 Network structure diagram

In order to be consistent with the method selected based on 7.1, 52 sample pairs are obtained, 70% of which are treated as training samples for forming the network, 15% of which are set as the validation sample, and 15% of which are viewed as the test samples.

Resultantly, Figure 7-3 shows the curve of the error performance, the relationship between the predicted value and the true value is shown in Figure 7-4. As it can be seen from the actual and predicted value of the curve, the predicted results are almost the same as the actual one, which proves that the future trend of sectional passenger flow can be well predicted by the scheme.

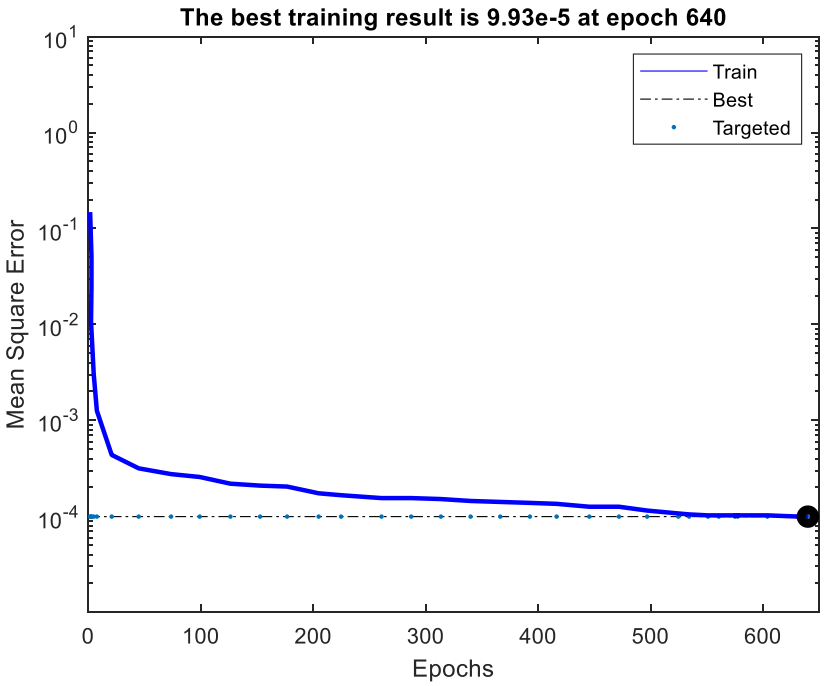

Fig. 7-3 Predicting outcomes

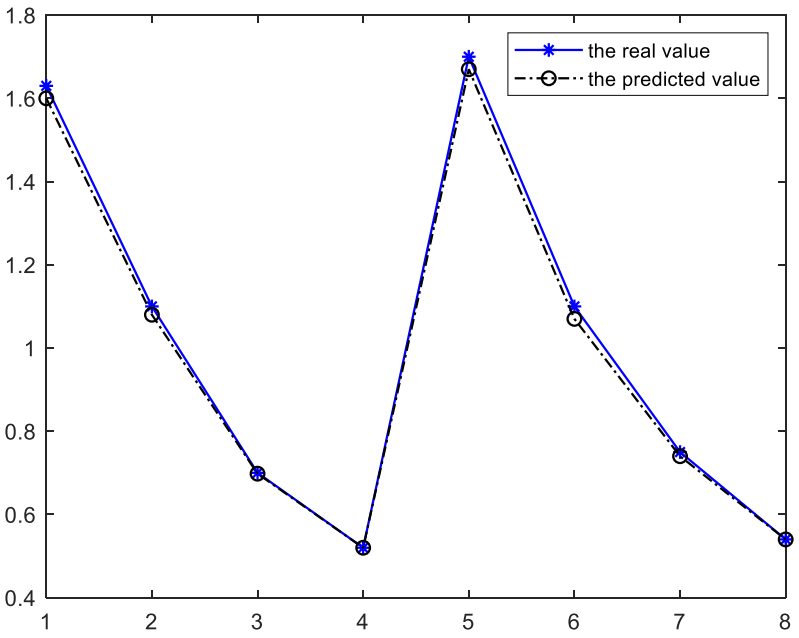

Fig. 7-4 Predicting outcomes

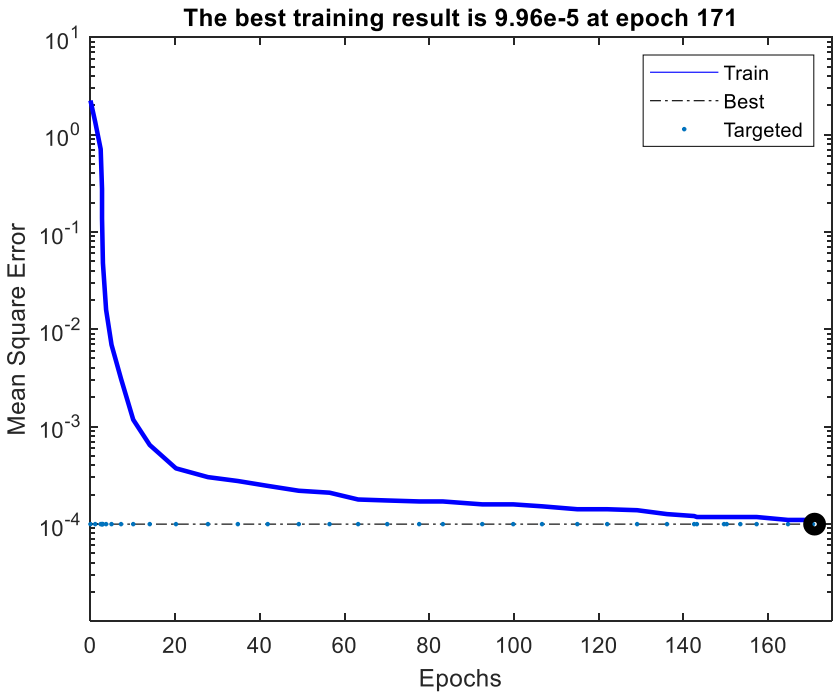

Fig. 7-5 Predicting outcomes

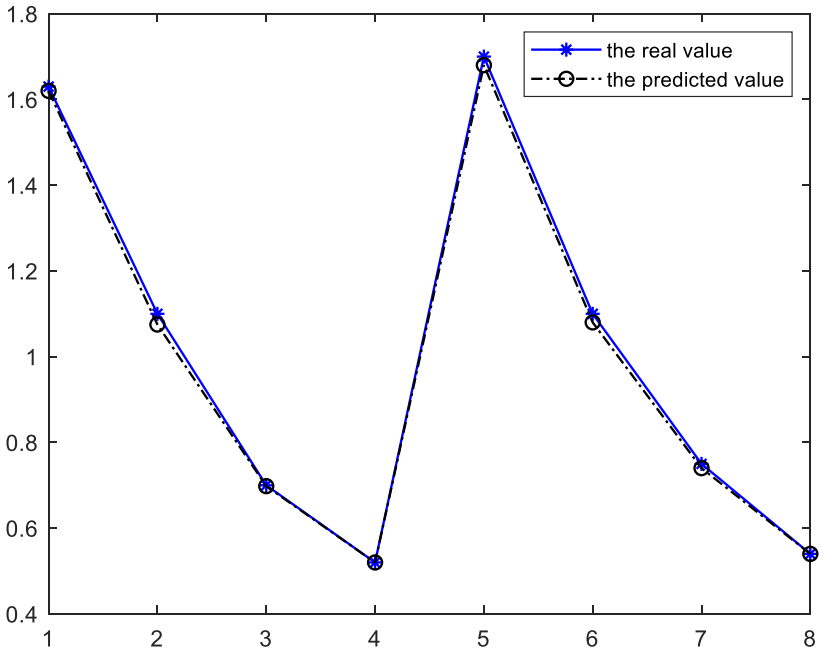

Fig. 7-6 Predicting outcomes

Fig. 7-7 Predicting outcomes

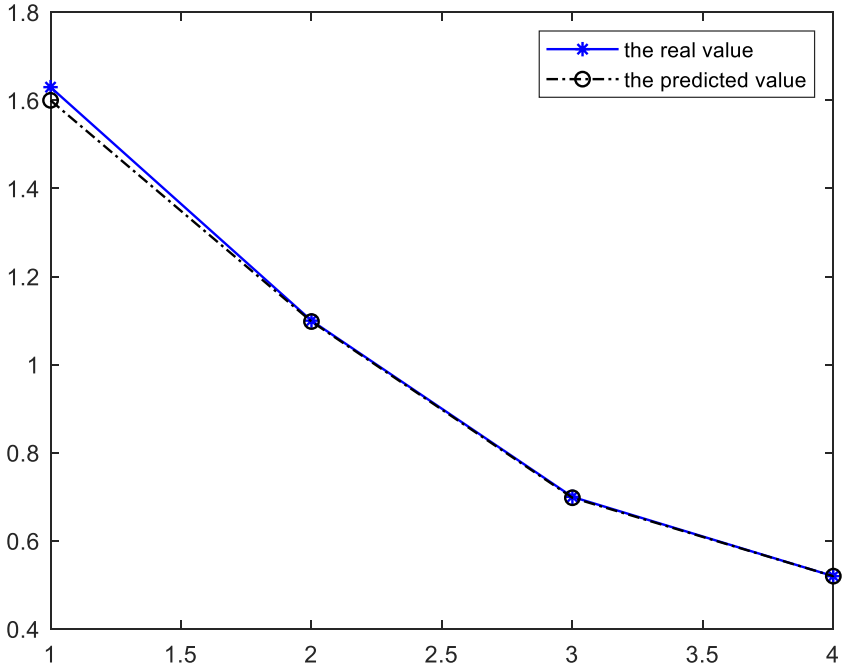

Fig. 7-8 Predicting outcomes

Due to the strong correlation between the sectional passenger flow of Fuxingmen to Fuchengmen and its adjacent sections, the next time passenger volume of Fuxingmen to Fuchengmen section can be predicted by the input vectors composed of four sections including section of Fuxingmen transfer station, Changchunjie to Fuxingmen, Fuxingmen to Fuchengmen, Xuanwumennei to Chang- chunjie current period passenger volume and the section of Fuxingmennei to Fuchengmen in front of three periods.

Consequently, the error performance curve is displayed in Figure 7-5, while the relationship between the predicted and the true value is presented in Figure 7-6. As it is clearly shown, the predicted results are consistent with the actual value so that the fact the future trend of sectional passenger flow can be predicted by the scheme can be proved.

The prediction accuracy can also be improved by the introduction of external factors which includes weekends, holidays, weather conditions, season, and other unexpected events. The factors of weather conditions and weekends are considered by this thesis. In this case, weekend is defined as 1, with weekday as 0, sunny weather as 0, overcast sky as 0.5 and rain and snow as 1.

As a result, the error performance curve is displayed in Figure 7-7, while the relationship between the predicted and the true value is presented in Figure 7-8. As it is clearly shown, the predicted results are consistent with the actual one, and the fact that the future trend of sectional passenger flow can be predicted by the scheme can be proved.

The above three schemes shown in Figures. 7-4, 7-6 and 7-8 all revealed the relations between the actual section flow and the predicted one. Hence section flow can be forecast by the method.

The results selected from 8:00 to 10:00 on March 7th of three schemes for comparison is shown in Table 7-2.

Based on the data above, a higher precision can be obtained when using the relevant section data than only using the relevant time. And error can be made smaller when considering other external factors.

Table 7-2. The comparison results of three schemes

Time interval	The actual section flow	The predicted value of Scheme 1	The predicted value of Scheme 2	The predicted value of Scheme 3
8:00 - 8:30	16,482	16,202	16,301	16,120
8:30 - 9:00	11,251	10,632	11,319	11,217
9:00 - 9:30	6922	6714	6713	6887
9:30 - 10:00	5186	4963	5046	5134
Time interval	Relative error of Scheme 1	Relative error of Scheme 2	Relative error of Scheme 3	
8:00 - 8:30	1.7%	1.1%	2.2%	
8:30 - 9:00	5.5%	0.6%	0.3%	
9:00 - 9:30	3.0%	3.0%	0.5%	
9:30 - 10:00	4.3%	2.7%	1.0%	

7.5. Summary

BP neural network and the features of sectional passenger flow are combined to predict, the results of which show that the three schemes are all feasible. Collected historical data is used in this thesis. However if Recurrent neural networks was involved with the deep learning a better prediction results can be obtained because recurrent networks are neural networks with backward connections[167-171]. They are dynamical systems with temporal state representations.

8. Summary and Prospect

8.1. Conclusions

In this thesis, the research work concentrates on the development of synthetic acquisition method of traffic flow based on multi-functional geomagnetic sensor and Auto-Calibration of Tri-axial Accelerometers and Magnetometers as well as the urban railway sectional passenger flow prediction.

Firstly, the method of multi-parameter comprehensive acquisition of traffic information based on MFGS is studied chapter 3. The algorithms of DWVDA, SVDA and ADWVDA are used to solve the fast and accurate vehicle detection under different application conditions. On this basis, it can realize the comprehensive acquisition of traffic flow parameters such as traffic, speed, occupancy, vehicle existence, vehicle stop, headway and so on based on single MFGS, The research of microcosmic layer provides TIASN network with abundant functions, wireless networking and long-life detection nodes.

In Chapter 4, the TIASN topology optimization and network construction method in multi-lane, multi-section or intersection traffic information acquisition are studied. By analysing the particularity of TIASN network, the hierarchical architecture and node functions of TIASN are given. The network topology and the communication topology optimization are implemented to ensure the economy of TIASN network deployment and the high efficiency of information transmission. The TIASN node semantic coding method developed in this thesis is expected to promote traffic information sharing and TIASN.

In Chapter 5, the calibration of the tri-axial accelerometers (TAs) in a micro Inertial Measurement Unit (μ-IMU) is investigated. Two experimental schemes based on the Central Composite design (CCD) and Box–Behnken design（BBD）are developed. We also compared them with the Icosahedron design proposed by our previous study whose optimality and relatability have been proved. Furthermore, we introduce some indices to assess the quality of each individual experiment in terms of desired experimental characteristics, such as orthogonality, D-optimality, and G-optimality. Finally, the proposed experimental schemes have been applied for the auto calibration of a recently developed μ-IMU which includes a 9-axis motion tracking chips. Both 6-paramter and 9-parammeter models have been applied for the auto-calibration of the TAs inside of μ-IMU. It is concluded that both models can achieve similar accuracy if the experimental data utilized for the estimation of the coefficient of the models can reach the required level of quality in terms of one of the proposed quality index.

In Chapter 6, we applied the Icosahedron design for the calibration of TM for both 6-parameter and 9-parameter models. Secondly, we proposed a method to simultaneously identify both the TA and TM 9-parameter models with certain optimality. Thirdly, based on the identified TA and TM models the angle between the local gravity and local magnetic field can be estimated with relative accuracy.

In Chapter 7, short-term sectional passenger flow forecasting methods are discussed using BP neural network. Furthermore, the method for instance of predicting sectional passenger flow is described. It is found that a better prediction results can be obtained if neural network with station control system is introduced to make real-time training and on-line prediction.

8.2. Research Outlook

It is a complex system engineering, which involves traffic engineering, electronic technology, data communication, intelligent algorithm, network optimization, signal processing and so on. In this thesis, although in the road traffic information acquisition sensor network, the road traffic information acquisition sensor network technology is in the ascendant, technical aspects of the work done to obtain a certain degree of research results, there are related issues and methods to be further studied and expanded, specifically in the following areas:

(1) Multi-sensor node-based cross-section traffic information multi-parameter acquisition and field test. In this thesis, we study the traffic information acquisition of single sensor node, which proves the validity of the MFGS node to obtain real-time road traffic information. It forms the foundation of TIASN network. Next, we need to extend the application range of MFGS node. In addition, according to the different traffic flow information of MFGS detection, a variety of application scenarios of TIASN based on MFGS are expanded and realized, such as large-scale parking management, large-scale traffic flow investigation, self-test of self- Adapt to traffic control, real-time traffic guidance, traffic incident identification.

(2) Multi-vehicle waveform acquisition and verification based on the geomagnetic sensor nodes. In this thesis, an on-line recognition algorithm based on time-frequency domain is proposed and tested in the field to prove the effectiveness of the method. Due to the limitations of on-site data acquisition and the complexity of video data calibration, only car and bus are used as the basic data. In order to meet the needs of the field application, the vehicle classification data acquired in this thesis are collected and calibrated on the basis of the field test to further validate the vehicle classification method proposed in this thesis.

(3) To achieve multi-type detection node integrated access hybrid TIASN network optimization. In this thesis, we focus on the physical topology and communication topology

optimization of TIASN as the detection node of MFGS nodes. In order to realize the comprehensive access of ED nodes in hybrid networks, it is becoming more and more common in traffic information acquisition system. The next step is to apply the method proposed in this thesis. To the physical topology of hybrid networks and communication topology optimization development, in order to improve the adaptability of this method.

(4) BP neural network and the features of sectional passenger flow are combined to predict, the results of which show that the three schemes are all feasible. Collected historical data is used in this thesis. Moreover, a better prediction results can be obtained if neural network with station control system is introduced to make real-time training and on-line prediction.

With the rapid development of CCTV surveillance technology, it makes head counting over video camera much easier and more accurate. In the future the CCTV system can provide every solid real-time data as training input and the prediction source. As the facing recognition system become more advanced, it helps not only count the head also identify the passengers going into the station as well as their route. It definitely creates large database of the people’s movement history and with the analysis of these data it will show regular movement of majority of people. It also helps data matching and makes on-line prediction more practical.

Reference

[1] Akyildiz, I.F., Su, W., Sankarasubramaniam, Y. and Cayirci, E., 2002. Wireless sensor networks: a survey. *Computer networks*, *38*(4), pp.393-422.

[2] Anon, What is wireless sensor network (WSN)? - Definition from WhatIs.com. SearchDataCenter. Available at: https://searchdatacenter.techtarget.com/definition/sensor-network [Accessed Jun 5, 2014].

[3] Oteafy, S.M. & Hassanein, H.S., 2014. Evolution of Wireless Sensor Networks. *Dynamic Wireless Sensor Networks*, pp.1–8.

[4] ElProCus - Electronic Projects for Engineering Students. (2019). *Introduction to Wireless Sensor Networks Types and Applications*. [online] Available at: https://www.elprocus.com/introduction-to-wireless-sensor-networks-types-and-applications/

[5] Anon, Wireless Sensor Networks. Wireless Sensor Networks - an overview | ScienceDirect Topics. Available at: https://www.sciencedirect.com/topics/computer-science/wireless-sensor-networks [Accessed July 3, 2014].

[6] Matin, M. & Islam, M., 2012. Overview of Wireless Sensor Network. *Wireless Sensor Networks - Technology and Protocols*.

[7] Wang, Q. & Balasingham, I., 2010. Wireless Sensor Networks - An Introduction. *Wireless Sensor Networks: Application-Centric Design*.

[8] Zheng, J. & Jamalipour, A., Introduction to Wireless Sensor Networks. *Wireless Sensor Networks*, pp.1–18.

[9] Soparia, J. & Bhatt, N., 2014. A Survey on Comparative Study of Wireless Sensor Network Topologies. *International Journal of Computer Applications*, 87(1), pp.40–43.

[10] Li, F., Chen, Z. & Wang, Y., 2012. Localized geometric topologies with bounded node degree for three-dimensional wireless sensor networks. *EURASIP Journal on Wireless Communications and Networking*, 2012(1).

[11] Karim, L. et al., 2012. The significant impact of a set of topologies on wireless sensor networks. *EURASIP Journal on Wireless Communications and Networking*, 2012(1).

[12] Yang, Chaoyu et al. (2013) Wireless Sensor Network Topology Control Based on Agent. *Sensors & Transducers*. 160 (12), 374–374. [online]. Available from: http://search.proquest.com/docview/1530995167/.

[13] Olexandr, Zuk et al. (2010) 'Wireless sensor network topology control', in *2010 International Conference on Modern Problems of Radio Engineering, Telecommunications and Computer Science (TCSET)*. February 2010 IEEE. pp. 160–160.

[14] Sultana, Marzia et al. (2014) 'Delaunay Triangulation and st-numbering in Wireless Sensor Network topology', in *2014 International Conference on Electrical Engineering and Information & Communication Technology*. [Online]. April 2014 IEEE. pp. 1–7.

[15] Guan, Jing et al. (2013) 'Topology structure design for underwater acoustic Wireless Sensor Network', in *The Institute of Electrical and Electronics Engineers, Inc. (IEEE) Conference Proceedings*. [Online]. 1 October 2013 pp. 1–4. [online]. Available from: http://search.proquest.com/docview/1732829084/.

[16] Feng, Yong et al. (2013) '*Hole patching strategy with the least mobile nodes in wireless sensor network of agriculture*', in [Online]. 4 March 2013 SPIE. pp. 876119–876119–6.

[17] Zhu Jian-Hong et al. (2011) 'Design of a Wireless Sensor Network node based on nRF2401', in *2011 IEEE International Conference on Computer Science and Automation Engineering*. [Online]. June 2011 IEEE. pp. 203–206.

[18] Sasanth, Tummala et al. (2013) A Study on ASCENT in Wireless Sensor Networks. *International Journal of Science, Engineering and Computer Technology*. 3 (8), 267–267. [online]. Available from: http://search.proquest.com/docview/1825467762/.

[19] Khedr, Ahmed M. & Osamy, Walid (2011) Effective target tracking mechanism in a self-organizing wireless sensor network. *Journal of Parallel and Distributed Computing*. [Online] 71 (10), 1318–1326.

[20] Filonenko, A et al. (2012) 'Self-configuration for surveillance sensor network', in *2012 9th International Conference on Ubiquitous Robots and Ambient Intelligence (URAI)*. [Online]. November 2012 IEEE. pp. 425–428.

[21] Becher, K. et al. (2011) Evaluation, validation and optimization of a self-sufficient medical Wireless Sensor Network.(Posterausstellung P101-P120). *Biomedizinische Technik / Biomedical Engineering*. 56 (S1), .

[22] Yang, Dequan (2013) A Mixture Approach of Data Fusion and Reliability in Wireless Sensor Network. *Sensors & Transducers*. 150 (3), 46–50. [online]. Available from: http://search.proquest.com/docview/1506154035/.

[23] Feng, Hai-Lin & Liu, San-Yang (2010) Reliability analysis of a wireless sensor network based on a physical model. *Journal of the Chinese Institute of Industrial Engineers*. [Online] 27 (1), 22–27.

[24] Pan, Shuxia et al. (2010) 'Reliability research of wireless sensor network node', in *2010 14th International Conference on Computer Supported Cooperative Work in Design*. [Online]. April 2010 IEEE. pp. 444–447.

[25] Dong Ting (2012) 'A Clustering Routing Algorithm Based on Reliability in Wireless Sensor Network', in *2012 International Conference on Cyber-Enabled Distributed Computing and Knowledge Discovery*. [Online]. October 2012 IEEE. pp. 389–392.

[26] Rodriguez, M. G et al. (2011) 'Wireless sensor network for data-center environmental monitoring', in *2011 Fifth International Conference on Sensing Technology*. [Online]. November 2011 IEEE. pp. 533–537.

[27] Ke Hong et al. (2013) 'A Synergy of the Wireless Sensor Network and the Data Center System', in *2013 IEEE 10th International Conference on Mobile Ad-Hoc and Sensor Systems*. [Online]. October 2013 IEEE. pp. 263–271.

[28] Nikolaidis, I. & Wu, Kui (2010) *Ad-Hoc, Mobile and Wireless Networks : 9th International Conference, ADHOC-NOW 2010, Edmonton, AB, Canada, August 20-22, 2010. Proceedings* . Berlin, Heidelberg: Springer Berlin Heidelberg.

[29] Yang, Dequan (2013) A Mixture Approach of Data Fusion and Reliability in Wireless Sensor Network. *Sensors & Transducers*. 150 (3), 46–50. [online]. Available from: http://search.proquest.com/docview/1506154035/.

[30] Gao, Liai et al. (2013) An Intelligent Irrigation System Based on Wireless Sensor Network and Fuzzy Control. *Journal of Networks*. [Online] 8 (5), 1080–1087. [online]. Available from: http://search.proquest.com/docview/1366056490/.

[31] Liu, Bo et al. (2013) '*Application of wireless sensor network based on ZigBee technology in photo-bioreactors system*', in [Online]. 14 March 2013 SPIE. p. 87687I–87687I–5.

[32] Santi, Paolo (2012) *Mobility models for next generation wireless networks : ad hoc, vehicular, and mesh networks* . [Online]. Hoboken, New Jersey: Wiley.

[33] Lasheng, Yu et al. (2013) An effective data collection algorithm for wireless sensor network. *Computing*. [Online] 95 (9), 723–738.

[34] Wang, Jianxin et al. (2010) The application research of wireless sensor networks for SHM. *Proceedings of SPIE - The International Society for Optical Engineering*. 7648. [online]. Available from: http://search.proquest.com/docview/1671264915/.

[35] Liu, Yide & Liu, Yide (2012) Wireless Sensor Network Applications in Smart Grid: Recent Trends and Challenges. *International Journal of Distributed Sensor Networks*. [Online] 2012 (9), 8. [online]. Available from: http://search.proquest.com/docview/1349424277/.

[36] Gajjar, S. H et al. (2011) 'Wireless Sensor Network: Application led research perspective', in *2011 IEEE Recent Advances in Intelligent Computational Systems*. [Online]. September 2011 IEEE. pp. 025–030.

[37] Ban-teng, Liu et al. (2013) Research on the optimal design of repeaters for WSNs based on CTCSS.(continuous tone-coded squelch system)(wireless sensor network). *Journal of Software*. [Online] 8 (4), 785–790.

[38] Wang, Jianxin et al. (2010) 'The application research of wireless sensor networks for SHM', in *Proceedings of SPIE.* [Online]. 25 March 2010 pp. 764818–764816.

[39] Hayek, A et al. (2012) 'FPGA-based wireless sensor network platform for safety systems', in *2012 19th International Conference on Telecommunications (ICT)*. [Online]. April 2012 IEEE. pp. 1–6.

[40] Bathula, Manohar et al. (2009) 'A Sensor Network System for Measuring Traffic in Short-Term Construction Work Zones', in *Distributed Computing in Sensor Systems: 5th IEEE International Conference, DCOSS 2009, Marina del Rey, CA, USA, June 8-10, 2009. Proceedings*. [Online]. Berlin, Heidelberg: Springer Berlin Heidelberg. pp. 216–230.

[41] Nagavignesh, M & Nagavignesh, M (2011) Design of Wireless Sensor Network For Tactical Military Application. *i-Manager's Journal on Electronics Engineering*. [Online] 2 (1), 51–57. [online]. Available from: http://search.proquest.com/docview/1692360283/.

[42] Liang Zhou & Han-Chieh Chao (2011) Multimedia traffic security architecture for the internet of things. *IEEE Network*. [Online] 25 (3), 35–40.

[43] Chin, T.-L. & Yen, Y.-T., 2012. Load balance for mobile sensor patrolling in surveillance sensor networks. *2012 IEEE Wireless Communications and Networking Conference (WCNC)*.

[44] Tiwari, Vinodkumar (2016) Study of Internet of Things (IoT): A Vision, Architectural Elements, and Future Directions. *International Journal of Advanced Research in Computer Science. 7 (7)*, . [online]. Available from: http://search.proquest.com/docview/1871595491/.

[45] Jauregui-Ortiz, Salvador et al. (2012) 'Smart Environmental Architecture for Node Localization in a Wireless Sensor Network', in *2012 Eighth International Conference on Intelligent Environments*. [Online]. June 2012 IEEE. pp. 222–227.

[46] El Emary, Ibrahiem M. M. & Ramakrishnan, S. (2013) *Wireless Sensor Networks : From Theory to Applications.* Hoboken: CRC Press.

[47] Vairamani, K. et al. (2013) Environmental parameter monitoring using wireless sensor network. *Instruments and Experimental Techniques.* [Online] 56 (4), 468–471.

[48] Guevara, J et al. (2012) Environmental wireless sensor network for road traffic applications. *IET Intelligent Transport Systems.* [Online] 6 (2), 177–186. [online]. Available from: http://search.proquest.com/docview/1637583094/.

[49] Lim, Hock et al. (2007) 'The national weather sensor grid', in *Proceedings of the 5th international conference on embedded networked sensor systems*. [Online]. 6 November 2007 ACM. pp. 369–370.

[50] Murty, R.N et al. (2008) 'CitySense: An Urban-Scale Wireless Sensor Network and Testbed', in *2008 IEEE Conference on Technologies for Homeland Security*. [Online]. May 2008 IEEE. pp. 583–588.

[51] Dickerson, R.F et al. (2008) ‘MetroNet: Case Study for Collaborative Data Sharing on the World Wide Web’, in *2008 International Conference on Information Processing in Sensor Networks* (ipsn 2008). [Online]. April 2008 IEEE. pp. 557–558.

[52] Bohli, J.M., Hessler, A., Ugus, O. and Westhoff, D., 2008, March. A secure and resilient WSN roadside architecture for intelligent transport systems. In *Proceedings of the first ACM conference on Wireless network security* (pp. 161-171). ACM.

[53] Wang, Ruchuan & Xiao, Fu (2013) *Advances in Wireless Sensor Networks : 6th China Conference, CWSN 2012, Huangshan, China, October 25-27, 2012, Revised Selected Papers* . Berlin, Heidelberg: Springer Berlin Heidelberg.

[54] Li, Li et al. (2013) A routing algorithm for WiFi-based wireless sensor network and the application in automatic meter reading.(Research Article)(Report). *Mathematical Problems in Engineering*. [Online] 20131–9.

[55] Shuang-Chun Yang & Yi Pan (2010) ‘The Application of the Wireless Sensor Network (WSN) in the Monitoring of Fushun Reach River in China’, in *2010 Second International Conference on Computer and Network Technology*. [Online]. April 2010 IEEE. pp. 331–333.

[56] Wang, Bei et al. (2011) ‘Application of Wireless Sensor Network in Farmland Data Acquisition System’, in Applied Informatics and Communication: International Conference, ICAIC 2011, Xi’ian, *China, August 20-21, 2011. Proceedings, Part III*. [Online]. Berlin, Heidelberg: Springer Berlin Heidelberg. pp. 672–678.

[57] Zeng, Yuanyuan et al. (2016) Opportunistic fleets for road event detection in vehicular sensor networks. *Wireless Networks.* [Online] 22 (2), 503–521.

[58] Eng-Han Ng et al. (2009) ‘Road traffic monitoring using a wireless vehicle sensor network’, in *2008 International Symposium on Intelligent Signal Processing and Communications Systems*. [Online]. February 2009 IEEE. pp. 1–4.

[59] Zhang, Ge et al. (2019) Application research of image compression and wireless network traffic video streaming.(Report). *Journal of Visual Communication and Image Representation*. [Online] 59168–175.

[60] Ye, Zhoujing et al. (2018) The Strip Clustering Scheme for data collection in large-scale Wireless Sensing Network of the road. *International Journal of Pavement*

Research and Technology. [Online] 11 (2), 138–145. [online]. Available from: http://search.proquest.com/docview/2021694338/.

[61] Oh C, Ritchie S G. Recognizing vehicle classification information from blade sensor signature. *Pattern recognition letters*, 2007, 28(9): 1041-1049.

[62] Cheung, S.Y. et al., 2004. *Traffic Measurement and Vehicle Classification with a Single Magnetic Sensor*.

[63] Reimer M J, Regehr J D. Hybrid Approach for Clustering Vehicle Classification Data to Support Regional Implementation of Mechanistic-Empirical Pavement Design Guide. *Transportation Research Board 92nd Annual Meeting*. 2013 (13-2849).

[64] Swan, D et al. (2008) Development of Regional Traffic Data for the Mechanistic-Empirical Pavement Design Guide. *Transportation Research Record.* 2049 (2049), 54–62.

[65] Sayyady, Fatemeh et al. (2009) Clustering Analysis to Characterize Mechanistic-Empirical Pavement Design Guide Traffic Data in North Carolina. *Transportation Research Record.* 2160 (1), 118–127.

[66] Z. Chen, N. Pears, M. Freeman, J. Austin, "Road vehicle classification using support vector machines", Proc. IEEE Int. Conf. Intell. *Comput. Intell. Syst.*, vol. 4, pp. 214-218, 2009-Nov.

[67] Kafai M, Bhanu B. Dynamic Bayesian networks for vehicle classification in video[J]. *IEEE Transactions on Industrial Informatics*, 2012, 8(1): 100-109.

[68] Rajesh P, Geetha M K, Ramu R.,2013, Traffic density estimation, vehicle classification and stopped vehicle detection for traffic surveillance system using predefined traffic videos, *Computer Science and Engineering*, 56A: 13671-13676.

[69] Guo, B., Nixon, M.S. and Damarla, T.R., 2008, June. Acoustic information fusion for ground vehicle classification. In *2008 11th international conference on information fusion* (pp. 1-7). IEEE.

[70] Wu, H. and Mendel, J.M., 2007. Classification of battlefield ground vehicles using acoustic features and fuzzy logic rule-based classifiers. *IEEE transactions on fuzzy systems*, *15*(1), pp.56-72.

[71] Guo, B., Gunn, S.R., Damper, R.I. and Nelson, J.D., 2006. Band selection for hyperspectral image classification using mutual information. *IEEE Geoscience and Remote Sensing Letters*, *3*(4), pp.522-526.

[72] Guo, B., Damper, R.I., Gunn, S.R. and Nelson, J.D., 2008. A fast separability-based feature-selection method for high-dimensional remotely sensed image classification. *Pattern Recognition*, *41*(5), pp.1653-1662.

[73] Paulraj, M.P., Adom, A.H., Sundararaj, S. and Rahim, N.B.A., 2013. Moving vehicle recognition and classification based on time domain approach. *Procedia Engineering*, *53*, pp.405-410.

[74] Averbuch, A., Hulata, E., Zheludev, V. and Kozlov, I., 2001. A wavelet packet algorithm for classification and detection of moving vehicles. *Multidimensional Systems and Signal Processing*, *12*(1), pp.9-31.

[75] Jeng, S.T., Chu, L. and Hernandez, S., 2013. Wavelet–k nearest neighbor vehicle classification approach with inductive loop signatures. *Transportation Research Record*, *2380*(1), pp.72-80.

[76] Vanajakshi, L.D., Williams, B.M. and Rilett, L.R., 2009. Improved flow-based travel time estimation method from point detector data for freeways. *Journal of Transportation Engineering*, *135*(1), pp.26-36.

[77] Coifman, B. and Kim, S., 2009. Speed estimation and length based vehicle classification from freeway single-loop detectors. *Transportation research part C: emerging technologies*, *17*(4), pp.349-364.

[78] Jain, M. and Coifman, B., 2005. Improved speed estimates from freeway traffic detectors. *Journal of Transportation Engineering*, *131*(7), pp.483-495.

[79] He, Y., Du, Y. and Sun, L., 2012. Vehicle classification method based on single-point magnetic sensor. *Procedia-Social and Behavioral Sciences*, *43*, pp.618-627.

[80] Lan, J., Xiang, Y., Wang, L. and Shi, Y., 2011. Vehicle detection and classification by measuring and processing magnetic signal. *Measurement*, 44(1), pp.174-180.

[81] Kaewkamnerd, S., Pongthornseri, R., Chinrungrueng, J. and Silawan, T., 2009, September. Automatic vehicle classification using wireless magnetic sensor. In *2009*

IEEE International Workshop on Intelligent Data Acquisition and Advanced Computing Systems: Technology and Applications (pp. 420-424). IEEE.

[82] Yang Z., Yang Z., Zhao D.,2002, Research on Vehicle Auto-classification of Freeway Toll Collection System. Journal of Jilin University, 32(3): 6-9

[83] Liu, H.X. and Sun, J., 2014. Length-based vehicle classification using event-based loop detector data. *Transportation Research Part C: Emerging Technologies*, *38*, pp.156-166.

[84] Liu, H.X., Wu, X., Ma, W. and Hu, H., 2009. Real-time queue length estimation for congested signalized intersections. *Transportation research part C: emerging technologies*, 17(4), pp.412-427.

[85] Bathula, M., Ramezanali, M., Pradhan, I., Patel, N., Gotschall, J. and Sridhar, N., 2009, June. A sensor network system for measuring traffic in short-term construction work zones. In *International Conference on Distributed Computing in Sensor Systems* (pp. 216-230). Springer, Berlin, Heidelberg.

[86] Awad, A., Frunzke, T. and Dressler, F., 2007, August. Adaptive distance estimation and localization in WSN using RSSI measures. In *10th Euromicro Conference on Digital System Design Architectures, Methods and Tools (DSD 2007)* (pp. 471-478). IEEE.

[87] Shuai, M., Xie, K., Ma, X. and Song, G., 2008, October. An on-road wireless sensor network approach for urban traffic state monitoring. In *2008 11th International IEEE Conference on Intelligent Transportation Systems* (pp. 1195-1200). IEEE.

[88] Guitton, A., Skordylis, A. and Trigoni, N., 2007, March. Utilizing correlations to compress time-series in traffic monitoring sensor networks. In *2007 IEEE Wireless Communications and Networking Conference* (pp. 2479-2483). IEEE.

[89] Sawant, H., Tan, J. and Yang, Q., 2004, October. A sensor networked approach for intelligent transportation systems. In *2004 IEEE/RSJ International Conference on Intelligent Robots and Systems (IROS)(IEEE Cat. No. 04CH37566)* (Vol. 2, pp. 1796-1801). IEEE.

[90] Wang, Q., 2010. *Traffic analysis, modeling and their applications in energy-constrained wireless sensor networks: on network optimization and anomaly detection* (Doctoral dissertation, Tryckeriet Mittuniversitetet).

[91] Wang, R., Zhang, L., Sun, R., Gong, J. and Cui, L., 2010. EasiTia: A pervasive traffic information acquisition system based on wireless sensor networks. *IEEE Transactions on Intelligent Transportation Systems*, *12*(2), pp.615-621.

[92] Kong, Q.J., Li, Z., Chen, Y. and Liu, Y., 2009. An approach to urban traffic state estimation by fusing multisource information. *IEEE Transactions on Intelligent Transportation Systems, 10*(3), pp.499-511.

[93] Zhou, B., Cao, J., Zeng, X. and Wu, H., 2010, September. Adaptive traffic light control in wireless sensor network-based intelligent transportation system. In *2010 IEEE 72nd Vehicular Technology Conference-Fall* (pp. 1-5). IEEE.

[94] Wu, H., Cao, J. and Fan, X., 2016. Dynamic collaborative in-network event detection in wireless sensor networks. *Telecommunication Systems*, *62*(1), pp.43-58.

[95] Pascale, A. et al., 2012. Wireless sensor networks for traffic management and road safety. *IET Intelligent Transport Systems*, 6(1), p.67.

[96] Tadigadapa, S. & Mateti, K., 2009. Piezoelectric MEMS sensors: state-of-the-art and perspectives. *Measurement Science and Technology*, 20(9), p.092001.

[97] Chinrungrueng, J., Sununtachaikul, U. and Triamlumlerd, S., 2006, June. A vehicular monitoring system with power-efficient wireless sensor networks. In *2006 6th International Conference on ITS Telecommunications* (pp. 951-954). IEEE.

[98] Ndzi, D.L., Arif, M.A., Shakaff, A.Y.M., Ahmad, M.N., Harun, A., Kamarudin, L.M., Zakaria, A., Ramli, M.F. and Razalli, M.S., 2012. Signal propagation analysis for low data rate wireless sensor network applications in sport grounds and on roads. *Progress In Electromagnetics Research*, *125*, pp.1-19.

[99] Wu, L., Yu, K., Du, T. and Wang, Z., 2014, June. Efficient information transmission under lossy WSNs link using compressive sensing. In *2014 9th IEEE Conference on Industrial Electronics and Applications* (pp. 493-498). IEEE.

[100] Daponte, P., De Vito, L., Rapuano, S., Riccio, M. and Tudosa, I., 2012, October. Wireless sensor network for traffic safety: analysis of measurement uncertainties. In *2012 International Conference and Exposition on Electrical and Power Engineering* (pp. 882-887). IEEE.

[101] De Vito, L., Cocca, V., Riccio, M. and Tudosa, I., 2012, September. Wireless active guardrail system for environmental measurements. In *2012 IEEE Workshop on Environmental Energy and Structural Monitoring Systems (EESMS)* (pp. 50-57). IEEE.

[102] Sen, R., Maurya, A., Raman, B., Mehta, R., Kalyanaraman, R., Vankadhara, N., Roy, S. and Sharma, P., 2012, November. Kyun queue: a sensor network system to monitor road traffic queues. In *Proceedings of the 10th ACM Conference on Embedded Network Sensor Systems* (pp. 127-140). ACM.

[103] Yoo J J, Kim D H, Kim K H, et al.,2012 On-Road Wireless Sensor Networks for Traffic Surveillance. *The Second International Conference on Mobile Services, Resources, and Users* pp. 131-135.

[104] Karpiriski, M., Senart, A. and Cahill, V., 2006, March. Sensor networks for smart roads. In *Fourth Annual IEEE International Conference on Pervasive Computing and Communications Workshops (PERCOMW'06)* (pp. 5-pp). IEEE.

[105] Megalingam, R.K., Mohan, V., Leons, P., Shooja, R. and Ajay, M., 2011, October. Smart traffic controller using wireless sensor network for dynamic traffic routing and over speed detection. In *2011 IEEE Global Humanitarian Technology Conference* (pp. 528-533). IEEE.

[106] Corredor, I., García, A., Martínez, J.F. and López, P., 2008. Wireless sensor network-based system for measuring and monitoring road traffic. *6th Collaborative Electronic Communications and eCommerce Technology and Research (CollECTeR 2008), Madrid, Spain*.

[107] Feng, Y. et al., 2019. MagSpeed: A Novel Method of Vehicle Speed Estimation Through A Single Magnetic Sensor. *2019 IEEE Intelligent Transportation Systems Conference (ITSC)*..

[108] WONG, W. and QI, Y. (2009). BP NEURAL NETWORK-BASED EFFECTIVE FAULT LOCALIZATION. *International Journal of Software Engineering and Knowledge Engineering*, 19(04), pp.573-597.

[109] Liu, Chao & Han, Jiawei (2006) 'Failure proximity: a fault localization-basedapproach', in *Proceedings of the 14th ACM SIGSOFT international symposium on foundations of software engineering*. 5 November 2006 ACM. pp. 46–56.

[110] Yi, J. et al., 2007. BP neural network prediction-based variable-period sampling approach for networked control systems. *Applied Mathematics and Computation*, 185(2), pp.976–988.

[111] Wu, A., Wang, D. and Liang, J. (2004). Application of generalized predictive control with neural network error correction in networked control system. *Fifth World Congress on Intelligent Control and Automation* (IEEE Cat. No.04EX788).

[112] Liu, J. et al., 2000. Prediction of the flow stress of high-speed steel during hot deformation using a BP artificial neural network. *Journal of Materials Processing Technology*, 103(2), pp.200–205.

[113] Wang, Y. et al., 2009. Back Propagation Neural Network for Short-term Electricity Load Forecasting with Weather Features. *2009 International Conference on Computational Intelligence and Natural Computing.*

[114] Benaouda, D. and Murtagh, F., 2006. Electricity load forecast using neural network trained from wavelet-transformed data. In *2006 IEEE International Conference on Engineering of Intelligent Systems,* pp. 1-6. IEEE

[115] Wang, Y.L., Niu, D.X. and Liu, J.Y., 2008, October. Optimization of artificial neural networks based on chaotic time series in power load forecasting model. *In 2008 Fourth International Conference on Natural Computation*, Vol. 2, pp. 106-110. IEEE.

[116] Park, P., Fischione, C. & Johansson, K.H., 2010. *Adaptive IEEE 802.15.4 Medium Access Control Protocol for Control and Monitoring Applications*. Wireless Networking Based Control, pp.271–300.

[117] Koubaa, A et al. (2006) 'GTS allocation analysis in IEEE 802.15.4 for real-time wireless sensor networks', in *Proceedings 20th IEEE International Parallel & Distributed Processing Symposium*. 2006 IEEE. p. 8 pp.

[118] Zhang, Y. & Dolmans, G., 2009. A New Priority-Guaranteed MAC Protocol for Emerging Body Area Networks. *2009 Fifth International Conference on Wireless and Mobile Communications*.

[119] Van Dam, T. and Langendoen, K., 2003, November. An adaptive energy-efficient MAC protocol for wireless sensor networks. In *Proceedings of the 1st international conference on Embedded networked sensor systems,* pp. 171-180. ACM.

[120] Sanli, H.O. & Çam, H., 2010. Collaborative Event-Driven Coverage and Rate Allocation for Event Miss-Ratio Assurances in Wireless Sensor Networks. *EURASIP Journal on Wireless Communications and Networking*, 2010(1), p.345052.

[121] Tian, D. and Georganas, N.D., 2003. A node scheduling scheme for energy conservation in large wireless sensor networks. *Wireless Communications and Mobile Computing*, *3*(2), pp.271-290.

[120] SIMONWEGMÜLLER, M.S. 2007, *Intra-body communication for biomedical sensor networks*, Doctoral Thesis, Engineering Information, Swiss Federal Institute of Technology, ZURICH.

[123] Wegmueller, M. et al., 2009. Galvanic Coupling Enabling Wireless Implant Communications. *IEEE Transactions on Instrumentation and Measurement*, 58(8), pp.2618–2625.

[124] Zhou, J. et al., 2012. Abnormalities Detection of IMU Based on PCA in Motion Monitoring. *Applied Mechanics and Materials*, 224, pp.533–538.

[125] Sun, S. & Liu, R., 2009. Error Calibration and FDI Technology of Gyros in Redundant IMU. *2009 First International Workshop on Database Technology and Applications*.

[126] Hu, W. et al., 2010. An Energy-efficient Rate Adaptive Media Access Protocol (RA-MAC) for Long-lived Sensor Networks. *Sensors*, 10(6), pp.5548–5568.

[127] Le, T. et al., 2009. ERTP: Energy-efficient and Reliable Transport Protocol for data streaming in Wireless Sensor Networks. *Computer Communications*, 32(7-10), pp.1154–1171.

[128] Aguiar, P.D. et al., 1995. D-optimal designs. *Chemometrics and Intelligent Laboratory Systems*, 30(2), pp.199–210.

[129] Frosio, I., Stuani, S. & Borghese, N.A., 2006. Autocalibration of MEMS Accelerometer. *2006 IEEE Instrumentation and Measurement Technology Conference Proceedings*.

[130] Wu, Z.C., Wang, Z.F. and Ge, Y., 2002. Gravity based online calibration for monolithic triaxial accelerometers' gain and offset drift. In *Proceedings of the 4th World Congress on Intelligent Control and Automation (Cat. No. 02EX527)* (Vol. 3, pp. 2171-2175). IEEE.

[131] Khuri, A.I. & Mukhopadhyay, S., 2010. Response surface methodology. *Wiley Interdisciplinary Reviews: Computational Statistics*, 2(2), pp.128–149.

[132] Khuri, A.I., 2006. Mixed Response Surface Models With Heterogeneous Within-Block Error Variances. *Technometrics*, 48(2), pp.206–218.

[133] Ye, L. & Su, S.W., 2015. Experimental Design and Its Posterior Efficiency for the Calibration of Wearable Sensors. *Journal of Intelligent Learning Systems and Applications*, 07(01), pp.11–20.

[134] López-Fidalgo, J. & Garcet-Rodríguez, S.A., 2004. Optimal Experimental Designs When Some Independent Variables Are Not Subject to Control. *Journal of the American Statistical Association*, 99(468), pp.1190–1199.

[135] Torsney, B. & Mandal, S., 2001. Construction of Constrained Optimal Designs. *Nonconvex Optimization and Its Applications Optimum Design 2000*, pp.141–152.

[136] Pedley M., 2013 “Tilt Sensing Using a Three-Axis Accelerometer,” *Free. Semicond. Appl. Note*.

[137] Won, S.P. & Golnaraghi, F., 2010. A Triaxial Accelerometer Calibration Method Using a Mathematical Model. *IEEE Transactions on Instrumentation and Measurement*, 59(8), pp.2144–2153.

[138] Umeda, A., Onoe, M., Sakata, K., Fukushia, T., Kanari, K., Iioka, H. and Kobayashi, T., 2004. Calibration of three-axis accelerometers using a three-dimensional vibration generator and three laser interferometers. *Sensors and Actuators A: Physical*, *114*(1), pp.93-101.

[138] Wardrop, D.M. & Myers, R.H., 1990. Some response surface designs for finding optimal conditions. *Journal of Statistical Planning and Inference*, 25(1), pp.7–28.

[140] Montgomery, D.C., 2017. *Design and analysis of experiments*, Hoboken: Wiley.

[141] Myers, R.H. & Montgomery, D.C., 1995. *Response surface methodology: process and product optimization using designed experiments*, New York: Wiley.

[142] Krohn, A., Beigl, M., Decker, C., Kochendörfer, U., Robinson, P. and Zimmer, T., 2004, November. Inexpensive and automatic calibration for acceleration sensors.

In *International Symposium on Ubiquitious Computing Systems*, pp. 245-258. Springer, Berlin, Heidelberg.

[143] Wu, Z.C., Wang, Z.F. and Ge, Y., 2002. Gravity based online calibration for monolithic triaxial accelerometers' gain and offset drift. In *Proceedings of the 4th World Congress on Intelligent Control and Automation,* Vol. 3, pp. 2171-2175. IEEE.

[144] Cook, D. & Fedorov, V., 1995. Invited Discussion Paper Constrained Optimization of Experimental Design. *Statistics*, 26(2), pp.129–148.

[145] Banaee, H., Ahmed, M. & Loutfi, A., 2013. Data Mining for Wearable Sensors in Health Monitoring Systems: A Review of Recent Trends and Challenges. *Sensors*, 13(12), pp.17472–17500.

[146] Glueck, M. et al., 2014. Real-Time Autocalibration of MEMS Accelerometers. *IEEE Transactions on Instrumentation and Measurement*, 63(1), pp.96–105.

[147] Breed, D., 2011, *Vehicle-traffic control device communication techniques,* US7983836B2

[148] Chaloner, K. & Verdinelli, I., 1995. Bayesian Experimental Design: A Review. *Statistical Science*, 10(3), pp.273–304.

[149] Rojas, C.R. et al., 2007. Robust optimal experiment design for system identification. *Automatica*, 43(6), pp.993–1008.

[150] Mehra, R., 1974. Optimal input signals for parameter estimation in dynamic systems--Survey and new results. *IEEE Transactions on Automatic Control*, 19(6), pp.753–768.

[151] Asprey, S. & Macchietto, S., 2002. Designing robust optimal dynamic experiments. *Journal of Process Control*, 12(4), pp.545–556.

[152] Patan, M. & Uciński, D., 2008. Configuring A Sensor Network for Fault Detection in Distributed Parameter Systems. *International Journal of Applied Mathematics and Computer Science*, 18(4), pp.513–524.

[153] Wei, Yu & Chen, Mu-Chen (2011) Forecasting the short-term metro passenger flow with empirical mode decomposition and neural networks. *Transportation Research Part C*. [Online] 21 (1), 148–162.

[154] Xie, Mei-Quan et al. (2014) Forecasting the short-term passenger flow on high-speed railway with neural networks. *Computational intelligence and neuroscience*. [Online] 2014 (2014), 375487–375487. [online]. Available from: http://search.proquest.com/docview/1641016391/.

[155] Zhang Dongquan & Wang Lina (2011) 'Passenger Flow Forecast of Urban Rail Transit Based on BP Neural Networks', in *2011 3rd International Workshop on Intelligent Systems and Applications*. [Online]. May 2011 IEEE. pp. 1–4.

[156] Dan Zheng & Yao Wang (2011) ‘Application of an artificial neural network on railway passenger flow prediction’, in *Proceedings of 2011 International Conference on Electronic & Mechanical Engineering and Information Technology*. [Online]. August 2011 IEEE. pp. 149–152.

[157] Li, Haiguang et al. (2013) A real-time transportation prediction system.(Report). *Applied Intelligence*. 39 (4), .

[158] Leng, Biao et al. (2013) Probability tree based passenger flow prediction and its application to the Beijing subway system. *Frontiers of Computer Science*. [Online] 7 (2), 195–203.

[159] Li, Wei et al. (2014) Design and Application of Mass Passenger Flow Precautionary and Forecasting System in Rail Transit Based on the Internet of Things Technology. *Applied Mechanics and Materials*. [Online] 556-5626366–6369.

[160] Mo Yikui & Su Yongyun (2009) ‘Neural networks based real-time transit passenger volume prediction’, in *2009 2nd International Conference on Power Electronics and Intelligent Transportation System (PEITS)*. [Online]. December 2009 IEEE. pp. 303–306.

[161] Zhang Haili et al. (2010) ‘Research on passenger flow model based on individual behavior in rail transit system’, in *2010 International Conference on Computer, Mechatronics, Control and Electronic Engineering*. [Online]. August 2010 IEEE. pp. 405–408.

[162] Ma, Zhenliang et al. (2012) ‘Dynamic Public Transport Passenger Flow Forecast Based on IMM Method’, in *Advances in Multimedia, Software Engineering and Computing Vol.2: Proceedings of the 2011 MSEC International Conference on Multimedia, Software Engineering and Computing, November 26–27, Wuhan, China*. [Online]. Berlin, Heidelberg: Springer Berlin Heidelberg. pp. 675–683.

[163] Rumelhart, Davide et al. (1986) Learning representations by back-propagating errors. *Nature*. 323533–536. [online]. Available from: http://search.proquest.com/docview/24094821/.

[164] Liu, Y. et al., 2018. Short-term forecasting of rail transit passenger flow based on long short-term memory neural network. *2018 International Conference on Intelligent Rail Transportation (ICIRT)*.

[165] Chen, Q., Wen, D., Li, X., Chen, D., Lv, H., Zhang, J. and Gao, P. (2019). Empirical mode decomposition based long short-term memory neural network forecasting model for the short-term metro passenger flow. *PLOS ONE*, 14(9), p.e0222365.

[166] Li, H., Wang, Y., Xu, X., Qin, L. and Zhang, H. (2019). Short-term passenger flow prediction under passenger flow control using a dynamic radial basis function network. *Applied Soft Computing*, 83, p.105620.

[167] Cashman, D. et al., 2018. RNNbow: Visualizing Learning Via Backpropagation Gradients in RNNs. *IEEE Computer Graphics and Applications*, 38(6), pp.39–50.

[168] Tang, H. & Glass, J., 2018. On Training Recurrent Networks with Truncated Backpropagation Through time in Speech Recognition. *2018 IEEE Spoken Language Technology Workshop (SLT)*.

[169] Bianchi, F.M. et al., 2017. Recurrent Neural Networks for Short-Term Load Forecasting. *SpringerBriefs in Computer Science*.

[170] G.c, M.P. et al., 2017. Back propagation genetic and recurrent neural network applications in modelling and analysis of squeeze casting process. *Applied Soft Computing*, 59, pp.418–437.

[171] Trischler, A.P. & D'Eleuterio, G.M., 2016. Synthesis of recurrent neural networks for dynamical system simulation. *Neural Networks*, 80, pp.67–78.